Alma Mater Studiorum · University of Bologna

School of Science
Department of Physics and Astronomy
Master Degree in Physics

Dark Sector searches at Neutrino Experiments

Supervisor:
Prof. Silvia Pascoli

Co-supervisor:
Prof. Pilar Coloma

Submitted by:
Sara Bianco

Academic Year 2022/2023

Dark Sector searches at Neutrino Experiments

Sara Bianco

September 2023

Acknowledgments

I am deeply grateful to my supervisor Silvia Pascoli for her invaluable guidance and support throughout my master's thesis journey. She has been a steadfast mentor who introduced me to the world of research and nurtured my growth in this direction. Thank you for your constant assistance, which extended beyond my thesis work. I am especially appreciative of your help in securing a PhD position, for which I am genuinely thankful.

I would also like to express my sincere gratitude to my co-supervisor, Pilar Coloma, who provided invaluable assistance during my time at the *Instituto de Física Teórica* in Madrid. Your constant availability and willingness to lend a helping hand whenever I needed it were truly important to me. Thank you for consistently being there to support me.

Lastly, I extend my thanks to all the incredible people I had the privilege of meeting in Madrid while conducting my research for this thesis. You made my time at IFT truly unforgettable. It is also thanks to all of you that I was really able to appreciate this world.

Abstract

Despite considerable progress in the understanding of fundamental particles and interactions and the striking predictive power of the Standard Model in collider experiments, some key questions in the understanding of Nature still remain unanswered. What is the origin of neutrino masses? What is dark matter made of? Why is there an imbalance between baryons and anti-baryons in the Universe? These questions call for new physics beyond the Standard Model. For decades, the majority of the experimental effort has been directed to the search for new particles with sizeable couplings to the Standard Model and masses at the TeV scale, motivated by some popular extensions of the SM. However, recent theoretical and experimental developments have brought new attention to the dark sectors, i.e. extensions of the Standard Model at scales below the electroweak scale and which are weakly coupled to the visible sector. In some of these rich dark sector models, it is possible to have dark photons decaying semi-visibly, meaning that the final state contains both visible and invisible particles, making it possible to circumvent current experimental constraints on the masses of the dark photons $m_{A'}$ and mixing ε with the SM photon. This project will focus on models containing multiple dark fermions, where the lighter of these can be made stable through some additional symmetry that forbids the mixing with active neutrinos, making it a viable dark matter candidate. This model can leave visible signatures in ProtoDUNE detectors, located at CERN. Protons extracted from the CERN Super Proton Synchrotron (SPS), with energies up to 400 GeV, can generate a flux of BSM particles that can reach the ProtoDUNE detectors. These are liquid Argon Time Projection Chambers (LArTPCs) constructed to test and consolidate the technologies of the DUNE Far Detector. Thanks to its large volume and the high density of liquid argon, stable particles coming into the detector can interact, leading to an excess of electron recoil.

Contents

Introduction

By observing the Universe and the galaxies it contains, we can gain information about the matter it is made of. What we find is that there are *dark* footprints, whose form we do not recognise, etched by something beyond our current understanding and whose origin remains a mystery. The cosmic microwave background, gravitational lensing, and large-scale structures, all show that ordinary matter is insufficient to account for all the matter inferred from observations[1–3]. Some additional elusive dark matter (DM) is necessary to explain these phenomena.

As sure as we are that there is something we are missing that contributes to the total matter in the universe from astronomical observations, we still have no idea what this dark matter is and what is its origin. The Standard Model of particle physics (SM), the currently most successful theory in describing fundamental particles and their interactions, lacks an explanation for DM.

Alongside dark matter, there are numerous pieces of evidence that show that the SM is incomplete. Neutrino masses, the uneven distribution of matter and antimatter in the universe, known as *baryon asymmetry*, and the precise value of the mass of Higgs bosons hint at some new physics that is able to address these problems. However, determining the energy scale at which this new physics might manifest remains an open question. Several prominent theories aiming to extend the SM, including Type-I seesaw, WIMP dark matter, and the 'vanilla leptogenesis' model designed to explain baryon asymmetry, suggest the presence of high-energy new physics. New physics at high energy is very important in solving the hierarchy problem, where supersymmetric theories have been proposed to address this issue. From an experimental viewpoint, the will to explore the energy frontier has led to searches in high-energy experiments, with the goal of looking for a resonance that could indicate a new particle. However, the lack of experimental evidence in this range has led to contemplating alternative avenues, in particular investigating particles that have weaker interactions with the known particles. These particles can have lighter masses and are referred to as "dark sectors" (DS).

Dark sectors provide new opportunities for theory, phenomenology and experiments. They could be imagined as a world parallel to our own, that could contain many states - either fermions or scalars. If the only interaction between the dark sectors and regular matter were through gravity, it would be exceedingly challenging to detect these new particles in laboratory experiments. Therefore some sort of *portal* interaction must be introduced, in order to allow us to have an interaction other than gravitational between these states. These *portals* can take different forms depending on the type and dimension of its operator. Dimension four portals are, in particular, the vector portal, the scalar portal and the fermion portal. The first one is mediated by a new

dark $U(1)_D$ gauge boson called *dark photon*, the second by an additional scalar that mixes with the SM Higgs boson, while the latter is mediated by a heavy neutral lepton (HNL) interacting with one of the left-handed SM doublets and the Higgs boson. There is an additional portal, the pseudoscalar portal, mediated by an axion (or axion-like particle). This portal has dimension five and is suppressed by the axion decay constant. The interest in dark sectors stems mainly from the power they offer in explaining the aforementioned problems by evading experimental bounds, and for the possibility of exploring many of these models in a short span of time as they can be investigated in existing experimental facilities. This thesis will focus on one of these mediators, the dark photon, that couples to the ordinary photon through kinetic mixing. Specifically, we consider the semi-visible dark photon models presented in [4], where the lightest particle in the dark sector can be regarded as a DM candidate. Expanding their discussion on searches for the dark photon at BaBar and NA64, in this work we analyze whether ProtoDUNE is sensitive to this model, following the idea in [5].

After a brief introduction to the standard model in Ch. 1 and an overview of DM in Ch. 2, we present a more general and in-depth analysis of a rich dark sector including all renormalizable portals in Ch. 3. Finally, we discuss the result of the current work in Ch. 4. We are particularly interested in the region of the parameter space that is compatible with a dark photon explanation of the anomalous muon magnetic moment $(g-2)_\mu$. Models that allow for the dark photon to decay semi-visibly are able to evade current constraints that exclude this region. Additionally, the lightest of the dark sector particles can constitute a dark matter candidate, allowing constraints coming from CMB and relic density. We see that ProtoDUNE can expand in some cases the current sensitivities for the dark photon mixing ε and masses $m_{A'}$, partially covering the newly open Δa_μ parameter space.

Chapter 1

The Standard Model and Beyond

The Standard Model of particle physics is a highly successful theoretical framework that describes particles' behaviour and interactions 1.1. It encompasses the electroweak theory, formulated by S. Weinberg [6] and A. Salam [7], building upon the model initially proposed by S.L. Glashow in 1961 [8]. Furthermore, it incorporates quantum chromodynamics [9–11], along with the Brout-Englert-Higgs (BEH) mechanism [12, 13], which imparts masses to matter and interaction fields. It has been extensively tested through various experiments over the past several decades, and its predictions have been found to be in agreement with experimental results. With the discovery of the Higgs boson at LHC [14, 15], the last missing experimental evidence of the Standard Model has been put into place, further proving the Standard Model to be the most accurate and reliable theory for describing the behaviour of the known subatomic particles and their interactions.

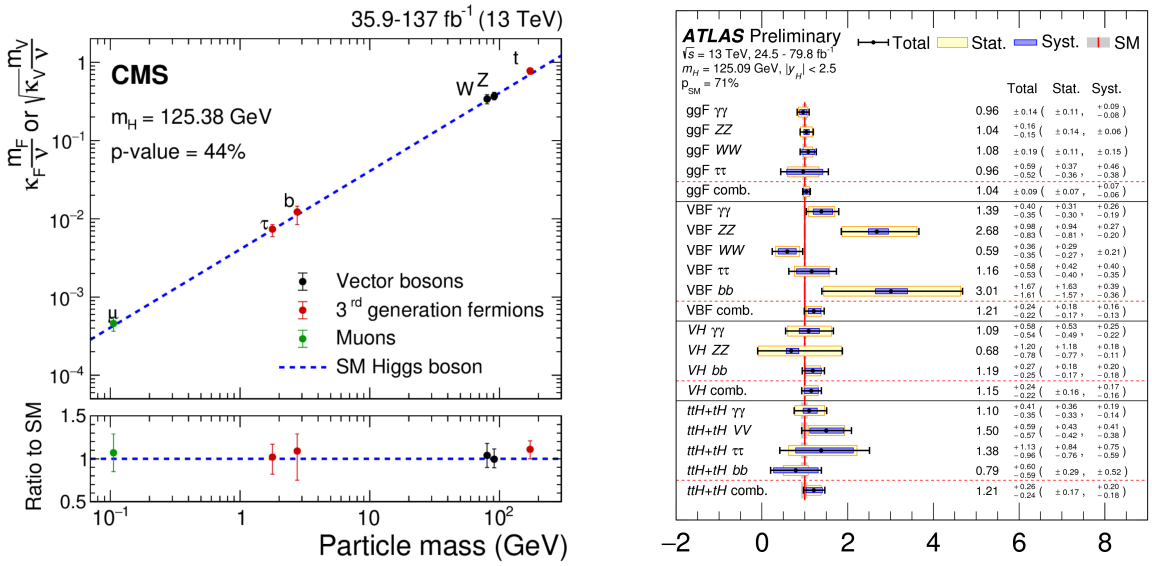

FIGURE 1.1: (Left) Best fit values of the Higgs boson couplings to the different particles as a function of particle mass for the CMS data [16]. (Right) Cross sections time branching fraction for the main Higgs production modes at the LHC (ggF, VBF, VH and ttH+tH) in each relevant decay mode ($\gamma\gamma$, WW, ZZ, $\tau\tau$, bb). All values are normalized to Standard Model predictions. Figure taken from [17]

.

Despite all of its success in explaining a wide range of experimental results, some questions remain unanswered and call for new physics Beyond the Standard Model, such as neutrino masses and oscillation, the baryon asymmetry of the universe (BAU) and Dark Matter (DM). However, it still constitutes the foundations upon which our quest for new physics must be built. For this reason, we start the present work by briefly introducing the theoretical framework of the Standard Model, focusing on the problem of Dark Matter.

1.1 The Standard Model of particle physics

The Standard Model is a renormalizable quantum field theory [18] described by the gauge group

$$G_{SM} = SU(3)_c \times SU(2)_L \times U(1)_Y, \tag{1.1}$$

that describes the fundamental interactions, with the exception of gravity. G_{SM} is a twelve-dimensional Lie group, with twelve different generators, each corresponding to a particle mediating a SM interaction. The generators of $SU(3)$ are the gluons responsible for the strong interaction, while the generators of $SU(2)_L \times U(1)_Y$ mediate the electroweak interaction. The theoretical formulation of the standard model relies on the same idea of Maxwell's equation, the *principle of gauge invariance*. Requiring that the Lagrangian is gauge invariant, forces us to introduce *covariant derivatives*, which leads to interactions between the gauge fields and the matter content of $\mathcal{L}_{SM}$.

In order to have a complete description of particle physics, we need two other ingredients: the **particle content** and the **scalar sector**. Fermions in the standard model are divided into three families or generations, as depicted in fig. 1.2. The three families all have the same quantum numbers as the particle in each family corresponds to the same irreducible representation of the gauge group. Table 1.1 summarizes the particle content and representations of all the fields of the model. Finally, a scalar sector is required, where a scalar field, the Higgs boson [12] behaves as a singlet under the SU(3) group, a doublet under SU(2) and has a hypercharge $Y = 1/2$. The Higgs boson is fundamental in the SM in order to break the $SU(2)_L \times U(1)_Y$ symmetry into $U(1)_{EM}$ and to give mass to the $W^{\pm}$ and Z bosons and to fermions [6, 7]. It was finally discovered in 2012, almost 50 years after being first proposed, when ATLAS and CMS collaborations announced the observation of a new boson with a mass of 125 GeV at 5 σ significance 1.3.

The standard model Lagrangian is constructed as follows:

$$\mathcal{L}_{SM} = \mathcal{L}_{gauge} + \mathcal{L}_{kin} + \mathcal{L}_{Higgs} + \mathcal{L}_{Yukawa},$$

where $\mathcal{L}_{kin}$ contains the kinetic terms of the fermions, $\mathcal{L}_{gauge}$ the gauge interactions, $\mathcal{L}_{Higgs}$ is the Higgs interactions and potential, and $\mathcal{L}_{Yukawa}$ the Yukawa couplings of the fermions.

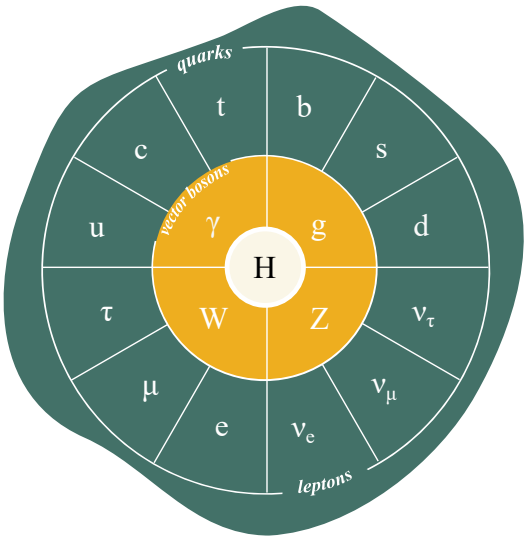

FIGURE 1.2: Particles in the standard model.

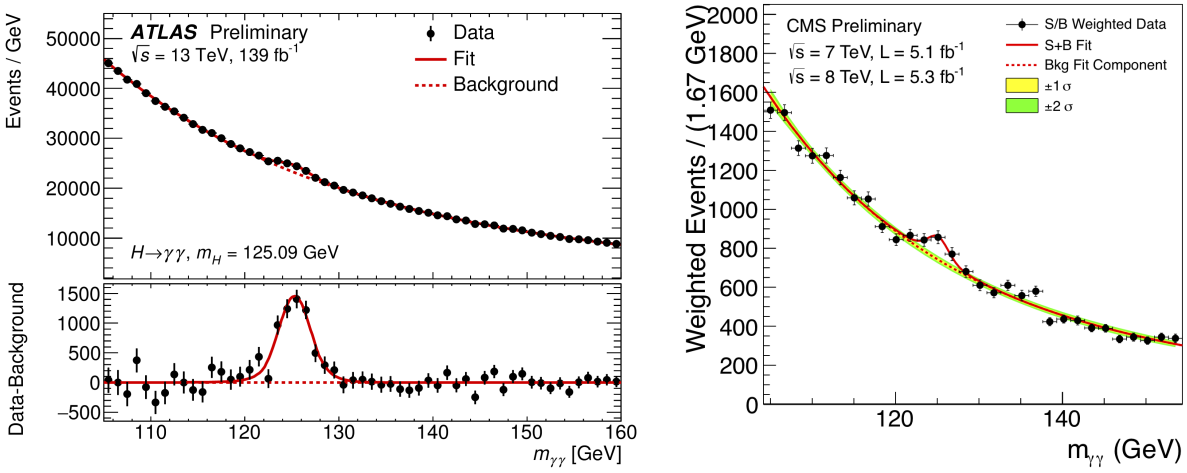

FIGURE 1.3: Distribution of the invariant mass of the two photons measured in the ATLAS and CMS experiment. Figures from [14, 15].

Gauge terms

The gauge invariant kinetic terms for the gauge bosons are:

$$\mathcal{L}_{gauge} = -\frac{1}{4}G^a_{\mu\nu}G^{\mu\nu}_a - \frac{1}{4}W^a_{\mu\nu}W^{\mu\nu}_a - \frac{1}{4}B_{\mu\nu}B^{\mu\nu},$$

where $F^a_{\mu\nu} = \partial_\mu F^a_\nu - \partial_\nu F^a_\mu - g_F f^{abc} F_{\mu,b} F_{\nu,c}$, g_F being the gauge coupling constant and f_{abc} the structure constant of the particular gauge group defined by the commutator

$$[t_a, t_b] = i f_{abc} t_c, \tag{1.2}$$

	Generations			G_{SM}		
	I	II	III	$SU(3)_c$	$SU(2)_L$	$U(1)_Y$
Quarks	$\begin{pmatrix} u \\ d \end{pmatrix}_L$	$\begin{pmatrix} c \\ s \end{pmatrix}_L$	$\begin{pmatrix} t \\ b \end{pmatrix}_L$	3	2	1/6
	u_R	c_R	t_R	3	1	2/3
	d_R	s_R	b_R	3	1	-1/3
Leptons	$\begin{pmatrix} e \\ \nu_e \end{pmatrix}_L$	$\begin{pmatrix} \mu \\ \nu_\mu \end{pmatrix}_L$	$\begin{pmatrix} \tau \\ \nu_\tau \end{pmatrix}_L$	1	2	-1/2
	e_R	μ_R	τ_R	1	1	-1
Higgs	H			1	2	1/2

TABLE 1.1: Quantum number for different representations of the gauge group for the fermions and the Higgs boson. Families are sorted in mass order, the third generation being the heavier one. The electric charge of the particle $Q = T_3 + Y$, where T_3 is the third component of the isospin and Y is the hypercharge.

where t_i are the generators of the group. In an Abelian group, the structure constant vanishes since all generators commute with each other. Therefore, the last term exclusively exists for non-Abelian groups, introducing the 3-point and 4-point interactions among the gauge bosons. On the other hand, the first two terms constitute the propagator of the gauge bosons.

Kinetic terms

The kinetic Lagrangian is responsible for the interactions between the gauge bosons and fermions ψ:

$$\mathcal{L}_{kin,\psi} = \sum \overline{\psi} i\gamma^\mu D_\mu \psi,$$

where the sum runs over all chiral fermions of the model.
The covariant derivative is $D_\mu = \partial_\mu - ig_S G^a_\mu \lambda_a - igW^a_\mu \sigma_a - ig'YB_\mu$, λ and σ being the generators of respectively $SU(3)_C$ and $SU(2)_L$, and Y the hypercharge of ψ. The $SU(3)_C$, $SU(2)_L$ and $U(1)_Y$ gauge coupling are respectively g_S, g and g'.

Scalar terms

Let's now briefly review the two last missing pieces in the picture. The Higgs field is a complex scalar field and a doublet under $SU(2)_L$, which can be represented as

$$H = \frac{1}{\sqrt{2}} \begin{pmatrix} G_1^+ + iG_2^+ \\ h^0 + iG_3^0 \end{pmatrix} = \frac{e^{iG_a\tau^a}}{\sqrt{2}} \begin{pmatrix} 0 \\ h \end{pmatrix}. \tag{1.3}$$

The Higgs Lagrangian reads

$$\mathcal{L}_{Higgs} = (D_\mu H)^\dagger (D^\mu H) - V(H), \quad \text{with} \quad V(H) = \mu^2 H^\dagger H + \lambda \left(H^\dagger H\right)^2. \tag{1.4}$$

In particular, μ^2 has mass dimension 2, and when it takes negative values H acquires a vacuum expectation value (*vev*) and breaks the electroweak group $SU(2)_L \times U(1)_Y \to U(1)_{EM}$. The vev of the field is $\langle H \rangle = \begin{pmatrix} 0 & v/\sqrt{2} \end{pmatrix}^T$, where $v^2 = -\mu^2/\lambda$. At this point, the lagrangian can be expanded around the true vacuum of the theory through the field redefinition $G_a \to G_a/v$ and $h \to h + v$. What arises is a mass term for the scalar field and its interactions with the gauge bosons, stemming from the covariant derivative. In accordance with the Goldstone theorem [19][20], which states that for each broken generator of the symmetry, there corresponds a massless field known as the Goldstone boson, we observe that $G_1, G_2,$ and G_3 are indeed massless, whereas h possess a mass term.

A very popular choice for fixing the gauge is the so-called *unitary gauge*, where the Goldstone bosons do not appear in the lagrangian. This is realized through a rotation such that:

$$H = \frac{1}{\sqrt{2}} \begin{pmatrix} 0 \\ h \end{pmatrix}. \tag{1.5}$$

The Goldstone bosons' degrees of freedom are "*eaten*" by the gauge bosons, that become massive. In conclusion, we get three massive and one massless vector bosons, defined as

$$W_\mu^\pm = \frac{1}{\sqrt{2}} \left(W_\mu^1 \mp i W_\mu^2 \right), \quad Z_\mu = c_W W_\mu^3 - s_W B_\mu, \quad A_\mu = c_W B_\mu + s_W W_\mu^3, \tag{1.6}$$

where we have defined $c_W(s_W) = g(g')/\sqrt{g^2 + g'^2}$ and $g = e/s_W, g' = e/c_W$. The value of the masses of the vector bosons are:

$$\begin{aligned} M_W &= \frac{gv}{2} \approx 80.387\text{GeV}, \\ M_Z &= \frac{v}{2}\sqrt{g^2 + g'^2} \approx 91.188\text{GeV}, \\ M_A &= 0. \end{aligned}$$

Yukawa terms

The EW sector is also responsible for the generation of fermion masses in the SM. All left-handed fermions are doublet under $SU(2)_L$, just like the Higgs. This allows us to write

$$\mathcal{L}_{Yukawa} = y^e_{\alpha\beta}(\overline{L}^\alpha H) e^\beta_R + y^u_{\alpha\beta}(\overline{Q}^\alpha_L \tilde{H}) u^\beta_R + y^d_{\alpha\beta}(\overline{Q}^\alpha_L H) d^\beta_R + \text{h.c.}, \tag{1.7}$$

where we have defined $\tilde{H} \equiv i\sigma_2 H^*$. $y^{e,u,d}_{\alpha\beta}$ are the Yukawa couplings. After SSB, these interaction terms give the charged leptons and quarks a Dirac mass term of the form

$$m_\psi \overline{\psi}\psi = m_\psi \left(\overline{\psi}_L \psi_R + \overline{\psi}_R \psi_L \right), \tag{1.8}$$

with $m_\psi = y_\psi v/\sqrt{2}$, where v is the vev of the scalar field, and $\psi_{L,R} = P_{L,R}\psi = \frac{1\pm\gamma^5}{2}\psi$.

The one just described is the Yukawa Lagrangian for the first family of fermions. The complete Lagrangian is obtained by promoting $y^\psi \to Y^\psi$, a 3×3 matrix. In the quark sector, the Yukawa matrix is off-diagonal and the different generations mix. The Yukawa matrices can be diagonalized by

$$Y^\psi = U_a^\psi Y_{diag}^\psi U_R^{\psi\dagger}. \tag{1.9}$$

The physical quark masses are found after rotating the up and down quarks through the Cabibbo-Kobayashi-Maskawa (CKM) matrix [21, 22]

$$U_{CKM} = U_L^{u\dagger} U_L^d. \tag{1.10}$$

The CKM matrix has 4 free parameters: three angles and a complex phase that allows for CP violation in the quark sector. It can be parametrized as

$$U_{CKM} = \begin{pmatrix} 1 & 0 & 0 \\ 0 & c_{23} & -s_{23} \\ 0 & s_{23} & c_{23} \end{pmatrix} \begin{pmatrix} c_{13} & 0 & -e^{-i\delta}s_{13} \\ 0 & 1 & 0 \\ e^{i\delta}s_{13} & 0 & c_{13} \end{pmatrix} \begin{pmatrix} c_{12} & -s_{12} & 0 \\ s_{12} & c_{12} & 0 \\ 0 & 0 & 1 \end{pmatrix}. \tag{1.11}$$

The angles and the phase of the CKM matrix are found to be:

$$\theta_{12} \approx 13^\circ, \quad \theta_{23} \approx 2^\circ, \quad \theta_{13} \approx 0.2^\circ \tag{1.12}$$

and

$$\delta \approx 70^\circ. \tag{1.13}$$

The CKM matrix is nearly diagonal, so the mixing between the quark and flavour mass eigenstates is small.

This concludes our review of the Standard Model of particle physics. Over the years, the SM has demonstrated its impressive accuracy, successfully aligning with experimental data from numerous collider experiments. However, as we previously hinted, certain theoretical and experimental inconsistencies require new physics beyond the standard model. In the following section, we will delve into these matters, providing a concise explanation of why the SM falls short in addressing these facts. Additionally, we will explore some ideas proposed to resolve these issues.

1.2 Open questions in the Standard Model

While the mass generation mechanism in the Standard Model is elegant in its simplicity, there are certain aspects that raise questions and challenge its completeness. There is no theoretical

explanation as to why the Yukawa couplings (and hence the masses) have those specific values. Indeed, the SM has 19 free parameters in the Lagrangian, that must be determined through experimental measurements. Although this may not be considered a fundamental flaw, the sheer abundance of free parameters hints at a deeper underlying structure yet to be uncovered. This conundrum is commonly referred to as the "flavour puzzle." The flavour puzzle becomes more pronounced when we consider the existence of neutrino masses and the significant difference between leptonic mixing and the one in the quark sector. This raises the second problem of the mass generation in the SM, which is that it does not predict a mass term for neutrinos due to the absence of ν_R.

It is already quite evident that the Standard Model is not sufficient to explain fully fundamental particles and their interactions. Furthermore, the SM is not the final theory, since it does not explain gravity.

In this section, we will outline the main limitations of the Standard Model and examine the areas where it fails to provide an explanation for observed phenomena. In particular, we will focus on the issue of dark matter, which we will discuss in more detail later.

The hierarchy problem. The SM must be treated as an effective field theory (EFT) valid up to the Planck mass $M_{Pl} \approx 10^{19} GeV$, where the effects of gravity are expected to not be negligible anymore. If there is no physics all the way up the Planck scale, then the cutoff would be $\Lambda = M_{Pl}$. This constitutes a problem when we consider quantum corrections to the Higgs mass, $m_h^2 = m_{bare}^2 + \delta m_h^2$, where $\delta m_h^2 = y_t^2 \Lambda^2 / 8\pi^2$. The presence of quantum corrections implies that the Higgs mass receives contributions proportional to the cutoff scale, potentially leading to a significant discrepancy between the observed Higgs mass and its bare value. This mismatch necessitates an explanation and fine-tuning of parameters to maintain the observed Higgs mass within the expected range. Supersymmetric theories have been proposed as potential solutions to address these issues. However, the lack of compelling evidence in support of these theories necessitates ongoing exploration and search for alternative solutions. A very comprehensive and in-depth analysis on the hierarchy problem by C. Csáki et al, can be found in [23].

Neutrino masses. One of the most compelling experimental pieces of evidence revealing the incompleteness of the Standard Model is the phenomenon of neutrino oscillation, first observed in 1998 by the atmospheric neutrino experiment Super-Kamikande [24]. Neutrino oscillation implies that neutrinos have a non-zero mass, in contradiction with the SM prediction of massless neutrinos. This observation highlights the necessity for extensions to the SM that can account for small neutrino masses and explain the phenomenon of neutrino oscillations.
Exploring the nature of neutrino mass gives rise to a multitude of questions, that any new physics beyond the Standard Model (BSM) must address. Primarily, some mechanism is required to generate neutrino masses. Type I seesaw is a commonly cited example, which introduces new heavy

degrees of freedom to explain the smallness of neutrino masses. Another fundamental question regards the nature of neutrinos themselves — whether they are Dirac particles or Majorana particles. Ongoing experiments investigating neutrinoless double beta decay ($0\nu2\beta$), first proposed by W.H. Furry in 1939 to test the nature of neutrinos [25], are actively seeking answers to this question [26–29].

Matter-Antimatter asymmetry. The baryon asymmetry of the Universe (BAU) we observe has no clear origin in the Early Universe, where matter and antimatter were created in equal amounts. This asymmetry is commonly quantified using the parameter $\eta_B = (n_B - n_{\overline{B}})/n_\gamma$, where the difference between the number density of baryons and antibaryons is divided by the number density of photons. Experimental measurements indicate that this parameter is extremely small, approximately $\eta_B \approx 10^{-10}$, as measured by WMAP[30]. The ingredients required to generate the observed baryon asymmetry are Sakharov's conditions, namely: (i) baryon number violation; (ii) C-symmetry and CP-symmetry violation; (iii) departure from thermal equilibrium [31]. The SM alone does not possess sufficient sources of CP violation to account for the observed baryon asymmetry. To address this issue, alternative scenarios have been proposed, such as EW baryogenesis and leptogenesis [32]. Leptogenesis is particularly relevant to neutrino physics, as it relies on CP violation in the lepton sector. In this scenario, CP violation in the decay of heavy right-handed neutrinos generates a lepton asymmetry. This asymmetry is then converted into a baryon asymmetry through non-perturbative processes known as *sphaleron processes*[33], which violate the total B + L number.

Dark Matter. Numerous pieces of evidence support the existence of dark matter, which constitutes approximately 25% of our universe, with dark energy comprising around 70% and ordinary matter accounting for a mere 5%. The nature of dark matter remains one of the most intriguing mysteries in our understanding of the universe. While Modified Newtonian Dynamics (MOND) theories can explain certain local astrophysical observations, they struggle in providing a consistent and comprehensive explanation for a broad range of cosmological phenomena and observations [34]. Another hypothesis that has been considered is the presence of primordial black holes as a potential explanation for dark matter [35]. However, the most widely accepted and extensively studied hypothesis suggests that dark matter consists of particles. Dark matter particles are expected to be electrically neutral to explain their elusiveness in detection. Additionally, they should possess long lifetimes to account for the substantial amount of dark matter still present in the universe today.

In the following section, we will delve into the specific characteristics that dark matter particles must possess. We will also review the current state of knowledge in this field, referring to comprehensive reviews [36–38] that summarize crucial aspects, such as the evidence for dark matter, potential candidates, and detection methods.

Chapter 2

A Dark Universe

Dark matter, inferred from astrophysical observations and gravitational effects, poses one of the most intriguing puzzles in current physics. Our efforts to understand its fundamental nature, whether it is a particle, its interactions with standard model particles, and its cosmological origin, have prompted extensive research. In this chapter, we provide an in-depth review of dark matter, drawing upon previous reviews[36–38]. In Section 2.1, we summarize the existing evidence supporting the existence of dark matter. We then delve into its astrophysical properties, including its distribution within galaxies. In Section 2.2, we explore various dark matter candidates, including some non-particle explanations such as primordial black holes and MACHOs (Massive Compact Halo Objects). A detailed discussion of thermal dark matter follows in 2.2.1, where we review the computations for the relic abundance and we motivate Weakly Interacting Massive Particles. Finally, we conclude by reviewing current and ongoing searches for Weakly Interacting Massive Particles (WIMPs) in 2.3.

2.1 Evidence and candidate for Dark Matter

Ninety years ago, Fritz Zwicky published a groundbreaking paper that showed that the galaxies in the Coma Cluster were moving too fast to be bound together by the visible matter of its galaxies [1]. He observed that the average density in the Coma Cluster would have to be at least 400 times larger than that derived from the observation of luminous matter. *If this should be verified*, he claimed, *it would lead to the surprising result that dark matter exists in much greater density than luminous matter.* However, the very first persuasive evidence supporting the existence of dark matter, only arrived in the 1970s, when Vera Rubin studied the rotation curves of spiral galaxies [2].

From Newtonian gravity, we know that $v_c(r) = \sqrt{GM/r}$, where v_c is the circular velocity. For distances that extend beyond the galactic disk, M should remain constant assuming that all the mass is concentrated in the disk. Therefore, we would expect to see $v_c \propto r^{-1/2}$. Instead, observations reveal that the velocity flattens at large distances, as shown in 2.1, implying that $M(r) \propto r$. This suggests that there must be an additional "dark" component to the galaxy's matter distribution.

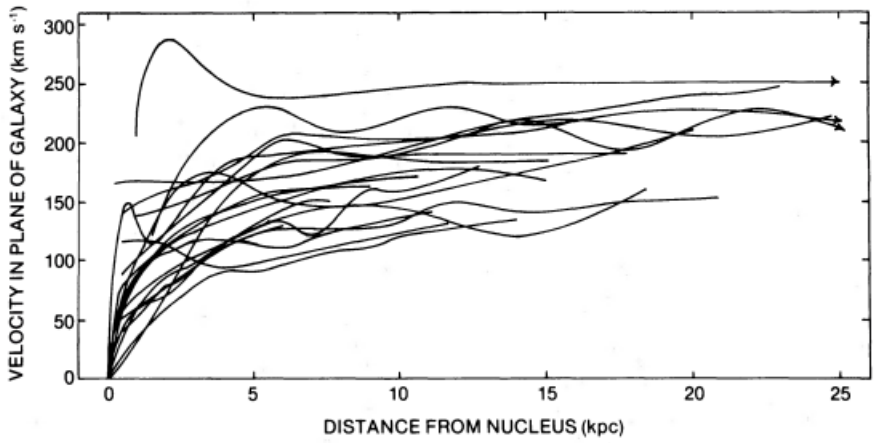

FIGURE 2.1: Rotational curves of spiral galaxies as measured in the original paper by V. Rubin et al in 1980 [39]. Most galaxies show a flattering in of the circular velocity at large radial distances.

Since then, the presence of dark matter has been observed in several ways. Gravitational lensing, namely the bending of light around massive objects, suggests the presence of unseen matter. This effect has been observed in cases like the Bullet Cluster [3]. A spatial separation is identified by comparing the mass distribution deduced from gravitational lensing with the distribution of visible matter detected via X-rays, indicating a nearly collisionless dark matter abundance.

Additionally, the cosmic microwave background (CMB) radiation, the afterglow of the Big Bang, provides strong evidence for the existence of dark matter. The observed patterns in the CMB radiation are consistent with the presence of large amounts of non-interacting matter. The latest results were published by the Planck collaboration in 2018 [40], where it has been inferred that the DM density today is

$$\Omega_{DM}h^2 = 0.120 \pm 0.001, \tag{2.1}$$

with $\Omega_{DM} = \rho_{DM}/\rho_c$ the energy density of DM in units of the critical density $\rho_c \approx 10^{-26} kg/m^3$, and $h = H_0/(100 kms^{-1}/Mpc) = 0.674 \pm 0.005$ the scaled Hubble expansion rate. This is around five times larger than the density of baryons, defined as all other non-relativistic matter. The density of baryons has also been measured through the relative abundances of light elements during Big Bang Nucleosynthesis (BBN) [41], where DM plays no role, and provides further evidence for the non-baryonic nature of DM. Many experiments have attempted to directly detect dark matter particles but no definitive detection has yet been made. While there is clear evidence for the existence of DM, its particle-physics identity still remains unknown. Over time, a plethora of candidates for DM has emerged, and in the next section we will delve into some of the most prominent contenders.

2.1.1 Astrophysical distribution

We saw in the previous section, that in order to account for the observed rotational velocity, $M(r) \propto r$. This means that the DM mass density distribution is

$$\rho(r) \propto \frac{M(r)}{r^3} \sim \frac{1}{r^2}, \tag{2.2}$$

where it was assumed that DM is distributed in a spherically symmetric halo around the centre of the Galaxy. This is quite different from baryons, that being able to strongly interact amongst themselves, dissipate energy and collapse into a disk. Since DM doesn't interact, it forms spherical halos. A very rough estimate done in [37] can give an idea of the size of the DM halo:

$$R_{halo} \sim 100\text{kpc} \tag{2.3}$$

and average velocity of the DM in the halo, obtained using the virial theorem, of:

$$\langle v \rangle \sim \sqrt{\frac{GM_{halo}}{R_{halo}}} \sim 200\text{km/s}. \tag{2.4}$$

From this rapid calculation, we can already deduce that DM exhibits non-relativistic behaviour, a crucial characteristic with significant implications for predicting observational signatures. To obtain a more accurate estimation of DM velocity, we can employ the Boltzmann equation and the Jeans Theorem.

The Boltzmann equation describes the evolution of the phase-space density $f(x, v)$ of DM in the halo:

$$\mathbf{L}[f] = \mathbf{C}[f], \tag{2.5}$$

where $\mathbf{L}$ is the Liouville operator and $\mathbf{C}$ is the collision operator. The most general form of $\mathbf{L}$ is

$$\mathbf{L}[f] = p^\alpha \frac{\partial f}{\partial x^\alpha} - \Gamma^\alpha_{\beta\gamma} p^\beta p^\gamma \frac{\partial f}{\partial p^\alpha}, \tag{2.6}$$

that in the non-relativistic limit simplifies to

$$\mathbf{L}_{nr}[f] = \frac{\partial f}{\partial t} + \dot{x}\frac{\partial f}{\partial x} + \dot{v}\frac{\partial f}{\partial v}. \tag{2.7}$$

The operator $\mathbf{C}[f]$ includes interactions between DM and other particles. Since a good approximation for dark matter is that it is collisionless, it is possible to simplify the Boltzmann equation as follows:

$$\mathbf{L}_{nr}[f] = \frac{\partial f}{\partial t} + \dot{x}\frac{\partial f}{\partial x} + \dot{v}\frac{\partial f}{\partial v} = 0. \tag{2.8}$$

Before introducing Jeans Theorem, we define as **integral of motion** $I(x, v)$ a function of the phase-space coordinates alone that is constant along an orbit, namely:

$$I[x(t_1), v(t_1)] = I[x(t_2), v(t_2)]. \tag{2.9}$$

This implies that a function of the phase-space coordinates is an integral if and only if:

$$\frac{d}{dt} I[x(t), v(t)] = 0 \tag{2.10}$$

along any orbit. Jeans Theorem states that any steady-state solution of the collisionless Boltzmann equation depends on the phase-space coordinates only through integrals of motion in the given potential, and any function of the integrals yields a steady-state solution of the collisionless Boltzmann equation. The Hamiltonian is an integral of motion. In this case, Jeans Theorem implies that the phase-space distribution is a function of the only energy E:

$$f(x, v) = f(E), \qquad E = \Psi - \frac{1}{2} v^2, \tag{2.11}$$

where Ψ is the gravitational potential.

For an isotropic halo in steady-state with $f(E) \propto e^E$, we have

$$\rho \propto \int_0^\infty dv v^2 f(v) = \int_0^\infty dv v^2 e^{\frac{\Psi - v^2/2}{\sigma^2}} \propto e^{\Psi/\sigma^2}, \tag{2.12}$$

with σ being the velocity dispersion. Using Poisson's equation $\nabla^2 \Psi = -4\pi G\rho$, we can find the radial dependence of the density distribution:

$$\rho(r) = \frac{\sigma^2}{2\pi G r^2}. \tag{2.13}$$

The phase-space distribution for a spherical isotropic halo in steady-state can be modelled by:

$$\rho(r) \propto 1/r^2, \qquad f(v) \propto e^{-v^2/\sigma^2}, \tag{2.14}$$

which is exactly what we found before by looking at the rotation curves of galaxies. However, while this is a good approximation, it is not entirely accurate, as it leads to an infinitely massive halo due to the proportionality of mass ($M(r) \propto r$) at large distances. Moreover, the dynamics of dark matter can be further influenced by galaxy mergers, rendering the steady-state assumption inadequate. Consequently, numerical simulations are essential to more precisely model the density distribution of dark matter halos. The Navarro-Frenk-White (NFW) profile or Einasto profile appears to offer improved descriptions of the density distribution: their profiles approach zero with increasing distance from the galaxy's center, thus avoiding the issue of predicting infinitely

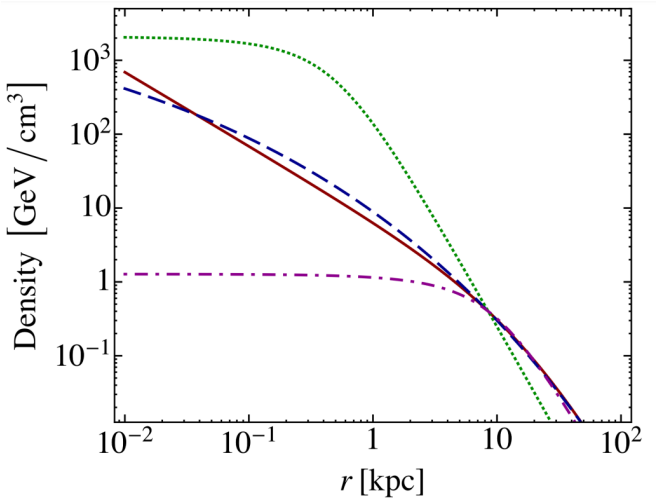

FIGURE 2.2: The NFW [solid red], Einasto [dashed blue], and Burkert with r_s = 0.5 [green dotted] and 10 kpc [purple dot-dashed] profiles as a function of the distance from the Galactic Centre. Figure from [44].

massive halos.

$$\rho_{NFW}(r) = \frac{\rho_0}{r/r_s(1+r/r_s)^2}, \tag{2.15}$$

with $r_s = 20kpc$ is the scale radius. The Einasto profile takes the form:

$$\rho_{Ein}(r) = \rho_0 \exp\left[-\frac{2}{\gamma}\left(\left(\frac{2}{2_s}\right)^{\gamma} - 1\right)\right], \tag{2.16}$$

where $\gamma = 0.17$. Both NFW and Einasto profiles are described as "cuspy" because of their steeper inner slopes. The Burkert profile has a flatter slope:

$$\rho_{Burk}(r) = \frac{\rho_0}{(1+r/r_s)(1+(r/r_s)^2)}. \tag{2.17}$$

N-body simulations provide evidence for substructure in the dark matter (DM) phase-space distribution [42, 43]. These structures arise from minor mergers between the Milky Way and other galaxies. When a DM subhalo falls into orbit around the Milky Way, tidal effects strip DM (and possibly stars) along its path, creating "debris" that eventually becomes part of the Milky Way's halo. However, some of this debris may not have reached equilibrium at any given time and can exhibit unique features that affect observations. Examples of substructure include **clumps**, which lead to localized DM overdensities, and **streams**, where debris is left behind along the orbits of infalling sub-halos.

2.2 Overview of Dark Matter candidates

Although the nature of DM is still unknown, astrophysical and cosmological observations can give us some clues about its identity and the characteristics that a DM candidate should have.

- **Neutral**. The possibility of DM being charged was first introduced in [45]. However, if dark matter (DM) possesses an electric charge or is "milli-charged," meaning it has a small electric charge, it could interact with the baryon-photon plasma during the cosmic recombination era. This interaction might influence the behaviour of DM density fluctuations. The presence of charged DM could lead to effects such as radiation pressure and photon diffusion, which could further modify the characteristic structure of the baryon acoustic peak. In [46], the requirement that DM must be entirely decoupled from the baryon-photon plasma during recombination leads to a maximum limit on the "milli-electric" charge of dark matter, expressed in units of the electron charge, of 3.5×10^{-7} for $m_{DM} > 1$ GeV, and of 4.0×10^{-7} for $m_{DM} < 1$ GeV.

- **Cold (non-relativistic)**. If DM was relativistic, it would tend to disperse structures like galaxies. If it were the dominant component of the DM, the observed structures would look significantly different, and the anisotropies in the cosmic microwave background (CMB) would be more prominent. Consequently, hot dark matter can only account for a small fraction of the total DM content. Under the assumption of the ΛCDM model, all dark matter is considered to be cold.

- **Stable or very long lived** In the case of decaying DM, its lifetime must be long compared to cosmological timescales [47].

- **Consistent with BBN**. Light elements were formed during BBN, and their primordial abundance depends on the total energy density through the expansion rate, which puts a constraint on the energy density in dark sector particles at the time of BBN [48].

- **Collisionless** Self-interacting dark matter is severely constrained, e.g. by observations of merging clusters [49]. The relevant parameter in this case is the ratio of DM-DM cross section and the DM mass, σ_{DM-DM}/m_{DM}. This value has been bound to be smaller than 0.84 barn/GeV at 95% C.L.[50]. However, certain theories try to go beyond the collisionless paradigm, as self-interactions could be useful to explain small-scale structure observations that are in tension with collisionless cold DM predictions [51].

Finally, of course, it should account for the observed abundance and be compatible with exclusion limits set by DM search experiments [52].

Certain model-independent statements can be made about the mass range of dark matter by considering the formation of DM halos. The lower limit of allowed masses is determined by the

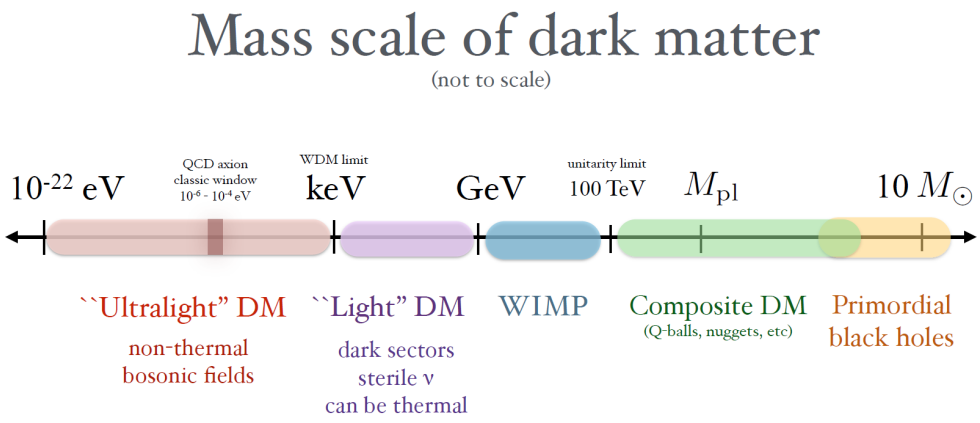

FIGURE 2.3: Mass range of allowed DM candidates, from particles to primordial black holes (figure by T. Lin in [38]).

number of particles that can be confined within a given cell of phase space, which, in turn, is governed by the particle's spin statistics. For instance, if DM is composed of ultra-light scalar particles, Bose-Einstein statistics dictate that an unlimited number of particles can occupy the same point in phase space. This implies that a classical field treatment can be applied and the stability of the halo is set by the uncertainty principle $\Delta x \Delta p \sim 1$, where $\Delta p \sim m_\chi v$ and $\Delta x \sim 2R_{halo}$. Dwarf galaxies set the tightest boundaries, with $R_{halo} \sim 1$ kpc and $v \sim 100 km/s$, giving the lower bound:

$$m_{scalar} \gtrsim 10^{-22} \text{ eV}. \tag{2.18}$$

Ultra-light scalar DM particles near the bottom of this bound are referred to as 'fuzzy' dark matter [53].
In the case of fermions, the Pauli exclusion principle applies [54]. This means:

$$M_{halo} = m_{ferm} V \int f(p) d^3p \lesssim m_{ferm} V \int d^3p \sim m_{ferm} R_{halo}^3 (m_{ferm} v)^3. \tag{2.19}$$

The inequality arises from the fact that each unit volume of phase space can have no more than one fermionic particle, on average. Substituting in v the virial velocity gives:

$$m_{ferm} \gtrsim (G^3 M_{halo} R_{halo}^3)^{-1/8} \gtrsim O(10) \text{eV}. \tag{2.20}$$

The upper bounds come from gravitational lensing. The lack of lensing events excludes MACHOs with masses between 10^{57-67} eV. In figure 2.3, a concise overview of potential candidates for dark matter is presented. Before delving into the specifics of the particle nature of dark matter, let's first discuss the heaviest possible candidates for dark matter.

Primordial black holes

Primordial black holes could have been formed in the early Universe, for instance in the era of radiation domination due to the gravitational collapse of large curvature perturbations generated during inflation. Constraints on PBHs as dark matter candidates come from CMB observations, gravitational lensing and evaporation. For instance, in the early Universe, massive PBHs can accrete matter, resulting in the emission of ionizing radiation that is strongly constrained by CMB observations. PBHs with masses up to $10^{-17}M_{\odot}$ evaporate enough that they are not sufficiently dark, and are therefore not good DM candidates. Between $10^{-17}M_{\odot}$ and 50 $M_{\odot}$, gravitational lensing constraints the fraction of DM that could be made of PBHs to 10%. There remains still an open window for PBHs to make up for all the observed abundance of dark matter in the region between $10^{-16}M_{\odot}$ - $10^{-11}M_{\odot}$ [55, 56].

MACHOs

MACHOs are massive astrophysical compact halo objects. For masses above the Planck mass, DM could be a composite object, such as bound states or nuggets of lighter fundamental particles [57]. Boson stars could also be a viable candidate in this mass range [58]. Another possibility is that of *Q-balls*, non-topological solitons that carry a conserved charge which guarantees stability [59].
Now, let's shift our focus to the particle candidates for dark matter.

2.2.1 Thermal DM

The most largely explored and studied region of DM masses is the one going from keV to $\sim$ 100 TeV, which includes thermal candidates and WIMPs. With thermal DM we refer to DM that was in thermal equilibrium with the rest of SM in the early Universe. This possibility is particularly appealing as it implies some interaction between dark matter and the rest of the standard model particles, leading to a variety of testable signatures. The keV mass scale "separates" thermally produced dark matter from non-thermally produced bosonic DM. We saw already that fermion DM candidate must have mass greater than $O(keV)$ to be consistent with observations of galaxies. Additionally, dark matter that is thermally produced from the SM bath must have mass greater then $O(keV)$ to be consistent with observations of large scale structure. On the opposite end of the spectrum, dark matter particles with masses exceeding $\sim$ 100 TeV encounter significant issues as unitarity would be violated [60]. In this range, a further distinction can be made:

- *10 GeV - 100 TeV*: weakly interactive massive particles (WIMPs).
- *keV - 10 GeV*: this range corresponds to the so-called "light DM". Thermal candidates here are typically embedded in dark sector models, which will be discussed later.

Within these masses, other interesting scenarios are those of DM candidates that were never in thermal equilibrium, such as sterile neutrinos, and freeze-in DM.

We now review the computations for the DM relic density. In the early Universe, when the interaction $\chi\chi \leftrightarrow XX$ is in equilibrium, the DM particles are produced and annihilated at the same rate. As the universe expands, the chances for a dark matter particle to encounter another particle for annihilation decrease. Eventually, the forward reaction of annihilation becomes less frequent until it shuts off completely. At this stage, the DM density remains unchanged, effectively "frozen" in time. This process, known as "freeze-out," takes place when the annihilation rate Γ becomes comparable to the Hubble rate H:

$$\Gamma = n_\chi \langle \sigma v \rangle \sim H, \tag{2.21}$$

where n_χ is the DM number density while $\langle \sigma v \rangle$ is the velocity-averaged cross section. Cold DM is non-relativistic at freeze-out, meaning $n_\chi \sim T^{3/2} e^{-m_\chi/T}$, T being the temperature of the DM species.

In order to compute the DM number density today, we start from the Boltzmann equation previously introduced:

$$\mathbf{L}[f] = \mathbf{C}[f], \tag{2.22}$$

The Liouville operator can be written in the form

$$\mathbf{L}[f] = E\frac{\partial f}{\partial t} - \frac{\dot{a}}{a}|p|^2 \frac{\partial f}{\partial E}, \tag{2.23}$$

where a is the scale factor that parametrizes the expansion of the Universe. The number density of a given particle is related to its phase-space density $f(E,t)$ through

$$n = g \int f(E,t) \frac{d^3p}{(2\pi)^3}, \tag{2.24}$$

with g the number of spin degrees of freedom of the particle. If we integrate the Liouville operator we find:

$$g \int \mathbf{L}[f] \frac{d^3p}{(2\pi)^3} = \frac{1}{a^3}\frac{d}{dt}(na^3) = \frac{dn}{dt} + 3Hn, \tag{2.25}$$

where $H = \dot{a}/a$ is the expansion rate of the Universe.
The collision term for particle 1 in the interaction $1 + 2 \leftrightarrow 3 + 4$ is [61]:

$$g_1 \int \mathbf{C}[f] \frac{d^3p_1}{(2\pi)^3} = -\sum_{spins} \int \left[f_1 f_2 (1 \pm f_3)(1 \pm f_4) |\mathcal{M}_{12\to34}|^2 - f_3 f_4 (1 \pm f_1)(1 \pm f_2) |\mathcal{M}_{34\to12}|^2 \right] \times (2\pi)^4 \delta^4(p_1 + p_2 - p_3 - p_4) d\Pi_1 d\Pi_2 d\Pi_3 d\Pi_4, \tag{2.26}$$

where g_i and f_i are respectively the spin degrees of freedom and phase-space densities for the particle i, $\mathcal{M}_{x\to y}$ is the matrix element for the reaction $x \to y$. The terms $(1 \pm f)$ represent Pauli blocking and Bose enhancement. The minus sign applies to fermions while the + sign to bosons, meaning that it is easier (harder) for a boson (fermion) to transition to a state that already contains a boson (fermion). The last line contains the delta function that forces the energy and momentum conservation. The phase space integration factors are:

$$d\Pi_i = \frac{d^3p_i}{(2\pi)^3 2E_i}. \tag{2.27}$$

Under some assumptions it is possible to simplify the form of 2.26:

1. *T (or CP) invariance*: this implies that $|\mathcal{M}_{12\to34}|^2 = |\mathcal{M}_{34\to12}|^2$.
2. *Maxwell-Boltzmann statistics*: the second simplification is to use the Maxwell-Boltzmann statistics for all species instead of the Fermi-Dirac for fermions and Bose-Einstein for bosons. In this case $(1 \pm f) \sim 1$.
3. *Kinetic equilibrium*: for all species in kinetic equilibrium $f_i(E_i) = e^{-\frac{E_i - \mu_i}{T}}$.

Using these approximations, we get:

$$\frac{dn}{dt} + 3Hn = \int (2\pi)^4 \delta^4(p_1 + p_2 - p_3 - p_4) d\Pi_1 d\Pi_2 d\Pi_3 d\Pi_4 |\mathcal{M}|^2 (f_3 f_4 - f_1 f_2). \tag{2.28}$$

Using the kinetic equilibrium approximation,

$$(f_3 f_4 - f_1 f_2) \sim \left(e^{\frac{\mu_4 - E_4}{T}} e^{\frac{\mu_3 - E_3}{T}} - e^{\frac{\mu_1 - E_1}{T}} e^{\frac{\mu_2 - E_2}{T}} \right) = e^{-\frac{E_1 + E_2}{T}} \left(e^{\frac{\mu_3 + \mu_4}{T}} - e^{\frac{\mu_1 + \mu_2}{T}} \right), \tag{2.29}$$

where in the second equality we have used the conservation of energy. In the interaction $\chi\chi \leftrightarrow XX$, we can assume X to have thermal distributions with zero chemical potential. SM particles will usually have additional interactions than DM, so the assumption of equilibrium for the X's is almost always a good one. We can write $f_3 = exp(-E_3/T)$ and $f_4 = exp(-E_4/T)$. For conservation of energy:

$$f_3 f_4 = exp[-(E_3 + E_4)/T] = exp[-(E_1 + E_2)/T] = f_1^{eq} f_2^{eq}. \tag{2.30}$$

It follows that:

$$(f_1 f_2 - f_3 f_4) = (f_1 f_2 - f_1^{eq} f_2^{eq}). \tag{2.31}$$

With all the relations just found, we can finally write:

$$\frac{dn_\chi}{dt} + 3Hn_\chi = -\langle \sigma_{\chi\chi \to XX} v \rangle \left[n_\chi^2 - (n_\chi^{eq})^2 \right]. \tag{2.32}$$

It is useful to scale out this effect by defining $Y \equiv n/s$, with s the total entropy of the Universe. We find:

$$\frac{dY}{dt} = \langle \sigma v \rangle s \left(Y_{eq}^2 - Y^2 \right) \implies \frac{dY}{dx} = \frac{s\langle \sigma v \rangle}{xH(m)} \left(Y_{eq}^2 - Y^2 \right), \tag{2.33}$$

where in the equation on the right we have defined $x = m/T$, m being the mass of the DM candidate.

We have found an expression that describes the evolution of Y as the Universe cools. Y is the DM number density, rescaled to remove the effects of the Universe's expansion. This means that changes in Y arise purely from interactions of the DM with states that are in thermal equilibrium with the photon bath. The evolution of Y is governed by the velocity-averaged cross section:

$$\langle \sigma v \rangle = \frac{\int \sigma v dn_1^{eq} dn_2^{eq}}{\int dn_1^{eq} dn_2^{eq}} = \frac{\int \sigma v e^{E_1/T} e^{E_2/T} d^3p_1 d^3p_2}{\int e^{E_1/T} e^{E_2/T} d^3p_1 d^3p_2}. \tag{2.34}$$

By redefining the integration variables and using the K_i modified Bessel functions:

$$\langle \sigma v \rangle = \frac{1}{9m^4 T K_2^2(m/T)} \int_{4m^2}^{\infty} \sigma(\tilde{s} - 4m^2) \sqrt{\tilde{s}} K_1(\sqrt{\tilde{s}/T}) ds \xrightarrow{non-rel} b_0 + 6b_1 x^{-1} + \ldots \tag{2.35}$$

with $\tilde{s} = 2m^2 + 2E_1E_2 - 2\boldsymbol{p_1 p_2}$. The case in which b_0 dominates is called s-wave annihilation, while when b_1 dominates is called p-wave annihilation.

This leads to the final equation in terms of the variable $\Delta = Y - Y^{eq}$:

$$\Delta' = -Y'^{eq} - f(x)\Delta(2Y^{eq} + \Delta), \tag{2.36}$$

where ' denotes d/dx and

$$f(x) = \sqrt{\frac{\pi g_*}{45}} m M_{Pl} (b_0 + 6b_1/x) x^{-2}. \tag{2.37}$$

Let's now introduce the quantity $x_F \equiv m/T_F$, where T_F is the temperature at the time of freeze-out. Equation 2.36 can be solved analytically in the two extreme regions $x \ll x_F$ and $x \gg x_F$, respectively long before freeze-out and long after freeze-out:

$$\Delta = -\frac{Y^{eq'}}{2f(x)Y^{eq}} \text{ for } x \ll x_F, \tag{2.38}$$

$$\Delta' = -f(x)\Delta^2 \text{ for } x \ll x_F. \tag{2.39}$$

Integrating 2.39 between x_F and ∞, and using $\Delta_{x_F} \gg \Delta_\infty$, we can derive the value of Δ_∞ and find:

$$Y_\infty^{-1} = \sqrt{\frac{\pi g_*}{45}} m M_{Pl} x_F^{-1}(b_0 + 3b_1/x_F). \tag{2.40}$$

The density of a generic relic χ today is given by $\rho_\chi = m_\chi n_\chi = m_\chi s_0 Y_\infty$, where $s_0 \sim 3\times10^3\ cm^{-3}$ is the entropy today. The relic density can finally be expressed in terms of the critical density

$$\Omega_X h^2 \approx \frac{1.07\times10^9 GeV^{-1}}{M_{Pl}} \frac{x_F}{\sqrt{g_*}} \frac{1}{b_0 + 3b_1/x_F}, \tag{2.41}$$

where b_0 and b_1 are expressed in GeV^{-2} and g_* is that at the freeze-out temperature. The freeze-out temperature x_F can be estimated iteratively with [36]

$$x_F = ln\left[c(c+2)\sqrt{\frac{45}{8}}\frac{g}{2\pi^3}\frac{mM_{Pl}(b_0 + 6b_1/x_F)}{g_*^{1/2}x_F^{1/2}}\right], \tag{2.42}$$

where c is a constant of $O(1)$ determined by matching late-time and early-time solutions.

An estimate of 2.41 gives

$$\Omega_\chi h^2 \approx \frac{3\times10^{-27}\text{cm}^3\text{s}^{-1}}{\langle\sigma v\rangle}. \tag{2.43}$$

In order to obtain the correct DM relic abundance:

$$\langle\sigma v\rangle \approx 10^{-26}\text{cm}^3\text{s}^{-1} \approx 10^{-9}\text{GeV}^{-2}. \tag{2.44}$$

Let us now check how this cross-section can give us some insights on the mass of a DM candidate. We consider the case of an annihilation that occurs through s-channel with a mediator with mass m_V:

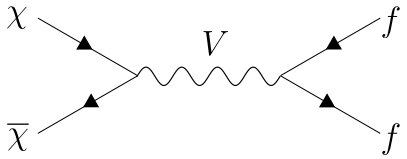

where the vector V has coupling g_χ with the DM and g_f with the fermions. In the non-relativistic limit, the cross section for this process is

$$\sigma = \int d\Omega_{cm} \frac{\mid \mathbf{p}_f \mid}{16\pi^2 E_{cm}^3 \mid \mathbf{v}_1 - \mathbf{v}_2 \mid} \mid \mathcal{M} \mid^2 = \int d\Omega_{cm} \frac{1}{\mid \mathbf{v}_1 - \mathbf{v}_2 \mid} \frac{\mid \mathcal{M} \mid^2}{32\pi^2 s}, \tag{2.45}$$

where Ω_{cm} are centre of mass scattering angles, and s is the centre of mass energy. We have used $\mid \boldsymbol{p}_f \mid \approx E_{cm}/2$ in the limit of massless fermions f. The thermally averaged cross section can be

approximated to be

$$\langle \sigma v \rangle \simeq \frac{\mid \mathcal{M} \mid^2}{32\pi m_\chi^2}. \tag{2.46}$$

In the case of Dirac fermion DM, a vector mediator and a single flavour for the fermion

$$\mid \mathcal{M} \mid^2 \approx g_\chi^2 g_f^2 \frac{32 m_\chi^4}{(s - m_V^2)^2} \tag{2.47}$$

in the non-relativistic limit.
We can now consider two cases:

- $m_V > m_\chi$: in this case, the heavy mediator generates a four-fermion interaction with amplitude $g_\chi g_f / m_V^2$. We have
$$\langle \sigma v \rangle \simeq \frac{16\pi \alpha_\chi \alpha_f m_\chi^2}{m_V^4}. \tag{2.48}$$
- $m_V < m_\chi$: in this case,
$$\langle \sigma v \rangle \simeq \frac{\pi \alpha_\chi \alpha_f}{m_\chi^2}. \tag{2.49}$$
However, in this case, a new process is allowed, namely $\chi\overline{\chi} \to VV$. If $m_V \ll m_\chi$:
$$\langle \sigma v \rangle_{\chi\overline{\chi}\to VV} \simeq \frac{\pi \alpha_\chi^2}{m_\chi^2}. \tag{2.50}$$
If $\alpha_\chi \gg \alpha_f$, the relic abundance may be primarily determined by the latter process.

In general, the thermally-averaged cross section is bounded

$$\langle \sigma v \rangle_{\lesssim} \frac{\pi \text{max}(\alpha_\chi \alpha_f, \alpha_\chi^2)}{m_\chi^2}. \tag{2.51}$$

By considering the cross section computed in 2.44, we can put an upper bound on the DM mass, if we assume perturbative couplings. Taking $\alpha_{\chi,f} \to 1$ in 2.51:

$$m_\chi \lesssim 50 - 100 \text{TeV}. \tag{2.52}$$

Additionally, we can derive the Lee-Weinberg bound from 2.48 by requiring that the couplings are the weak gauge couplings and that $m_V \sim 100$ GeV:

$$\langle \sigma v \rangle \approx \frac{\alpha_W^2 m_\chi^2}{m_V^4} \implies m_\chi \gtrsim 10 \text{GeV}. \tag{2.53}$$

Finally, if we consider SM typical values for the weak couplings, $g_{\chi,f} \sim 0.1, 0.3$, we find:

$$\langle \sigma v \rangle \approx \frac{\alpha_W^2}{1\text{TeV}^2}, \text{ with } \alpha_w \approx 0.03. \tag{2.54}$$

Assuming a weakly interacting DM particle with $\alpha \sim 0.03$ and $m_\chi \sim 100$ GeV, we remarkably obtain the correct abundance observed today, as measured by Planck [40]. This intriguing coincidence has become known as the "*WIMP miracle*", sparking extensive research and focus on this potential DM candidate. However, it is essential to take a moment to reflect on whether this alignment truly represents a miraculous occurrence or if there are underlying reasons that contribute to this intriguing agreement. Indeed, the WIMP miracle more than a coincidence between two demonstrated phenomena is a coincidence between two model paradigms. For getting the results in 2.44 we made some important assumptions. Let's analyze each one of them more carefully:

- *No chemical potential*: it was assumed that the annihilation rate of dark matter particles is proportional to their equilibrium number density. However, it is possible that an asymmetry exists between the number densities of dark matter particles and their corresponding antiparticles - in this case, the relic density depends also on the asymmetry [62, 63].

- *No resonances or threshold behaviour*: in the presence of threshold behaviour or resonances the cross section has a strong T-dependence. In our computations, it was assumed that σ is approximately constant throughout freeze-out.

- *Annihilation of DM DM $\rightarrow$ SM SM dominate*: e.g. in co-scattering [64], DM annihilates against a heavier state and inelastic DM scattering processes determine the relic abundance.

- *Annihilation during the radiation-dominated era in standard cosmology*: if a long-lived massive particle exists in the early universe, it could lead to a matter-dominated era. In such a scenario, if freeze-out occurs during this matter-dominated era, the annihilation cross-section could potentially be much smaller. This is because the density of dark matter is diluted following the decay of the massive particle. An example of this concept can be found in [65]. It's worth noting that this approach could also circumvent the necessity for new light mediators in sub-GeV thermal dark matter candidates.

Another possibility is that DM was never in equilibrium to start with. In this case, it's possible to encounter some problems as the relic abundance would depend too much on the initial condition (UV-dominated) and other assumptions at early times. However, it is possible to have a non-thermal DM candidate that is not UV-dominated and potentially observable.

Freeze-in. Freeze-in [66] is a mechanism where rare interactions within the SM thermal bath slowly build up an abundance of DM. An example could be the annihilation of SM particles, such as e^+e^-, into DM particles. If the coupling is sufficiently small, DM never gets in equilibrium. Another possibility is the freeze-in of DM through the decay of heavy particles. Since the heavy particles can have relatively larger coupling with the SM, they could be produced in colliders and decay with a long lifetime, giving an interesting observational handle of these types of freeze-in models.

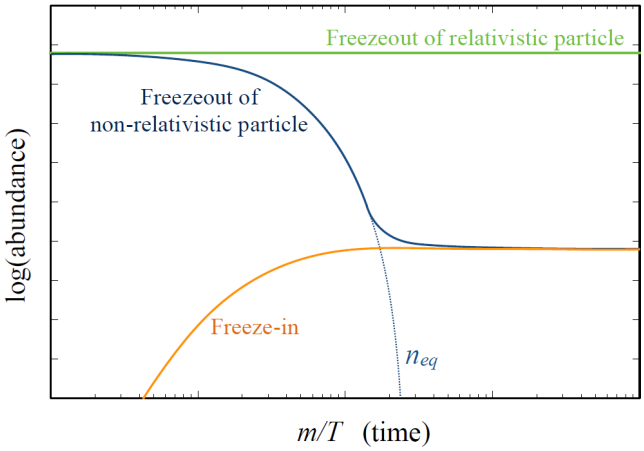

FIGURE 2.4: Illustration of the resulting abundance from freeze-out of relativistic particle, freeze-out of non-relativistic particle, and freeze-in. Figure from [38].

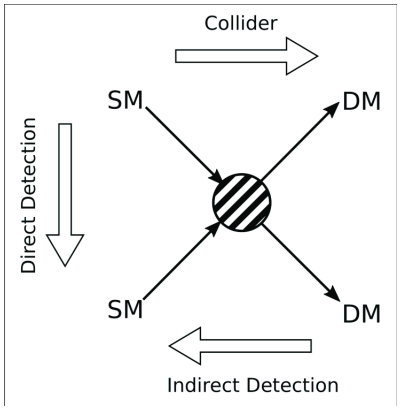

FIGURE 2.5: Schematic showing the possible dark matter detection channels. Figure from [67].

2.3 Looking for WIMPs

There are different ways to look for WIMP dark matter. In fig. 2.5 are summarized the possible channels of detection for dark matter:

- **Direct detection**: dark matter particles can scatter off nuclei in the detector, that then recoil with some energy E_R. If the recoil energy is large enough, it may be possible to detect the scattered particle and infer properties of dark matter [68].
- **Indirect detection**: dark matter can annihilate producing SM products that can be detected.
- **Collider searches**: If dark matter is produced e.g. in a p-p interaction at the LHC, it can escape detectors leading to missing energy signals.

Let's dive deeper into each one of them and present current bounds on dark matter searches.

2.3.1 Direct searches

If DM scatters off a nucleus with mass m_N, the recoil energy is

$$E_R = \frac{q^2}{2m_N} \simeq 50\text{keV} \left(\frac{m_\chi}{100\text{GeV}}\right)^2 \left(\frac{100\text{GeV}}{m_N}\right), \tag{2.55}$$

with $q \sim m_\chi v$, where we have taken $v \sim 10^{-3}$ as the non-relativistic speed of incoming DM. Experiments such as LUX [69] and Xenon100 [70] use a Xenon target with $m_N \sim 120$ GeV and have an energy threshold of a few keV, meaning that they are sensitive to masses for DM up to 10 GeV.

The kinetic energy of an incident DM particle with a mass of around a hundred GeV is $\sim$ 10 keV, much smaller than the $O(10)$ MeV nuclear binding energy of an atomic target. This allows to only consider the scattering of DM off the nucleus as a whole, without considering the scattering with its constituent.

The basic quantity of interest is the scattering rate of DM particles off nuclei. The differential rate per unit detector mass is

$$\frac{dR}{dE_R} = \frac{n_\chi}{m_N} \langle v \frac{d\sigma}{dE_R} \rangle, \quad n_\chi = \rho_\chi / m_\chi. \tag{2.56}$$

The quantity $d\sigma/dE_R$ is the differential scattering cross section. Equation 2.56 can be expanded:

$$\frac{dR}{dE_R} = \frac{\rho_\chi}{m_\chi m_N} \int_{v_{min}}^{v_{max}} d^3v v \tilde{f}(\mathrm{v}, t) \frac{d\sigma}{dE_R}, \tag{2.57}$$

where $\tilde{f}$ is the DM velocity distribution in the lab frame, v_{min} is the minimum velocity needed to cause a nucleus to scatter with energy E_R and v_{max} is the escape velocity, which is bound from measurements of the fastest stars in the Galaxy to be $\sim$500-600 km/s.

Let's compute the differential cross section $d\sigma/dE_R$. We assume DM to be a spin-1/2 Dirac fermion that interacts with quarks through a scalar or a vector boson ϕ with mass m_ϕ. Using an effective operator approach, the scattering Lagrangian can be written as the four-fermion interaction:

$$\mathcal{L}_{eff} = g(q^2, m_\phi) \overline{\chi} \Gamma_\chi \chi \overline{Q} \Gamma_Q Q. \tag{2.58}$$

We have introduced the following quantities: $g(q^2, m_\phi)$ is an effective coupling, Q represent the quark field and $\Gamma_{\chi,Q} = \{I, \gamma^5, \gamma^\mu, \gamma^\mu\gamma^5, \sigma^{\mu\nu}, \sigma^{\mu\nu}\gamma^5\}$. As an example, let's consider

$$\mathcal{L}_{eff} = g_\phi \overline{\chi} \chi \overline{Q} Q, \tag{2.59}$$

where g is independent of momentum transfer. The coupling of DM to nucleon fields n, p will be given by the scattering amplitude:

$$\mathcal{M} = f_p \overline{\chi}\chi\overline{p}p + f_n \overline{\chi}\chi\overline{n}n. \tag{2.60}$$

In many models, DM couples to n and p with the same strength, meaning $f_p \approx f_n$. We can rewrite in terms of the fields for the nuclei:

$$\mathcal{M} = [Zf_p + (A-Z)f_n]\,\overline{\chi}\chi\overline{N}\Gamma_N N, \tag{2.61}$$

where Z is the atomic number, A is the mass number, and Γ_N a Lorentz-invariant 4×4 matrix. Since the result can only depend on q_μ and P_μ,

$$\overline{N}\Gamma_N N = \overline{N}N\tilde{F}_1(q) + \overline{N}\gamma^\mu N q_\mu \tilde{F}_2(q) + \overline{N}\gamma^\mu N P_\mu \tilde{F}_3(q) + \overline{N}\sigma^{\mu\nu} N q_\mu P_\nu \tilde{F}_4(q), \tag{2.62}$$

where $\tilde{F}_i(q)$ are the nuclear form factors. In the limit of small momentum transfer, DM does not probe the size of the nucleus and the cross section is unaffected. As the momentum transfer increases, the interactions become sensitive to the size of the nucleus and the cross section is diminished. Using Dirac equation $\gamma^\mu p_\mu N(p) = m_N N(p)$ and $\overline{N}(p')\gamma^\mu p'_\mu = m_N \overline{N}(p')$:

$$\mathcal{M} = [Zf_p + (A-Z)f_n]\,\overline{\chi}\chi\overline{N}F(q), \tag{2.63}$$

where $F(q)$ is a linear combination of all the $\tilde{F}_i$. By taking the non-relativistic limit, averaging over the spins and sum we find

$$\frac{d\sigma}{dE_R} = \frac{2m_N}{\pi v^2}\left[Zf_p + (A-Z)f_n\right]^2 F^2(q). \tag{2.64}$$

We can note that for $f_p = f_n$, the average cross section $\frac{d\sigma}{dE_R} \propto A^2$. In this case DM couples coherently to the entire nucleus and the strength of the scattering interaction increases with the mass number of the nucleus. These effective interactions are called "spin-independent" since the cross-section does not depend on the nuclear spin. Bear in mind that the one we just consider is a simple example. Additional consideration can be made if, for example, the coupling $g_\phi \propto 1/q^2$. In this situation the differential cross section $d\sigma/dE_R \propto E_R^{-2}$, meaning that the scattering rate is enhanced at small recoil energies.

Let's go back to the scattering rate R. We have:

$$\frac{dR}{dE_R} = \frac{\rho_\chi}{m_\chi m_N}\int_{\sqrt{\frac{m_N E_{th}}{2\mu^2}}}^{v_{escape}} d^3v\, v\tilde{f}(\mathrm{v},t)\frac{d\sigma}{dE_R}. \tag{2.65}$$

The DM particle properties are encoded in m_χ and $d\sigma/dE_R$, while m_N and E_{th} depends on the detector.

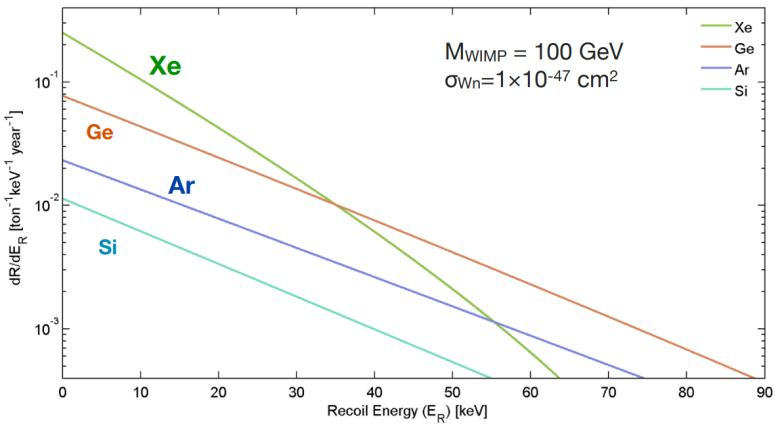

FIGURE 2.6: Scattering rate for different materials for a WIMP with mass 100 GeV [71].

In the Galactic rest frame, DM has no preferred direction. However, in the lab frame, the DM velocities are oriented opposite to the motion of the Sun. Therefore, there is a wind of DM in the Solar frame. In June, the Earth move towards this wind and an observer sees particles with higher velocities than when the Earth moves away from it in December. This implies that the DM flux will be larger in summer, resulting in an **annual modulation**. An additional effect called *gravitational focusing* derives from the relative position of the Earth with respect to the Sun: a DM particle travelling past the Sun is pulled closer to it by their mutual gravitational interaction. When the Earth is behind the Sun, the result is an enhancement in the DM phase-space distribution.

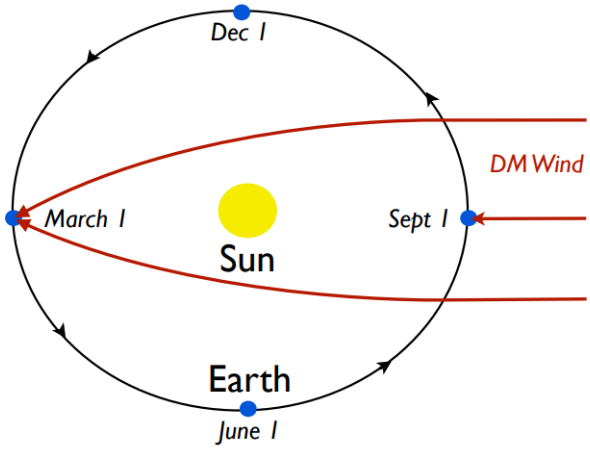

FIGURE 2.7: Schematic representation of annual modulation and gravitational focusing. Figure from [72].

A summary of current and projected is reported in fig. 2.8. Neutrinos are an irreducible source of background. They can come from various sources, e.g. atmospheric, solar or supernovae neutrinos, and their scattering mimics DM recoils.

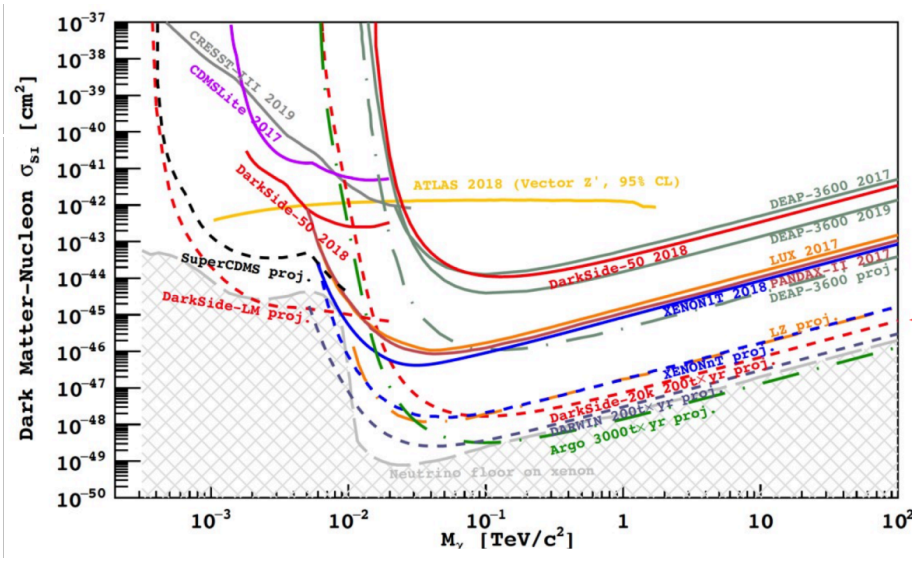

FIGURE 2.8: Summary of current and projected bounds on DM-SM scattering cross section σ. Figure from talk [73].

2.3.2 Indirect searches

Indirect detection searches [74] aim at identifying the products of DM annihilation occurring within our Galaxy or even beyond. Although DM annihilation is significantly suppressed after thermal freeze-out, it can still happen in the present epoch, in particular in regions of very high DM density. The products of DM annihilation may vary depending on the theoretical model, leading to direct production of photon pairs or other Standard Model states that subsequently generate photons through secondary interactions. These gamma-rays then travel relatively undisturbed until they reach the Earth, where they are detected by satellites or ground-based telescopes.

The flux of products is proportional to the number of annihilation per unit time and volume:

$$\Phi \propto \langle \sigma v \rangle \frac{\rho_{DM}^2}{m_{DM}^2}. \tag{2.66}$$

Indirect searches for DM look for high energy cosmic rays produced from DM annihilation.

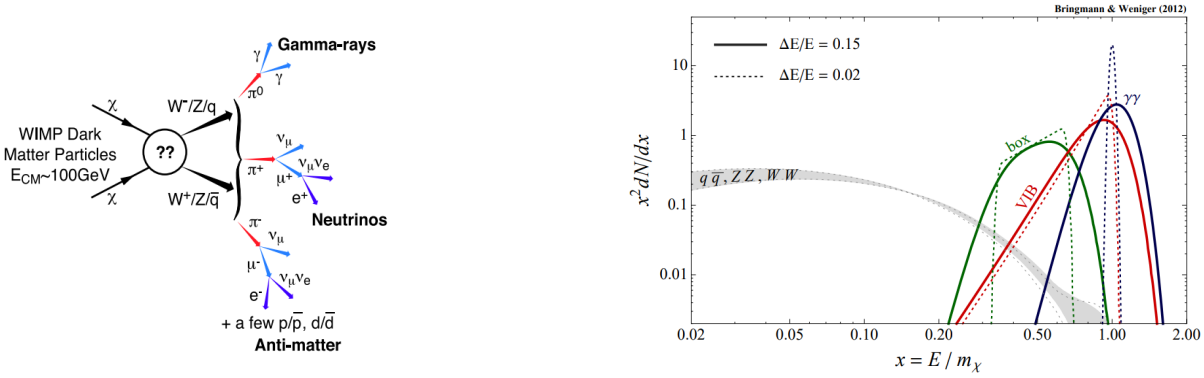

FIGURE 2.9: (Left) Schematic representation of how CRs are produced from DM annihilation. Figure from [75]. (Right) Photon energy spectrum for the $\gamma\gamma$ final state without (blue) and with (red) virtual internal bremsstrahlung. The box spectrum (green) can be produced if the DM annihilates to a new state, that then decays to photons. Figure from [76].

Photons from annihilation. Photons can be produced via:

- Direct annihilation via loops
- Final-state or intermediate state radiation
- Hadronization, e.g. $\chi\chi \to X\pi^0 \to X\gamma\gamma$

Gamma rays freely propagate in the galaxy and can give information on both the initial energy and the angular distribution. To calculate the spectrum and angular distribution of gamma rays from dark matter annihilation per unit time within a solid angle, we integrate the annihilation rate over the solid angle observed, and over the line-of-sight:

$$\Phi_\gamma(E_\gamma, \Delta\Omega) = \frac{1}{2}\frac{dN_\gamma}{dE_\gamma}\frac{\langle\sigma v\rangle}{4\pi m_\chi^2}\int_{\Delta\Omega}\int_{l.o.s.}\rho_\chi^2(l,\Omega)dld\Omega, \tag{2.67}$$

where dN_γ/dE_γ is the spectrum of gamma rays produced per annihilation, which depends on the DM particle's mass and on the particles produced in the process. The quantity in the integral is often referred to as J-factor and encapsulates the relevant astrophysical information. In the case of a spherical dwarf galaxy of radius r, density ρ and located at a distance $d \gg r$, the J-factor is

$$J \equiv \int_{\Delta\Omega}\int_{l.o.s.}\rho_\chi^2(l,\Omega)dld\Omega \simeq \frac{4\pi r^3\rho_\chi^2}{3d^2}. \tag{2.68}$$

This simple example gives us some insights on which are the best targets for gamma-ray searches of DM:

- High density of DM ($J \propto \rho_\chi^2$)
- Close ($J \propto d^{-2}$)

- Extended over a large volume ($(J \propto V)$
- Low or well-understood astrophysical background

The Galactic Center is one of the brightest source of DM annihilation. Also dwarf galaxies are a good target, having smaller J-factor compared to the Galactic center but a better understood astrophysical background. Other searches are focused on galaxy cluster, the halo of the Milky Way and the isotropic gamma-ray background [77–79].
Current experiments looking for DM annihilation products are Fermi Gamma-Ray Space Telescope [80] (in the energy range between 0.1 and 100 GeV), HESS[81], MAGIC [82], and in the future CTA [83].

Antimatter from annihilation. In the case in which the annihilation products are positrons and antiprotons, the signal can be more complicated. After production, charged cosmic rays walk through the Milky Way magnetic field and interact with the backgrounds leading to energy losses. To reduce backgrounds, one looks for specific features in the spectrum or for very low backgrounds.
Positrons can be emitted directly or can originate as secondary particles, e.g. from pion and kaon decays from high-energy cosmic rays interacting with gas. PAMELA and AMS-02 reported an excess that could be due to DM [84, 85], even though it is also compatible with the expected contribution for nearby pulsars.
Another excess of anti-protons was reported by AMS-02 at high energy. However, systematic uncertainties due to antiproton production cross-section, solar modulation and cosmic-ray transport are difficult to assess[86].

Neutrinos from annihilation. Neutrinos behave as photons as they travel freely. High-energy neutrinos can be detected by IceCube [87] or, at lower energies, Super-Kamiokande [88]. The searches for neutrinos produced from DM annihilation are similar to those used for gamma rays. Due to small interaction cross-sections, however, such constraints are usually much weaker than those derived from gamma-ray or cosmic-ray searches. The advantage of looking for neutrinos resides in their capability of penetrating large quantities of matter: this would allow us to detect dark matter annihilation in the core of the Sun or Earth[89].

2.3.3 Collider DM searches

Collider experiments have played a crucial role in testing the predictions of the Standard Model. Furthermore, they offer a valuable avenue for investigating dark matter particles, providing essential information and serving as a significant tool in the search for these elusive particles [91, 92].
Colliders can look for DM by inferring missing energy in the final states. Techniques like studying monophoton or monojet events, carefully vetting other objects, accurately modelling backgrounds, and analyzing the missing transverse energy (E_T^{miss}) can be employed to probe the

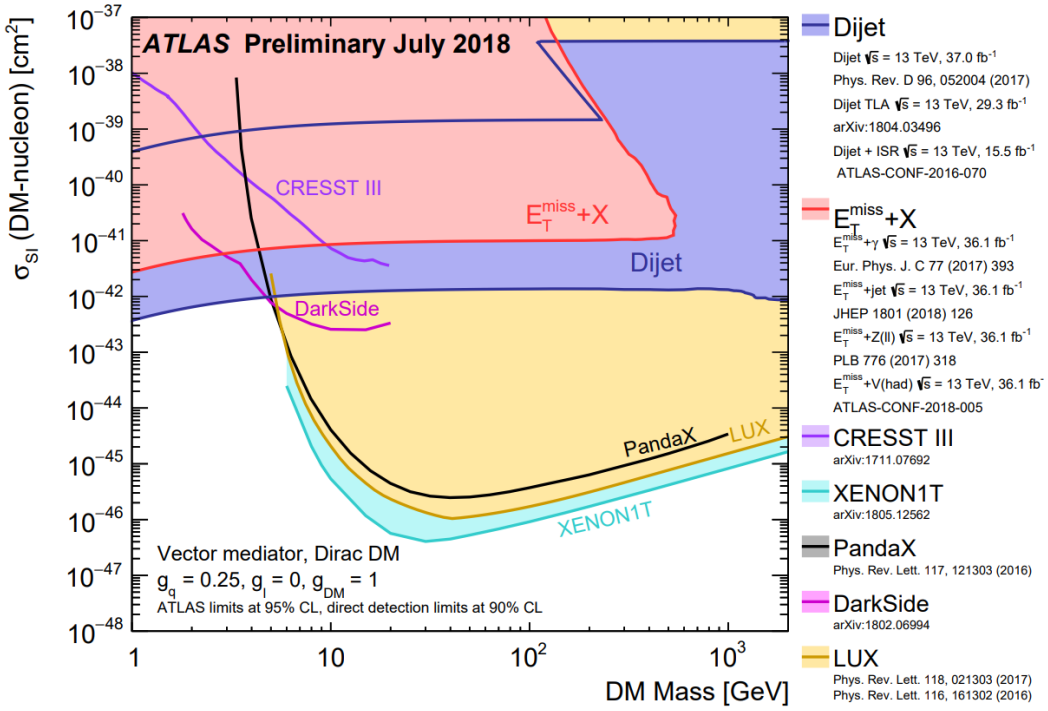

FIGURE 2.10: Dark-matter exclusion summary plot. Figure from [90].

presence of dark matter particles. LHC has already put strong constraints on DM interactions by looking for these signatures [90].

Chapter 3

Dark Sectors

The hunt for new physics Beyond the Standard Model has always focused primarily on searches at higher energies. Over the last decades, there has been a growing interest in **Dark Sectors**[93–96], a collection of particles that are not charged under any standard model gauge groups but can interact with known matter through *portals*. While searches for new heavy particles at the LHC continue, this possibility offers a new framework, that is easily accessible at current experimental facilities and that provides extensive capabilities for constructing and developing models, allowing for a wide range of possibilities to be explored. Dark sectors are particularly interesting for their power to explain a wide range of current open questions in physics in a fairly elegant and natural way. For example, dark matter, whose most relevant feature is the lack of strong and electromagnetic interactions, can be easily embedded in a dark sector model, producing the observed dark matter abundance through thermal freeze-in or freeze-out [97] [98]. Similarly, sterile neutrinos, amongst the most popular hypotheses for the origin of neutrino masses, can be included in dark sector models [99][100]. The interactions of sterile neutrinos or other more complex dark sectors could produce the Sakharov conditions [31] necessary to produce a baryon asymmetry [101] [102]. Rich dark sectors models could in principle also be able to explain some known discrepancies between theory and experiment, as explored in [103].

In this chapter, we will examine the three-portal model introduced by Ballett et al. in [99] as a prime example of a dark sector model. This model encompasses all the renormalizable portals, including the vector, fermion, and scalar portals. Our goal is to delve into the mathematical framework of these portals and understand how to derive their phenomenological implications.

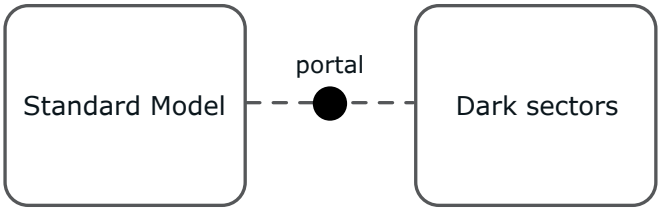

3.1 Portal interactions

Dark sectors typically include one or more mediators that interact with both SM and dark sector particles, acting as a bridge (or, indeed, a portal) and ensuring the possibility of having indirect interactions between the two sectors and hence a visible signal[104]. Lowest dimensional portals include the vector portal, mediated by a dark gauge boson usually referred to as dark photon; the scalar portal, mediated by a new scalar that mixes to the SM Higgs boson; the fermion portal, mediated by a heavy neutral lepton (HNL) interacting with one of the left-handed SM doublets and the Higgs boson. These three cases are all renormalizable and therefore unsuppressed by any physics scale. The pseudoscalar portal, mediated by an axion (or axion-like particle), has instead dimension five and is suppressed by the axion decay constant.

$$\mathcal{L} \supset \begin{cases} \frac{sin\chi}{2} B_{\mu\nu} X^{\mu\nu} & \textbf{vector portal} \\ \lambda (H^\dagger H)|\Phi|^2 & \textbf{scalar portal} \\ y_\nu^\alpha \left(\overline{L_\alpha} \cdot \tilde{H}\right) N^c & \textbf{neutrino portal} \\ \frac{a}{f_a} F_{\mu\nu} \tilde{F^{\mu\nu}} & \textbf{axion portal} \end{cases} . \tag{3.1}$$

3.1.1 Three Portal Model

In this section, we will present a dark sector model, which includes all renormalizable portals [100]. This comprehensive framework allows us to conduct an in-depth analysis of each of the aforementioned portals and their corresponding mathematical formalism. The particle content shown the Table 3.1 and the lagrangian is given by:

$$\begin{aligned} \mathcal{L} \supset & (D_\mu \Phi)^\dagger (D_\mu \Phi) - V(\Phi, H) - \frac{1}{4} X^{\mu\nu} X_{\mu\nu} + \overline{N} i \partial\!\!\!/ N + \overline{\nu_D} i \partial\!\!\!/ \nu_D \\ & - \left[y_\nu^\alpha \big(\overline{L_\alpha} \cdot \tilde{H}\big) N^c + \frac{\mu'}{2} \overline{N} N^c + y_N \overline{N} \nu_D^c \Phi + h.c. \right], \end{aligned} \tag{3.2}$$

where $D_\mu \equiv (\partial_\mu - i g_X X_\mu)$, $X_{\mu\nu} = \partial^\mu X^\nu - \partial^\nu X^\mu$, $L_\alpha \equiv \left(\nu_\alpha^T, l_\alpha^T\right)^T$ is the SM leptonic doublet of flavour $\alpha = e, \mu, \tau$ and $\tilde{H} \equiv i\sigma_2 H^*$ is the charge conjugate of the SM Higgs doublet. In the neutral fermion sector, there are the Yukawa couplings y_ν^α and y_N responsible for the interaction $L_\alpha - N$ and $\nu_D - N$ respectively, plus a Majorana mass term μ' for N. The latter one violates the lepton number assignment by two units. As it will be shown it plays an important role in the generation of neutrino masses.

	$SU(3)_C$	$SU(2)_L$	$U(1)_Y$	$U(1)_X$
N	1	1	0	0
ν_D	1	1	0	Q
Φ	1	1	0	Q

TABLE 3.1: The additional field content of our model. N and ν_D are left-handed fermions, while Φ is a complex scalar.

3.2 Scalar sector

3.2.1 Symmetry breaking

The scalar potential is

$$V(\Phi, H) = -m_\Phi^2|\Phi|^2 + \lambda_\Phi|\Phi|^4 - m_H^2 H^\dagger H + \lambda_H (H^\dagger H)^2 + \lambda (H^\dagger H)|\Phi|^2. \tag{3.3}$$

There are two possible parametrizations that can be used:

$$H = \frac{1}{\sqrt{2}} \begin{pmatrix} G_1^+ + iG_2^+ \\ h + iG^0 \end{pmatrix} \qquad \Phi = \frac{\phi + iG_\phi}{\sqrt{2}} \tag{3.4}$$

and

$$H = \frac{1}{\sqrt{2}} \begin{pmatrix} e^{i\eta^+} g^+ \\ e^{i\eta_h} h^0 \end{pmatrix} \qquad \Phi = \frac{e^{i\eta_\varphi}\varphi}{\sqrt{2}}. \tag{3.5}$$

In both the parametrizations, all the components of the scalar fields are real. Using 3.5, we can minimize the potential and find the vacuum expectation values of the two scalar fields:

$$V(\Phi, H) = -\frac{m_\Phi^2}{2}|\varphi|^2 + \lambda_\Phi|\varphi|^4 - \frac{m_H^2}{2}h^2 + \frac{\lambda_H}{2}h^4 + \frac{\lambda}{4}h^2\varphi^2. \tag{3.6}$$

By imposing:

$$\begin{cases} \frac{\partial V}{\partial h}\big|_{\langle h \rangle} = 0 \\ \frac{\partial V}{\partial \varphi}\big|_{\langle \varphi \rangle} = 0 \end{cases} \tag{3.7}$$

and doing some easy algebra, we obtain:

$$v_h^2 = \frac{\lambda_\Phi m_H^2 - \lambda m_\Phi^2/2}{\lambda_H \lambda_\Phi - \lambda^2/4}, \qquad v_\varphi^2 = \frac{\lambda_H m_\Phi^2 - \lambda m_H^2/2}{\lambda_H \lambda_\Phi - \lambda^2/4}. \tag{3.8}$$

We can now expand around the true vacuum:

$$\begin{aligned} &\varphi \to \varphi + v_\varphi, \qquad && h \to h + v_h \\ &\eta_\varphi \to \eta_\varphi / v_\varphi, \qquad && \eta_h \to \eta_h / v_h, \end{aligned} \tag{3.9}$$

and find the potential:

$$\begin{aligned} V(\Phi, H) = &- \frac{m_\Phi^2}{2}(\varphi^2 + 2v\varphi + v_\varphi^2) + \frac{\lambda_\Phi}{4}(\varphi^2 + 2v_\varphi + v_\varphi^2)^4 \\ &- \frac{m_H^2}{2}(h^2 + 2v_h h + v_h^2) + \frac{\lambda_H}{4}(h^2 + 2v_h h + v_h^2)^2 \\ &+ \frac{\lambda}{4}(h^2 + 2v_h h + v_h^2)(\varphi^2 + 2v_\varphi \varphi + v_\varphi^2) \\ &+ V_{Goldstone} + \text{constants}. \end{aligned} \tag{3.10}$$

From 3.8 we find the value for the masses given by

$$m_H^2 = \lambda_H v_h^2 + \frac{\lambda}{2} v_\varphi^2 \qquad\qquad m_\Phi^2 = \lambda_\Phi v_\varphi^2 + \frac{\lambda}{2} v_h^2. \tag{3.11}$$

We can finally substitute in eq.3.10:

$$\begin{aligned} V(\Phi, H) = &(\lambda_\Phi v_\varphi^2)\varphi^2 + (\lambda_H v_h^2)h^2 + (\lambda v_h v_\varphi)h\varphi \\ &+ \left(\frac{\lambda v_h}{2}\right)h\varphi^2 + \left(\frac{\lambda v_\varphi}{2}\right)h^2\varphi + (\lambda_\Phi v_\varphi)\varphi^3 + (\lambda_H v_h)h^3 \\ &+ \left(\frac{\lambda_\Phi}{4}\right)\varphi^4 + \left(\frac{\lambda_H}{4}\right)h^4 + \left(\frac{\lambda}{4}\right)h^2\varphi^2 \\ &+ V_{Goldstone} + \text{constants}. \end{aligned} \tag{3.12}$$

Scalar masses

To find the physical mass basis for the two scalar fields, we need to diagonalize our Lagrangian:

$$\begin{pmatrix} h & \varphi \end{pmatrix} \begin{pmatrix} \lambda_H v_h^2 & \frac{\lambda}{2} v_h v_\varphi \\ \frac{\lambda}{2} v_h v_\varphi & \lambda_\Phi v_\varphi^2 \end{pmatrix} \begin{pmatrix} h \\ \varphi \end{pmatrix} = \begin{pmatrix} h' & \varphi' \end{pmatrix} R(\theta) \begin{pmatrix} \lambda_H v_h^2 & \frac{\lambda}{2} v_h v_\varphi \\ \frac{\lambda}{2} v_h v_\varphi & \lambda_\Phi v_\varphi^2 \end{pmatrix} R(-\theta) \begin{pmatrix} h' \\ \varphi' \end{pmatrix}, \tag{3.13}$$

where

$$R(-\theta) = \begin{pmatrix} cos\theta & sin\theta \\ -sin\theta & cos\theta \end{pmatrix}, \qquad tan2\theta = \frac{\lambda v_h v_\varphi}{\lambda_H v_h^2 - \lambda_\Phi v_\varphi^2} \tag{3.14}$$

$$sin2\theta = \frac{\lambda v_\varphi v_h}{\sqrt{(\lambda_\Phi v_\varphi^2 - \lambda_H v_h^2)^2 + \lambda^2 v_h^2 v_\varphi^2}}, \qquad cos2\theta = \frac{\lambda_H v_h^2 - \lambda_\Phi v_\varphi^2}{\sqrt{(\lambda_\Phi v_\varphi^2 - \lambda_H v_h^2)^2 + \lambda^2 v_h^2 v_\varphi^2}}. \tag{3.15}$$

The masses will be the eigenvalues of the matrix:

$$\frac{m_{\varphi', h'}^2}{2} = \frac{\lambda_\Phi v_\varphi^2 + \lambda_H v_h^2}{2} \pm \frac{\sqrt{(\lambda_\Phi v_\varphi^2 + \lambda_H v_h^2)^2 + \lambda^2 v_h^2 v_\varphi^2}}{2}. \tag{3.16}$$

φ' will be the lightest state, while h' is like the SM Higgs. Note that if we take the portal coupling λ to zero, we recover a fully diagonal matrix and there's no mixing.

Gauge terms

Let's now focus on the scalar kinetic terms. The covariant derivative is

$$D_\mu \equiv \partial_\mu + ig\vec{W}_\mu \cdot \vec{\tau} + ig' B_\mu \frac{Y}{2} + ig_X Q_X X_\mu \tag{3.17}$$

$$= \partial_\mu + i\frac{g}{2}\begin{pmatrix} W_\mu^3 & \sqrt{2}W_\mu^+ \\ \sqrt{2}W_\mu^- & -W_\mu^3 \end{pmatrix} + ig' B_\mu \frac{Y}{2} + ig_X Q_X X_\mu, \tag{3.18}$$

where $W_\mu^\pm \equiv (W_\mu^1 \pm W_\mu^2)/\sqrt{2}$. From 3.4, we have $\Phi = (\phi + iG_\phi)/\sqrt{2}$. Since Φ is a singlet of $SU(2)_L$ and has zero charge under $U(1)_Y$:

$$\begin{aligned}(D_\mu\Phi)^*(D_\mu\Phi) =& \frac{1}{2}(\partial_\mu - ig_X X_\mu Q_X)(\phi - iG_\phi)(\partial^\mu + ig_X X_\mu Q_X)(\phi + iG_\phi) \\ =& \frac{1}{2}(\partial_\mu\phi - i\partial_\mu G_\phi - ig_X Q_X X_\mu \phi - g_X Q_X X_\mu G_\phi) \\ & (\partial^\mu\phi + i\partial^\mu G_\phi + ig_X Q_X X^\mu \phi - g_X Q_X X^\mu G_\phi) \\ =& \frac{1}{2}(\partial_\mu\phi)(\partial^\mu\phi) + \frac{1}{2}(\partial_\mu G_\phi)(\partial^\mu G_\phi) \\ & - g_X Q_X X_\mu(\phi\partial^\mu G_\phi + \partial^\mu\phi G_\phi) + \frac{g_X^2}{2} Q_X^2 X_\mu X^\mu(\phi^2 + G_\phi^2).\end{aligned} \tag{3.19}$$

For $Q_X = 1$, we find:

$$\begin{aligned}(D_\mu\Phi)^*(D_\mu\Phi) =& \frac{1}{2}(\partial_\mu\phi)(\partial^\mu\phi) + \frac{1}{2}(\partial_\mu G_\phi)(\partial^\mu G_\phi) \\ & - g_X X_\mu(\phi\partial^\mu G_\phi + \partial^\mu\phi G_\phi) + \frac{g_X^2}{2} X_\mu X^\mu(\phi^2 + G_\phi^2).\end{aligned} \tag{3.20}$$

After spontaneous symmetry breaking we get two additional terms

$$g_X^2 X_\mu X^\mu(2v_\varphi\phi + v_\varphi^2), \tag{3.21}$$

responsible for the $\phi - X^\mu - X^\mu$ interaction and for X_μ mass term.

For the Higgs boson kinetic term, ignoring charged Goldstone bosons and focusing only on the neutral part of the lagrangian:

$$H = \frac{1}{\sqrt{2}}\begin{pmatrix} 0 \\ h + iG_h \end{pmatrix}, \tag{3.22}$$

$$D_\mu H = \partial_\mu H + \frac{ig}{2}\begin{pmatrix} W_\mu^3 & 0 \\ 0 & -W_\mu^3 \end{pmatrix} H + \frac{ig'}{2} B_\mu H. \tag{3.23}$$

In this case, after spontaneous symmetry breaking

$$\begin{aligned}|D_\mu H|^2 =& \frac{1}{2}\Big[\partial_\mu h\partial^\mu h + \partial_\mu G_h\partial^\mu G_h + \\ & g(\partial^\mu h W_\mu^3 G_h - \partial^\mu B_\mu G_h - \partial^\mu G_h W_\mu^3 h - \partial^\mu G_h W_\mu^3 v_h) + \\ & g'(B_\mu h\partial^\mu G_h + B_\mu v_h\partial^\mu G_h) \\ & \frac{g^2}{4}W_\mu^3 W^{\mu 3}(G_h^2 + (h+v_h)^2) + \frac{g'^2}{4}B_\mu B^\mu(G_h^2 + (h+v_h)^2) \\ & \frac{gg'}{2}W_\mu^3 B^\mu(G_h^2 + (h+v_h)^2)\Big].\end{aligned} \tag{3.24}$$

3.3 Neutral Gauge Fields

3.3.1 Kinetic term

The kinetic term in the Lagrangian for the relevant gauge bosons is: Just considering the electroweak and dark sectors, the kinetic terms for the gauge fields in the Lagrangian are

$$\mathcal{L}_{kin} = -\frac{1}{4}B_{\mu\nu}B^{\mu\nu} - \frac{sin\chi}{2}B_{\mu\nu}X^{\mu\nu} - \frac{1}{4}X_{\mu\nu}X^{\mu\nu} - \frac{1}{4}W^a_{\mu\nu}W^{a\mu\nu}. \tag{3.25}$$

To be able to work with canonical propagators and Feynman rules, we will need diagonal kinetic terms, and perform a field redefinition:

$$\begin{pmatrix}\overline{X}^\mu \\ \overline{W}^\mu \\ \overline{B}^\mu\end{pmatrix} = \begin{pmatrix}1 & 0 & sin\chi \\ 0 & 1 & 0 \\ 0 & 0 & cos\chi\end{pmatrix}\begin{pmatrix}X^\mu \\ W^\mu \\ B^\mu\end{pmatrix}. \tag{3.26}$$

Substituting in 3.25 we get

$$\mathcal{L}_{kin} = -\frac{1}{4}\overline{B}_{\mu\nu}\overline{B}^{\mu\nu} - \frac{1}{4}\overline{W}^a_{\mu\nu}\overline{W}^{a,\mu\nu} - \frac{1}{4}\overline{X}_{\mu\nu}\overline{X}^{\mu\nu}. \tag{3.27}$$

3.3.2 Mass term

The mass terms for the gauge fields come from the covariant derivatives that act on the Higgs fields:

$$\mathcal{L}_{mass} \supset \frac{1}{2}\Big[\frac{g^2v_h^2}{4}W_\mu^3 W^{\mu 3} - \frac{gg'v_h^2}{2}W_\mu^3 B^\mu + \frac{g'^2v_h^2}{4}B_\mu B^\mu + g_X^2 v_\varphi^2 X_\mu X^\mu\Big]. \tag{3.28}$$

From the SM we have the following relations:

$$M_Z^{SM} \equiv \frac{v_h}{2}\sqrt{g^2+g'^2}, \qquad c_W \equiv \cos\theta_W = \frac{g}{\sqrt{g^2+g'^2}}, \qquad s_W \equiv \sin\theta_W = \frac{g'}{\sqrt{g^2+g'^2}}, \tag{3.29}$$

$$\mu^2 \equiv \frac{g_X^2 v_\varphi^2}{(M_Z^{SM})^2} = \frac{M_X^2}{(M_Z^{SM})^2}, \qquad e = g s_W. \tag{3.30}$$

Using the above definitions, and rewriting the fields in terms of the previously defined field $\overline{B_\mu}$, $\overline{W_\mu^3}$ and $\overline{X_\mu}$ the mass term can be rewritten as

$$\mathcal{L}_{mass} \supset \frac{(M_Z^{SM})^2}{2} \begin{pmatrix} \overline{B^\mu} & \overline{W^{3\mu}} & \overline{X^\mu} \end{pmatrix} \begin{pmatrix} \frac{s_W^2 + \mu^2 s_\chi^2}{c_\chi^2} & -\frac{s_W c_W}{c_\chi} & -\mu^2 t_\chi \\ -\frac{s_W c_W}{c_\chi} & c_W^2 & 0 \\ -\mu^2 t_\chi & 0 & \mu^2 \end{pmatrix} \begin{pmatrix} \overline{B^\mu} \\ \overline{W^{3\mu}} \\ \overline{X^\mu} \end{pmatrix}. \tag{3.31}$$

To diagonalize the mass matrix, we can first perform the following rotations:

$$R^y(\chi) \equiv \begin{pmatrix} c_\chi & 0 & -s_\chi \\ 0 & 1 & 0 \\ s_\chi & 0 & c_\chi \end{pmatrix} \qquad R^z(\theta_W) \equiv \begin{pmatrix} c_W & -s_W & 0 \\ s_W & c_W & 0 \\ 0 & 0 & 1 \end{pmatrix}. \tag{3.32}$$

We define $V \equiv R^y(\chi) R^z(\theta_W)$ and compute

$$V^\dagger M V = (M_Z^{SM})^2 \begin{pmatrix} 0 & 0 & 0 \\ 0 & 1 & s_W t_\chi \\ 0 & s_W t_\chi & \mu^2/c_\chi^2 + s_W^2 t_\chi^2 \end{pmatrix}. \tag{3.33}$$

The first diagonal entry corresponds to the mass of the photon, which is zero as expected. At this point, we can perform a rotation in the YZ plan that finally diagonalizes the mass matrix:

$$R^x(\beta) \equiv \begin{pmatrix} 1 & 0 & 0 \\ 0 & c_\beta & -s_\beta \\ 0 & s_\beta & c_\beta \end{pmatrix}, \tag{3.34}$$

$$R^x(\beta)^\dagger V^\dagger M V R^x(\beta) = \begin{pmatrix} 0 & 0 & 0 \\ 0 & M_Z^2 & 0 \\ 0 & 0 & M_{A'}^2 \end{pmatrix}, \tag{3.35}$$

where

$$\tan 2\beta = \frac{2 s_W s_\chi c_\chi}{c_\chi^2 - s_W^2 s_\chi^2 - \mu^2}, \tag{3.36}$$

$$\sin 2\beta = \frac{2 s_W s_\chi c_\chi}{\sqrt{(c_\chi^2 - s_W^2 s_\chi^2 - \mu^2)^2 + 4 s_W^2 s_\chi^2 c_\chi^2}}, \quad \cos 2\beta = \frac{c_\chi^2 - s_W^2 s_\chi^2 - \mu^2}{\sqrt{(c_\chi^2 - s_W^2 s_\chi^2 - \mu^2)^2 + 4 s_W^2 s_\chi^2 c_\chi^2}}. \tag{3.37}$$

The physical masses of the neutral gauge bosons are

$$\begin{aligned} m_A^2 &= 0, \\ M_Z^2 &= (M_Z^{SM})^2\Big(\frac{s_W^2 + c_W^2 c_\chi^2 + \mu^2}{2c_\chi^2} + \frac{\sqrt{(s_W^2 + c_W^2 c_\chi^2 + \mu^2)^2 - 4c_\chi^2\mu^2}}{2c_\chi^2}\Big) \\ &= (M_Z^{SM})^2\big(1 + s_W t_\chi t_\beta\big), \\ M_{A'}^2 &= (M_Z^{SM})^2\Big(\frac{s_W^2 + c_W^2 c_\chi^2 + \mu^2}{2c_\chi^2} - \frac{\sqrt{(s_W^2 + c_W^2 c_\chi^2 + \mu^2)^2 - 4c_\chi^2\mu^2}}{2c_\chi^2}\Big) \\ &= (M_Z^{SM})^2\big(1 - \frac{s_W t_\chi}{t_\beta}\big). \end{aligned} \tag{3.38}$$

Finally, putting it all together, we have the transformation to go from the off-diagonal flavour basis to the physical basis:

$$\begin{pmatrix} B^\mu \\ W^{3\mu} \\ X^\mu \end{pmatrix} = \begin{pmatrix} 1/\cos\chi & 0 & 0 \\ 0 & 1 & 0 \\ -\tan\chi & 0 & 1 \end{pmatrix} R^x(\chi) R^y(\theta_W) R^z(\beta) \begin{pmatrix} A^\mu \\ Z^\mu \\ A'^\mu \end{pmatrix}. \tag{3.39}$$

From the Standard Model we have:

$$A_\mu^{SM} = c_W B_\mu + s_W W_\mu^3 \qquad Z_\mu^{SM} = -s_W B_\mu + c_W W_\mu^3 \tag{3.40}$$

and we can write

$$\begin{cases} A_\mu = A_\mu^{SM} + c_W s_\chi X_\mu \\ Z_\mu = c_\beta Z_\mu^{SM} + s_\beta c_\chi X_\mu \\ A'_\mu = c_\beta c_\chi X_\mu - s_\beta Z_\mu^{SM} \end{cases}. \tag{3.41}$$

Other useful relations are:

$$\begin{cases} A_\mu^{SM} = A_\mu - c_\beta c_W t_\chi A'_\mu - s_\beta c_W t_\chi Z_\mu \\ Z_\mu^{SM} = (c_\beta + s_\beta s_W t_\chi) Z_\mu - (s_\beta - c_\beta s_W t_\chi) A'_\mu \\ X_\mu = \frac{s_\beta}{c_\chi} Z_\mu + \frac{c_\beta}{c_\chi} A'_\mu \end{cases}. \tag{3.42}$$

These relations are particularly useful if we take the Standard Model lagrangian:

$$-\mathcal{L}_{int}^{SM} \supset e A_\mu^{SM} J_{EM}^\mu + \frac{g}{2c_W} Z_\mu^{SM} J_{NC}^\mu. \tag{3.43}$$

Then in the new theory, we have

$$\begin{aligned}
-\mathcal{L}_{int} \supset & eA_\mu^{SM} J_{EM}^\mu + \frac{g}{2c_W} Z_\mu^{SM} J_{NC}^\mu + g_X X_\mu J_X^\mu \\
= & eA_\mu^{SM} J_{EM}^\mu \\
& Z_\mu \Big[(c_\beta + s_\beta s_W t_\chi) \frac{g}{2c_W} J_{NC}^\mu - s_\beta c_W t_\chi e J_{EM}^\mu + \frac{s_\beta}{c_\chi} g_X J_X^\mu \Big] \\
& A'_\mu \Big[-(s_\beta - c_\beta s_W t_\chi) \frac{g}{2c_W} J_{NC}^\mu - c_\beta c_W t_\chi e J_{EM}^\mu + \frac{c_\beta}{c_\chi} g_X J_X^\mu \Big],
\end{aligned} \tag{3.44}$$

where we have used 3.42. Note that the coupling χ is the mixing between SM hypercharge and X. For very light X, however, the mixing with the Standard Model Z is very small (X has small couplings to the SM neutral current), and we end up with large couplings only with the EM current. In this case, one usually defines:

$$\varepsilon \equiv c_W e. \tag{3.45}$$

3.3.3 Couplings to charged fermions

We want to compute the coupling between the dark photon and the matter fields. From the covariant derivative:

$$\overline{\psi} i \not{D} \psi = \overline{\psi} \left[i\not{\partial} - g' \frac{Y}{2} - g Q_L^3 \not{W}^3 - Q_X g_X \not{X} \right] \psi, \tag{3.46}$$

where $\psi = Q, L, e_R, u_R, d_R$. Using the relations found in the previous sections and exploiting the fact that $Q_e = Y/2 + Q_L^3$, we can combine the left- and right-handed fields to write the vector couplings

$$\begin{aligned}
-\mathcal{L}_I \supset \overline{\psi} \gamma^\mu \{ & A_\mu \left(e Q_e \right) \\
& + Z_\mu \left[\frac{e}{4 s_W c_W} \left(c_\beta \left(4 c_W^2 Q_e - Y_L - Y_R \right) - s_\beta s_W t_\chi \left(Y_L + Y_R \right) \right) + g_X Q_X \frac{s_\beta}{c_\chi} \right] \\
& + A'_\mu \left[\frac{e}{4 s_W c_W} \left(-s_\beta \left(4 c_W^2 Q_e - Y_L - Y_R \right) - c_\beta s_W t_\chi \left(Y_L + Y_R \right) \right) + g_X Q_X \frac{c_\beta}{c_\chi} \right] \Big\} \psi
\end{aligned} \tag{3.47}$$

and axial coupling

$$\begin{aligned}
-\mathcal{L}_I \supset -\overline{\psi} \gamma^\mu \gamma^5 \Big\{ & Z_\mu \left[\frac{e}{4 s_W c_W} \left(Y_L - Y_R \right) \left(c_\beta + t_\chi s_\beta s_W \right) \right] \\
& + A'_\mu \left[\frac{e}{4 s_W c_W} \left(Y_L - Y_R \right) \left(-s_\beta + t_\chi s_\beta s_W \right) \right] \Big\} \psi
\end{aligned} . \tag{3.48}$$

We can reorganize the above expressions and write the couplings to Z and A' in the following way:

$$\mathcal{L}_I \supset -\overline{\psi_f}\gamma^\mu \left\{ \left(c_V^f + c_A^f \gamma^5 \right) Z_\mu + \left(d_V^f + d_A^f \gamma^5 \right) A'_\mu \right\} \psi_f. \tag{3.49}$$

Z_μ	electron	$c_V^e = \frac{g}{2c_W}\left[c_\beta\left(-\frac{1}{2}+2s_W^2\right)+\frac{3}{2}s_\beta s_W t_\chi\right]$	$c_A^e = \frac{g}{2c_W}\left[-\frac{c_\beta+s_\beta s_W t_\chi}{2}\right]$
	up	$c_V^u = \frac{g}{2c_W}\left[c_\beta\left(\frac{1}{2}-\frac{4}{3}s_W^2\right)-\frac{5}{6}s_\beta s_W t_\chi\right]$	$c_A^u = \frac{g}{2c_W}\left[\frac{c_\beta+s_\beta s_W t_\chi}{2}\right]$
	down	$c_V^d = \frac{g}{2c_W}\left[c_\beta\left(-\frac{1}{2}+\frac{2}{3}s_W^2\right)+\frac{1}{6}s_\beta s_W t_\chi\right]$	$c_A^d = \frac{g}{2c_W}\left[-\frac{c_\beta+s_\beta s_W t_\chi}{2}\right]$
A'_μ	electron	$d_V^e = \frac{g}{2c_W}\left[-s_\beta\left(-\frac{1}{2}+2s_W^2\right)+\frac{3}{2}c_\beta s_W t_\chi\right]$	$d_A^e = \frac{g}{2c_W}\left[-\frac{-s_\beta+c_\beta s_W t_\chi}{2}\right]$
	up	$d_V^u = \frac{g}{2c_W}\left[-s_\beta\left(\frac{1}{2}-\frac{4}{3}s_W^2\right)-\frac{5}{6}c_\beta s_W t_\chi\right]$	$d_A^u = \frac{g}{2c_W}\left[\frac{-s_\beta+c_\beta s_W t_\chi}{2}\right]$
	down	$d_V^d = \frac{g}{2c_W}\left[-s_\beta\left(-\frac{1}{2}+\frac{2}{3}s_W^2\right)+\frac{1}{6}c_\beta s_W t_\chi\right]$	$d_A^d = \frac{g}{2c_W}\left[-\frac{-s_\beta+c_\beta s_W t_\chi}{2}\right]$

TABLE 3.2: Fermion neutral couplings

3.3.4 Couplings to neutral fermions

The Lagrangian for the active neutrinos is:

$$\mathcal{L}_\alpha \supset \sum_{\alpha=e,\mu,\tau} \left[\overline{\nu_\alpha} \left(i\not{\partial} + \frac{g'}{2}\not{B} - \frac{g}{2}\not{W}^3 \right) P_L \nu_\alpha + \overline{\nu_\alpha} \left(\frac{g}{\sqrt{2}}\not{W}^+ \right) P_L e_\alpha \right], \tag{3.50}$$

with $\nu_\alpha = \sum_{i=1,2,3} U_{\alpha i}\nu_i$.

We also need to consider the interaction lagrangian for the new heavy neutral lepton flavours:

$$\mathcal{L}' \supset \overline{\nu_D}\left(i\not{\partial} - Q_X g_X\right) P_L \nu_D + \overline{N}\left(i\not{\partial}\right) P_L N, \tag{3.51}$$

so that the interaction Lagrangian for the neutrinos can be written as follow:

$$\mathcal{L} \supset -\sum_{\alpha=e,\mu,\tau} \left[\overline{\nu_\alpha}\gamma^\mu\left(c^\alpha Z_\mu + d^\alpha A'_\mu\right) P_L\nu_\alpha\right] + \left[\overline{\nu_D}\gamma^\mu\left(c^D Z_\mu + d^D A'_\mu\right) P_L\nu_D\right] \tag{3.52a}$$

$$= -\sum_{i,j=1}^{5} \left[\overline{\nu_i}\gamma^\mu\left(c^{ij} Z_\mu + d^{ij} A'_\mu\right) P_L\nu_j\right] \tag{3.52b}$$

$$= -\sum_{\alpha,\beta=e,\mu,\tau} \left[\overline{\nu_\alpha}\gamma^\mu\left(U^*_{i\alpha}U_{j\beta}c^{ij} Z_\mu + U^*_{i\alpha}U_{j\beta}d^{ij} A'_\mu\right) P_L\nu_\beta\right] + \nu_D terms. \tag{3.52c}$$

We can make some additional manipulations and rewrite the above couplings in the following

Z_μ	$c^{ij} = \frac{g}{2c_W}\left[U^*_{\alpha i}U_{\alpha j}\left(c_\beta + s_W t_\chi s_\beta\right)\right] + U^*_{Di}U_{Dj}g_X Q_X \frac{s_\beta}{c_\chi}$	
	$c^\alpha = \frac{g}{2c_W}\left(c_\beta + s_\beta s_W t_\chi\right)$	$c^D = g_X Q_X \frac{s_\beta}{c_\chi}$
A'_μ	$d^{ij} = \frac{g}{2c_W}\left[U^*_{\alpha i}U_{\alpha j}\left(-s_\beta + s_W t_\chi c_\beta\right)\right] + U^*_{Di}U_{Dj}g_X Q_X \frac{c_\beta}{c_\chi}$	
	$d^\alpha = \frac{g}{2c_W}\left(-s_\beta + s_W t_\chi c_\beta\right)$	$d^D = g_X Q_X \frac{c_\beta}{c_\chi}$

TABLE 3.3: Neutrino neutral couplings

way:

$$\begin{aligned} c^{ij} &= \frac{g}{2c_W}\left[U^*_{\alpha i}U_{\alpha j}\left(c_\beta + s_W t_\chi s_\beta\right)\right] + U^*_{Di}U_{Dj}g_X Q_X \frac{s_\beta}{c_\chi} \\ &= \frac{c_\beta c_W M_Z^2}{M_W v_H}U^*_{\alpha i}U_{\alpha j} + \frac{s_\beta c_W M_Z M_{A'}}{M_W v_\phi}U^*_{Di}U_{Dj} \\ &= \frac{M_Z}{2}\left(C_{ij}P_L - C^*_{ij}P_R\right), \end{aligned} \tag{3.53}$$

where

$$C_{ij} = \frac{c_\omega}{v_H}U^*_{\alpha i}U_{\alpha j} - \frac{s_\omega}{v_\phi}U^*_{Di}U_{Dj} \tag{3.54}$$

and we have defined:

$$c_\omega \equiv \frac{c_\beta c_W M_Z}{M_W}, \qquad s_\omega \equiv -\frac{s_\beta c_W M_{A'}}{M_W}. \tag{3.55}$$

Note that $c_\omega \neq c_W$ and $c_\omega^2 + s_\omega^2 = 1$. We can do the same thing for the coupling to the A':

$$\begin{aligned} d^{ij} = d^{ij} &= \frac{g}{2c_W}\left[U^*_{\alpha i}U_{\alpha j}\left(-s_\beta + s_W t_\chi c_\beta\right)\right] + U^*_{Di}U_{Dj}g_X Q_X \frac{c_\beta}{c_\chi} \\ &= -\frac{s_\beta c_W M_{A'}^2}{M_W v_H}U^*_{\alpha i}U_{\alpha j} + \frac{c_\beta c_W M_Z M_{A'}}{M_W v_\phi}U^*_{Di}U_{Dj} \\ &= -\frac{M_Z}{2}\left(D_{ij}P_L - D^*_{ij}P_R\right), \end{aligned} \tag{3.56}$$

where

$$D_{ij} = \frac{s_\omega}{v_H}U^*_{\alpha i}U_{\alpha j} + \frac{c_\omega}{v_\phi}U^*_{Di}U_{Dj}. \tag{3.57}$$

3.4 Neutrino scalar interactions

The Lagrangian of the model also contains a term that takes into account the interaction between neutrinos and the scalar fields:

$$-\mathcal{L}^\nu_{scalar} = \frac{y^\alpha_\nu}{\sqrt{2}}\overline{nu_\alpha}N^C h + \frac{y_N}{\sqrt{2}}\overline{N}nu^C_D\phi + \text{h.c.} \tag{3.58}$$

Considering the Majorana nature of the neutrino fields, we can write

$$-\mathcal{L}^{\nu}_{scalar} = \overline{\nu_i}\left(\left(\Delta_h\right)_{ij} P_R + \left(\Delta_h\right)^*_{ij} P_L\right)\nu_j h + \overline{\nu_i}\left(\left(\Delta_\phi\right)_{ij} P_R + \left(\Delta_\phi\right)^*_{ij} P_L\right)\nu_j \phi, \tag{3.59}$$

where

$$\begin{aligned}\left(\Delta_h\right)_{ij} &= \frac{y^\alpha_\nu}{2\sqrt{2}}\left(U^*_{\alpha i}U^*_{Nj} + U^*_{\alpha j}U^*_{Ni}\right)\\ \left(\Delta_\phi\right)_{ij} &= \frac{y^\alpha_N}{2\sqrt{2}}\left(U^*_{Ni}U^*_{Dj} + U^*_{Nj}U^*_{Di}\right).\end{aligned} \tag{3.60}$$

In the presence of scalar mixing ($\lambda \neq 0$ in the scalar potential), we must also rotate the scalar sector to obtain the physical fields. This was done in section 3.2.1, were we found

$$h = c_\theta h' + s_\theta \phi' \tag{3.61}$$

$$\phi = -s_\theta h' + c_\theta \phi' \tag{3.62}$$

$$\tan(2\theta) = \frac{\lambda v_h v_\varphi}{\lambda_H v_h^2 - \lambda_\Phi v_\varphi^2}. \tag{3.63}$$

The final lagrangian will read:

$$\begin{aligned}\mathcal{L}^{\nu}_{scalar} = &-\overline{\nu_i}\left[\left(\left(\Delta_h\right)_{ij} P_R + \left(\Delta_h\right)^*_{ij} P_L\right)c_\theta - \left(\left(\Delta_\phi\right)_{ij} P_R + \left(\Delta_\phi\right)^*_{ij} P_L\right)s_\theta\right]\nu_j h'\\ &-\overline{\nu_i}\left[\left(\left(\Delta_h\right)_{ij} P_R + \left(\Delta_h\right)^*_{ij} P_L\right)s_\theta + \left(\left(\Delta_\phi\right)_{ij} P_R + \left(\Delta_\phi\right)^*_{ij} P_L\right)c_\theta\right]\nu_j \phi'.\end{aligned} \tag{3.64}$$

3.5 Neutrino masses

The mass terms of the Lagrangian for the neutrino masses are the following:

$$\begin{aligned}-\mathcal{L}^{\nu}_{mass} &= y^\alpha_\nu(\overline{L_\alpha}\cdot\tilde{H})N^C + \frac{\mu'}{2}\overline{N}N^C + y_N\overline{N}\nu^C_D\Phi + h.c.\\ &= \frac{y^\alpha_\nu}{\sqrt{2}}\begin{pmatrix}\overline{\nu_\alpha} & \overline{l_\alpha}\end{pmatrix}\begin{pmatrix}v_H\\0\end{pmatrix}N^C + \frac{\mu'}{2}\overline{N}N^C + y_N\overline{N}\nu^C_D v_\phi + \text{h.c.}\end{aligned} \tag{3.65}$$

We define:

$$\begin{aligned}m_D &= \left[\frac{y^\alpha_\nu}{\sqrt{2}}v_H\right]^T\\ \Lambda &= \left[\frac{y_N}{\sqrt{2}}v_\phi\right]^T.\end{aligned} \tag{3.66}$$

With the above definitions, we can rewrite 3.65 as

$$\mathcal{L}^{\nu}_{mass} = -\frac{1}{2}\left(\overline{\nu_\alpha}\,\overline{N}\,\overline{\nu_D}\right)\begin{pmatrix} 0_{3\times3} & m_D^T & 0 \\ m_D & \mu' & \Lambda^T \\ 0 & \Lambda & 0, \end{pmatrix}\begin{pmatrix} \nu_\alpha \\ N^C \\ \nu_D \end{pmatrix}. \tag{3.67}$$

The mass matrix thus obtained can be diagonalised by block, in order to find the physical value of the masses

$$\hat{M} = \begin{pmatrix} U_\alpha^T & U_N^T & U_D^T \end{pmatrix}\begin{pmatrix} 0_{3\times3} & m_D^T & 0 \\ m_D & \mu' & \Lambda^T \\ 0 & \Lambda & 0 \end{pmatrix}\begin{pmatrix} U_\alpha \\ U_N \\ U_D \end{pmatrix} = U^T M U. \tag{3.68}$$

In order to have an idea of the order of magnitude of the masses, we can consider just one generation of active neutrinos in order to simplify the computations:

$$M' = \left(R^y_\alpha\right)^T M R^y_\alpha = \begin{pmatrix} 0 & 0 & 0 \\ 0 & \mu' & \sqrt{m_D^2+\Lambda^2} \\ 0 & \sqrt{m_D^2+\Lambda^2} & 0 \end{pmatrix}, \tag{3.69}$$

where

$$R^y_\alpha = \begin{pmatrix} c_\alpha & 0 & s_\alpha \\ 0 & 1 & 0 \\ -s_\alpha & 0 & c_\alpha \end{pmatrix} \qquad \tan\alpha = \frac{m_D}{\Lambda}. \tag{3.70}$$

A last rotation is necessary to diagonalize the mass matrix completely, namely:

$$\hat{M} = \left(R^x_\delta\right)^T M R^x_\delta = \begin{pmatrix} 0 & 0 & 0 \\ 0 & c_\delta^2\mu' + 2s_\delta c_\delta\sqrt{m_D^2+\Lambda^2} & 0 \\ 0 & 0 & s_\delta^2\mu' - 2s_\delta c_\delta\sqrt{m_D^2+\Lambda^2} \end{pmatrix}, \tag{3.71}$$

where

$$R^x_\delta = \begin{pmatrix} 1 & 0 & 0 \\ 0 & c_\delta & s_\delta \\ 0 & -s_\delta & c_\delta \end{pmatrix} \qquad \tan\alpha = \frac{2\sqrt{m_D^2+\Lambda^2}}{\mu'}. \tag{3.72}$$

We have thus found that the masses are:

$$\begin{aligned} m_1 =& 0 \\ m_2 =& c_\delta^2 \mu' + 2 s_\delta c_\delta \sqrt{m_D^2 + \Lambda^2} \\ =& \frac{\mu'}{2}\left(1 + \frac{\mu'}{\sqrt{\mu'^2 + 4m_D^2 + 4\Lambda^2}}\right) + 2\frac{m_D^2 + \Lambda^2}{\sqrt{\mu'^2 + 4m_D^2 + 4\Lambda^2}} \\ m_3 =& s_\delta^2 \mu' - 2 s_\delta c_\delta \sqrt{m_D^2 + \Lambda^2} \\ =& \frac{\mu'}{2}\left(1 - \frac{\mu'}{\sqrt{\mu'^2 + 4m_D^2 + 4\Lambda^2}}\right) - 2\frac{m_D^2 + \Lambda^2}{\sqrt{\mu'^2 + 4m_D^2 + 4\Lambda^2}}. \end{aligned} \tag{3.73}$$

Active neutrinos are massless at tree-level. This is due to an accidental cancellation between two seesaw contributions to the light neutrino masses and is evident in equation (5) of [105]. In our case, having only one generation for each new HNF, it is trivial to see that the active neutrino mass matrix will be zero. However, the same holds given that the new HNFs have the same number of generations.

Another way to see this is to integrate out N by taking $\mu' \to \infty$. We are then left with the effective terms:

$$\begin{aligned} &\frac{1}{\Lambda_{NP}}(\overline{L}\tilde{H})(\Phi\nu_D^C) \to \frac{m_D\Lambda}{\mu'}\overline{\nu_L} \\ &\frac{1}{\Lambda_{NP}}(\overline{\nu_D^C}\varphi^*)(\nu_D\varphi^*) \to \frac{\Lambda^2}{\mu'}\overline{\nu_D^C}\nu_D \\ &\frac{1}{\Lambda_{NP}}(\overline{L^C}\tilde{H}^*)(\tilde{H}^\dagger L) \to \frac{m_D^2}{\mu'}\overline{\nu_L^C}\nu_L. \end{aligned} \tag{3.74}$$

The resulting mass matrix is:

$$\mathcal{L}^\nu_{mass} = \frac{1}{2}\begin{pmatrix}\overline{\nu_\alpha} & \overline{\nu_D}\end{pmatrix}\begin{pmatrix} m_D^2/\mu' & m_D\Lambda/\mu' \\ m_D\Lambda/\mu' & \Lambda^2/\mu' \end{pmatrix}\begin{pmatrix}\nu_\alpha^C \\ \nu_D^C\end{pmatrix} + \text{h.c.} \tag{3.75}$$

This matrix has determinant zero, meaning that the lightest neutrinos must be massless. We explore how light neutrinos could acquire a mass term in this particular model in Appendix A.

Chapter 4

ProtoDUNE searches for Semi-Visible Dark Photon

Among the different portals that can mediate an interaction between the Dark Sectors and the Standard Model particles, the vector portal is the one where the interaction takes place because of the kinetic mixing between one dark and one visible Abelian gauge boson.

Depending on the kinematics of the process, the dark photon can undergo two types of decays: one into Standard Model particles, leading to observable signatures, and the other into dark sector particles, resulting in invisible ones. In the former case, one looks for resonance in the invariant mass distribution of the decay products, while in the latter techniques like missing momentum, missing energy, and missing mass are used in order to identify a possible massive dark photon decaying into invisible final states. Another intriguing possibility arises when the dark photon undergoes semi-visible decay. This means that the final state will comprise both visible and invisible states, allowing us to evade constraints coming from fully visible or invisible dark photon searches. As we will discuss, this opens up new regions in the parameter space that are of significant interest from a theoretical standpoint.

In this final chapter, we present the results of the thesis work. Building upon the findings from [4], we consider the proposal presented by P. Coloma et al. in [5] to explore the potential of using ProtoDUNE for investigating rich dark sector models. Specifically, we focus on the semi-visible dark photon as considered by A. Abdullahi et al. in [4].

In section 4.1 we will discuss the theoretical motivation that drives such models. Moving forward to section 4.2, a detailed presentation of the model employed in this study will be provided. This includes an extensive examination of the implications resulting from variations in the particle composition within the dark sector. In 4.3 we will review current constraints on the dark photon masses $m_{A'}$ and mixing ε. In 4.4 we will introduce ProtoDUNE and explain how we can use it to search for this specific model. Lastly, in section 4.5 we will present and discuss the obtained research outcomes.

4.1 Theoretical motivation

As we saw in the previous chapter, unless explicitly forbidden, the dark gauge boson mixes with the SM hypercharge [106]. The naive one-loop expectation for the kinetic mixing ε is around 10^{-3} - 10^{-2} [107]. Many experimental efforts have focused on dark photons decaying either visibly or invisibly. In these scenarios, a huge part of the parameter space for the dark photon mixing ε and masses $m_{A'}$ has already been excluded, hinting at smaller dark couplings or higher-order origin for ε. However, the regions of parameter space characterized by such kinetic mixing values are specifically interesting in solving the anomalous magnetic moment of the muon Δa_μ [108, 109]. Dirac equation predicts fermion magnetic moments g to be precisely two. However, as has been measured in experiments, loop contributions lead to a departure from this precise value. Usually, the value $a_\mu = (g-2)/2$ is used in this context to refer to the departure from tree-level prediction. Loop corrections to the electron magnetic moment are consistent with the experimental measurement of this quantity; however, in the case of the muon anomalous magnetic moment, there is a discrepancy between the SM predictions and the experimental measurement. The latest results published by Fermilab in August 2023, show a departure of 5.1σ from the SM computation [110]. We will discuss more in detail about the anomalous muon magnetic moment in 4.3.

A dark photon can contribute at one loop to $a_\mu = (g-2)_\mu/2$ with a positive sign, fixing the observed discrepancy. This is possible for light mediator, with $m_{A'} \lesssim 3$ GeV and kinetic mixing in the range $\varepsilon \sim 10^{-3}$ - 10^{-2} [111]. While this explanation has been fully excluded for DP decaying in fully visible or invisible states, it still remains a viable possibility in the case of a dark photon decaying semi-visibly, as first shown in the minimal model in [112].
The model considered in [4] includes a dark sector containing multiple fermions, that can either be interpreted as a dark matter model (when the lightest candidate is stable) or seesaw neutrino mass models (when the fermions mix with the SM neutrinos). In this thesis, we focus on the stable case, where the coannihilation of the lighter fermions with heavier ones will be predominant. The minimal inelastic DM mediated by a DP proposed in [112], leaves very little parameter space open for Δa_μ explanation. Therefore, next-to-minimal models are considered, which have the potential to expand the accessible parameter space considerably, particularly within the specified region of interest. Building upon the groundwork laid in [4], this study aims to extend the analysis by scrutinizing each of the benchmark points (BPs) considered there. The primary objective is to determine whether ProtoDUNE can enhance the existing sensitivities for the model under examination, following the work presented in [5].

4.2 Semi-visible Dark Photon

The Lagrangian of the model is given by

$$\mathcal{L} = \mathcal{L}_{SM} - \frac{\epsilon}{2c_W} F_{\mu\nu} X^{\mu\nu} - \frac{1}{4} X_{\mu\nu} X^{\mu\nu} + g_D X_\mu \mathcal{J}_D^\mu + \frac{m_X^2}{2} X_\mu X^\mu, \tag{4.1}$$

where $X_{\mu\nu}$ is the field strength tensor of the dark photon and $\mathcal{J}_D^\mu$ is the dark current containing new degrees of freedom. In this particular model, we assume a Stückelberg mass for the dark photon, leaving unspecified the origin of its mass. After we canonically normalize the gauge kinetic term, we obtain a dark photon with mass $m_{A'} \simeq m_X$ that couples to both the dark sector and the SM electromagnetic (EM) and weak neutral current (NC)

$$\begin{aligned} \mathcal{L}_{int} \supset & A'_\mu \Big(g_D \mathcal{J}_D^\mu - e\varepsilon \mathcal{J}_{EM}^\mu - \varepsilon t_W \frac{m_{A'}^2}{m_Z^2} \frac{g}{2c_W} \mathcal{J}_{NC}^\mu \Big) + \\ & Z_\mu \Big(\frac{g}{2c_W} \mathcal{J}_{NC}^\mu + g_D t_W \varepsilon \mathcal{J}_D^\mu \Big) + O(\varepsilon^2), \end{aligned} \tag{4.2}$$

where $t_W = \tan(\theta_W)$, θ_W being the SM weak mixing angle.

In order to render the dark photon semi-visible, it must decay predominantly into dark particles, that then decay into lighter states producing missing energy and SM states, e.g. $\psi_i \to \psi_{i-1} e^+ e^-$. Our focus will be on a dark sector that includes only fermions:

$$\mathcal{J}_D^\mu \equiv \sum_{i,j=1}^{n} V_{ij} \overline{\psi_i} \gamma^\mu \psi_j, \tag{4.3}$$

where V_{ij} are the model-dependent coupling vertices.

This model offers two interesting phenomenological possibilities: if the Heavy Neutral Fermions (HNFs) mix with SM neutrinos, they are often referred to as Heavy Neutral Leptons (HNLs) denoted by N_4, N_5, etc. A comprehensive recent review is given in [113]. Alternatively, when the lightest HNF is stable, this could constitute a potential dark matter candidate. The heavier states, $\psi_{i=2,\dots,n}$, are expected to decay in cascades down to the lightest HNF, emitting two charged particles at each step. This idea is linked to the inelastic Dark Matter model, first presented in [114] to reconcile the DAMA and the CDMS experiments.

In this specific benchmark scenario, the dark photon is heavier than all HNFs, which permits only three-body decays. Furthermore, all decays involving 3 HNFs are prohibited to avoid constraints on invisible decays. In the upcoming sections, we will delve into the study of the model's fermionic content, starting with the simplest case featuring two Majorana fermions, and then extending up to 4 HNFs.

4.2.1 Two Heavy Neutral Fermions (HNFs)

We start by considering only two Majorana HNFs χ_L and χ_R with charges respectively Q_L and Q_R. The Lagrangian for this model is

$$\begin{aligned}\mathcal{L}_\chi = \overline{\chi_L} i\left(\partial\!\!\!/ - i g_D Q_L A\!\!\!/'\right)\chi_L + \overline{\chi_R^c} i\left(\partial\!\!\!/ + i g_D Q_R A\!\!\!/'\right)\chi_R^c \\ - \frac{1}{2}\left[\begin{pmatrix}\overline{\chi_L^c} & \overline{\chi_R}\end{pmatrix}\begin{pmatrix}\mu_L & m_D \\ m_D & \mu_R\end{pmatrix}\begin{pmatrix}\chi_L \\ \chi_R^c\end{pmatrix} + \text{h.c.}\right].\end{aligned} \tag{4.4}$$

To diagonalize the symmetric mass matrix, $\text{diag}(m_1,m_2) = U^T M U$, where $U = R(\theta)\text{diag}(e^{i\varphi},1)$, and $R(\theta)$ represents the rotation matrix with $\tan 2\theta = m_D/\Delta\mu$. We introduced $\Delta\mu = (\mu_R - \mu_L)/2$ and additionally define $\mu = (\mu_R + \mu_L)/2$, which will be used later. CP is conserved when $\varphi = 0, \pi/2$

In terms of Majorana mass eigenstates, the dark current is given by

$$\begin{aligned}\mathcal{J}_D^\mu = &\frac{Q_A - Q_V\cos 2\theta}{2}\overline{\psi_2}\gamma^\mu\gamma^5\psi_2 + \frac{Q_A + Q_V\cos 2\theta}{2}\overline{\psi_1}\gamma^\mu\gamma^5\psi_1 \\ &+ i\sin\varphi Q_V \sin 2\theta\overline{\psi_2}\gamma^\mu\psi_1 + \cos\varphi Q_V\sin 2\theta\overline{\psi_2}\gamma^\mu\gamma^5\psi_1\end{aligned}, \tag{4.5}$$

where $Q_V \equiv (Q_L + Q_R)/2$ and $Q_A \equiv (Q_L - Q_R)/2$. Gauge anomaly cancellation fixes $Q_A = 0$.

For $\Delta\mu \to 0$, $\tan 2\theta$ is maximal and the dark photon couples only off-diagonally to the mass eigenstates. The on-diagonal couplings can be made small through a C symmetry. The C operator U_c acts on Weyl fermions as:

$$U_c\chi_L U_c^{-1} = \eta_c\psi_R^c, \quad U_c\chi_R U_c^{-1} = \eta_c\psi_L^c. \tag{4.6}$$

We can define the eigenbasis for the C operator as:

$$\chi_+ = \frac{\chi_L + \chi_R^c}{\sqrt{2}}, \quad \chi_- = e^{i\varphi}\frac{\chi_L - \chi_R^c}{\sqrt{2}}. \tag{4.7}$$

Given that $C(A'_\mu) = -1$, the C parity of the fermions can be fixed as $C(\chi_\pm) = \pm 1$. In this basis, the Lagrangian can be rewritten as:

$$\begin{aligned}\mathcal{L}_\chi = \overline{\chi}_+ i\partial\!\!\!/\chi_+ + \overline{\chi}_- i\partial\!\!\!/\chi_- + g_D A'_\mu\left[\frac{Q_A}{2}(\overline{\chi}_+\gamma^\mu\gamma^5\chi_+ + \overline{\chi}_-\gamma^\mu\gamma^5\chi_-) + iQ_V\overline{\chi}_+\gamma^\mu\chi_-\right] \\ - \left[\frac{1}{2}\begin{pmatrix}\overline{\chi}_-^c & \overline{\chi}_+^c\end{pmatrix}\begin{pmatrix}m_D - \mu & i\Delta\mu \\ i\Delta\mu & m_D + \mu\end{pmatrix}\begin{pmatrix}\chi_- \\ \chi_+\end{pmatrix} + \text{h.c.}\right].\end{aligned} \tag{4.8}$$

This basis is identified with the physical basis when $\Delta\mu \to 0$.

In the C-symmetric limit, $\chi_\pm$ behaves like the components of a pseudo-Dirac particle with a mass gap of 2μ.

Inelastic dark matter (iDM). In the C-symmetric limit and with an anomaly-free charge assignment, we find exactly the iDM model [114]. In this case, the dark current would simply be, taking $Q_V = 1$ and $\varphi = \pi/2$:

$$\mathcal{J}^{\mu}_{iDM} = i\overline{\psi_2}\gamma^{\mu}\psi_1 + \text{h.c.} \tag{4.9}$$

This specific model faces challenges due to constraints imposed by invisible dark photon limits, as even small losses in the detector acceptance contribute to the invisible dark photon branching ratio. To avoid these limits, alternative approaches can be considered, involving additional unstable fermions accompanying the dark photon production. This can be achieved by either producing ψ_2 particles in pairs or by exploring models with three or more HNFs. Additionally, the dark photon's couplings are adjusted so that the dark photon predominantly interacts with the heavier and short-lived states. We will now analyze the case of three and four HNFs.

4.2.2 Three HNFs

Starting from the two HNFs model, we add to the particle content an additional fully sterile Weyl fermion η_L. In the interaction basis, we will have the Majorana fermions χ_L, χ_R and η_L. The model Lagrangian then reads:

$$\mathcal{L}_{3-HNFs} = \mathcal{L}_{\chi} + \overline{\eta}_L i\partial\!\!\!/\eta_L - \left[\frac{\mu'_L}{2}\overline{\eta^c}_L\eta_L + \Lambda_L\overline{\eta^c}_L\chi_L + \Lambda_R\overline{\eta^c}_L\chi^c_R + \text{h.c.}\right]. \tag{4.10}$$

The mixing term between η and χ causes the breaking of the $U(1)_D$ symmetry.

In this particular model, η_L is completely neutral, which allows it to couple to the SM lepton doublets via the Yukawa coupling $\overline{L}\tilde{H}\eta^c_L$. This coupling term is crucial in generating the masses of light neutrinos and would enable the lightest HNF to decay into SM neutrinos. However, to ensure the stability of the dark matter candidate, it is necessary to forbid these coupling terms. This is achieved by imposing a dark parity Z_2 under which all dark sector fermions are charged. By introducing this dark parity, we prevent the interaction terms that would otherwise allow η_L to couple to SM lepton doublets, ensuring that the lightest HNF remains a viable dark matter candidate. The dark parity can also be linked to the conservation of the lepton number if $L(\eta_L) = 1$, forbidding the neutrino Yukawa coupling in the model.

We use the left-handed dark fermion basis introduced in 4.7, and set the Majorana phase to be such that CP is conserved and the mass terms are positive when $M_X > \mu$. The DS fermion mass matrix is

$$-\mathcal{L}_{3-HNFs} = \frac{1}{2}\left[\begin{pmatrix}\overline{\eta^c_L} & \overline{\chi^c_-} & \overline{\chi^c_+}\end{pmatrix}\begin{pmatrix}\mu'_L & \Delta\Lambda & \Lambda \\ \Delta\Lambda & M_X - \mu & \Delta\mu \\ \Lambda & \Delta\mu & M_X + \mu\end{pmatrix}\begin{pmatrix}\eta_L \\ \chi_- \\ \chi_+\end{pmatrix} + \text{h.c.}\right], \tag{4.11}$$

with $\Lambda = (\Lambda_R + \Lambda_L)/\sqrt{2}$ and $\Delta\Lambda = (\Lambda_R - \Lambda_R)/\sqrt{2}$. By imposing C-symmetry in the χ sector, we can recover the limit where $\Delta\mu = \Delta\Lambda = 0$. In doing so, we encounter a situation analogous to the case of two HNFs, but with a difference: now χ_+ can mix with the fully sterile state. Indeed, as $C(\eta_L) = 1$, C-conservation implies that only C-even fermions can mix with η_L. Consequently, the particle spectrum can consist of one Dirac fermion and one Majorana fermion or three Majorana states.

The C-odd state, denoted as $\chi_- \equiv \psi_2$, decouples, while η and χ_+ mix with each other. In the mass basis, we find:

$$\psi_1 = c_\alpha \eta + s_\alpha \chi_+, \qquad m_1 = \mu'_L - M\frac{\sin^2\alpha}{\cos 2\alpha}, \tag{4.12}$$

$$\psi_2 = \chi_-, \qquad m_2 = M_X - \mu, \tag{4.13}$$

$$\psi_3 = -s_\alpha \eta + c_\alpha \chi_+, \qquad m_3 = \mu'_L + M\frac{\cos^2\alpha}{\cos 2\alpha}, \tag{4.13}$$

where $\tan 2\alpha = 2\Lambda/M$ and $M = M_X + \mu - \mu'_L$. In the limit $\tan 2\alpha \ll 1$, ψ_2 and ψ_3 form a pseudo-Dirac pair. In the other limit, $tan2\alpha \gg 1$, we have three Majorana fermions. The splitting in this case will be given by $m_3 - m_1 \sim M + 2\Lambda^2/M$ and $m_3 - m_2 \sim \Lambda^2/M + 2\mu$. In the C-symmetric case, the current will be fully off-diagonal:

$$\mathcal{J}^\mu_{3-HNF} \supset s_\alpha \overline{\psi_2}\gamma^\mu \psi_1 + c_\alpha \overline{\psi_2}\gamma^\mu \psi_3 + \text{h.c.} \tag{4.14}$$

As we anticipated above, two phenomenological models can arise from having three HNFs: mixed inelastic dark matter (mixed-iDM) and three Majorana fermions.

Mixed-iDM. If we take the limit of small α, ψ_2 and ψ_3 form a pseudo-Dirac pair, while ψ_1 remains a Majorana particle. When ψ_1 is a dark matter particle, its relic abundance is set only through the coannihilation with the lightest pseudo-Dirac partner. The self-annihilation of dark matter is forbidden by the C-symmetry, and not constrained by CMB limits. The dark current will be

$$\mathcal{J}^\mu_{mixed-iDM} = s_\alpha \overline{\Psi}_2 \gamma^\mu \psi_1 + c_\alpha \overline{\Psi}_2 \gamma^\mu \Psi_2 + \text{h.c.} \tag{4.15}$$

The important parameter, in this case, is the mass splitting between the Majorana fermion and its interaction partner Δ_{21}. The mass splitting between the fermions constituting the pseudo-Dirac pair, expressed in terms of $\tan 2\theta$ and Δ_{21}, is $\Delta_{32} = \frac{1}{4}\frac{\Delta_{21}}{1+\Delta_{21}}\tan^2 2\alpha$, which is small for $\tan^2 2\alpha \ll 1$. In this limit $\Delta_{32} \propto \alpha^2$, and if we take $\alpha \to 0$ we recover the exact Dirac case. The decay of $\psi_3 \to \psi_2 + ..$ are suppressed by Δ^5_{32}, so it is possible to safely neglect those.

Three Majorana fermions. By relaxing the condition $\alpha \ll 1$ and the C symmetry in the dark sector, we have three hierarchical Majorana HNFs. In this case the decay of $\psi_3 \to \psi_2$ is enhanced, while the on-diagonal terms are suppressed. This case can provide both a viable

inelastic DM candidate or a heavy neutral lepton interpretation, as has been analyzed in [103]. Depending on the mass hierarchy in this case, it would be possible for the heavier HNFs to decay in lighter states, for example into 3 ψ_1. The benchmarks chosen for the analysis are such that this possibility is forbidden as it would dominate and contribute to the invisible branching ratio of the dark photon.

4.2.3 Four HNFs

By adding another fermion, it is possible to go to the two Dirac fermions limit. In this scenario, we have two families of HNFs: one fully sterile, η, and the other charged under the dark gauge symmetry, χ. In this case, the Lagrangian is

$$\begin{aligned}\mathcal{L}_{4-HNF} =& \mathcal{L}_\chi + \overline{\eta} i\partial\!\!\!/ \eta - M_\eta \overline{\eta}\eta \\ &- \left[\frac{\mu'_R}{2}\overline{\eta_R}\eta^c_R + \Lambda'_R\overline{\eta_R}\chi^c_R + \frac{\mu'_L}{2}\overline{\eta^c_L}\eta_L + \Lambda_L\overline{\eta^c_L}\chi_L + \Lambda_R\overline{\eta^c_L}\chi^c_R + \text{h.c.}\right].\end{aligned} \tag{4.16}$$

In the C-symmetric limit, $\Lambda_R = \Lambda'_L$ and $\Lambda_L = \Lambda'_R$. The mass matrix in the C eigenbasis is

$$-\mathbf{L}_{4-HNF} \supset \frac{1}{2}\begin{pmatrix}\overline{\eta^c_-} & \overline{\eta^c_+} & \overline{\chi^c_-} & \overline{\chi^c_-}\end{pmatrix}\begin{pmatrix}M_\eta - \mu' & 0 & \Lambda_- & 0 \\ 0 & M_\eta + \mu' & 0 & \Lambda_+ \\ \Lambda_- & 0 & M_X - \mu & 0 \\ 0 & \Lambda_+ & 0 & M_X + \mu\end{pmatrix}\begin{pmatrix}\eta_- \\ \eta_+ \\ \chi_- \\ \chi_+\end{pmatrix} + \text{h.c.}, \tag{4.17}$$

where $\Lambda_\pm \equiv (\Lambda'_L + \Lambda_R)/2 \pm (\Lambda'_R + \Lambda_L)/2$. As before, the C-even and C-odd sectors decouple. We introduce the rotations defined by the mixing angles $\tan 2\beta_\pm = 2\Lambda_\pm/\Delta_\pm$, with $\Delta_\pm = \pm(M_X - M_\eta) + \mu - \mu'$. The mass basis will read:

$$\begin{aligned}\psi_1 &= c_{\beta_-}\eta_- + s_{\beta_-}\chi_-, \quad m_1 = M_\eta - \mu' + \Delta_-\frac{\sin^2\beta_-}{\cos 2\beta_-}, \\ \psi_2 &= c_{\beta_+}\eta_+ + s_{\beta_+}\chi_+, \quad m_2 = M_\eta + \mu' - \Delta_+\frac{\sin^2\beta_+}{\cos 2\beta_+}, \\ \psi_3 &= -s_{\beta_-}\eta_- + c_{\beta_-}\chi_-, \quad m_3 = M_X - \mu - \Delta_-\frac{\sin^2\beta_-}{\cos 2\beta_-}, \\ \psi_4 &= -s_{\beta_+}\eta_+ + c_{\beta_+}\chi_+, \quad m_4 = M_X - \mu + \Delta_+\frac{\sin^2\beta_-}{\cos 2\beta_-}.\end{aligned} \tag{4.18}$$

In the limit $\mu, \mu'\Lambda \ll M_X, M_\eta$, the spectrum is composed of two pseudo-Dirac particles, split by the $U(1)_D$-breaking terms. If we take the $U(1)_D$ to be broken by one unit, such that $\mu = \mu' = 0$ and $\Delta_- = \Delta_+ = \Delta$, the Dirac pairs are split by:

$$\Delta_{43} \sim \Delta_{21} \sim \Delta\left(\beta_+^2 - \beta_-^2\right), \tag{4.19}$$

which is small for small mixing angles and vanishes for $\beta_- = \beta_+$. In this last case, we recover the exact two Dirac fermions. In terms of mass eigenstates, the dark current is

$$\mathcal{J}^\mu_X = c_{\beta_+}c_{\beta_-}\overline{\psi_4}\gamma^\mu\psi_3 + s_{\beta_+}c_{\beta_-}\overline{\psi_4}\gamma^\mu\psi_1 + s_{\beta_-}c_{\beta_+}\overline{\psi_3}\gamma^\mu\psi_2 + s_{\beta_+}s_{\beta_-}\overline{\psi_2}\gamma^\mu\psi_1 + \text{h.c.} \tag{4.20}$$

Only interactions amongst C-odd and C-even states are allowed. The heaviest pseudo-Dirac pair couples most strongly to the dark photon. The dominant decays are $\psi_{4,3} \to \psi_{1,2}$.
The model allows for the possibility of recovering the inelastic dark matter case, the **Inelastic Dirac Dark Matter (i2DM)** [115]. In the exact Dirac limit, we only have two particles in the spectrum: a light, mostly neutral Dirac fermion Ψ_1, which is the dark matter candidate, and Ψ_2, that works as a coannihilator. The idea for the inelastic Dirac dark matter stems from the need to create a different paradigm to the simple iDM scenario, which is already strongly constrained. As discussed in [115], this leads to different cosmology and new phenomenology that can help us test this model in current and future experiments:

$$\mathcal{J}^\mu_{i2DM} = s^2_\beta\overline{\Psi_1}\gamma^\mu\Psi_1 + s_\beta c_\beta(\overline{\Psi_2}\Psi_1 + \text{h.c.}) + c^2_\beta\overline{\Psi_2}\Psi_2. \tag{4.21}$$

This model is different from the mixed-iDM in that the off-diagonal interaction is suppressed with respect to the self-annihilation of the heavier Dirac fermion. The branching ratios of the dark photon to the lighter fermions will be hierarchical, following a proportion of $(1{:}\beta^2{:}\beta^4)$ for $(\Psi_2\Psi_2,\ \Psi_2\Psi_1,\ \Psi_1\Psi_1)$

4.2.4 Mixing with light neutrinos

As we anticipated before, in general, in the presence of a fully sterile state, the Lagrangian should also contain the Yukawa couplings with both the SM leptonic doublet and the DS, which after symmetry breaking will lead to the mixing between neutrinos and HNFs (in this scenario they are usually referred to as HNLs).

The HNLs are unstable and the lightest particle in the spectrum cannot constitute dark matter. For example, considering the 3-HNF model, the Lagrangian would contain the additional term

$$\mathcal{L} = \mathcal{L}_{3-HNF} - \sum_{\alpha=e,\mu,\tau}\left(y_\alpha\overline{L_\alpha}\tilde{H}\eta^c_L + \text{h.c.}\right). \tag{4.22}$$

The mixing of active SM neutrinos and HNLs is constrained to be small by direct laboratory searches. The main consequence of having this mixing is that it could be a mechanism for light neutrino mass generation. Indeed, a GeV-scale seesaw mechanism has been extensively studied in the literature ([93, 116]. In Appendix A it has been explored as an example of how the three portal model presented in [100] can give rise to neutrino masses at loop level.

The breaking of the lepton number plays an important role in the generation of neutrino masses. In the dark sector, the charge assignment is arbitrary and depending on specific choices, lepton number can be broken by different terms, e.g. for $L(\chi_L) = L(\chi_R^c) = 0$ and $L(\chi_R) = L(\chi_L^c) = 1$, it will be broken by $\Lambda_{L,R}$, M_X and $\mu_{L,R}$. Light neutrino masses need to depend on all the $U(1)_L$-breaking parameters. One could also give charge assignment such that the Yukawa term itself is small, thus explaining naturally its smallness. For negligible μ'_L and $\Lambda_{L,R} \ll M_X$, we have that $m_1 \simeq \Lambda^2/M$, $m_2 \simeq m_3 = M$ and light neutrino masses will be:

$$m_\nu \simeq \frac{y^2 v_H^2}{\Lambda^2} M. \tag{4.23}$$

The case with four HNFs allows us to add two Yukawa interactions to the SM:

$$\mathcal{L} = \mathcal{L}_{4-HNF} - \sum_{\alpha=e,\mu,\tau} \left(y_\alpha \overline{L_\alpha} \tilde{H} \eta_R + y'_\alpha \overline{L_\alpha} \tilde{H} \eta_L^c + \text{h.c.} \right). \tag{4.24}$$

As before, the Yukawa can be suppressed by not charging η. If $L(\eta_L) = L(\eta_R) = 1$, M_η is allowed while L-conservation implies y'_α to be very small. An interesting case is the one in which $L(\chi_L) = L(\chi_R) = 1$, which is compatible with the C-symmetry discussed before. In this case, the lightest neutrino mass is zero as it is protected by the accidental lepton number symmetry.

4.3 Current experimental constraints

We now provide a brief summary of the constraints on the mass of the dark photon $m_{A'}$ and the mixing parameter ε based on reference [117]. Specifically, our focus lies on masses above 1 MeV, which are relevant for our analysis in the range 10 MeV $< m_{A'} <$ 10 GeV and $10^{-4} < \varepsilon < 0.1$. A more comprehensive analysis of some of these constraints within the context of the model studied in this thesis can be found in reference [4]. However, here we present a broader discussion, later touching upon model-independent limits.

The main production mechanisms of the dark photon are:

- *Bremmstrahlung*: the incoming electron scatters off the target nuclei (Z), goes off-shell and can thus emit the dark photon via $e^- Z \to e^- Z A'$.
- *Annihilation*: an elector-positron pair annihilates into an ordinary photon and a dark photon: $e^- e^+ \to \gamma A'$.
- *Meson decays*: a pseudoscalar meson φ can decay, producing a dark photon and an ordinary photon: $\varphi \to A'\gamma$. For a vector meson, V an off-shell dark photon can be produced which subsequently decays into SM or dark sectors particles: $V \to A'^* (\to l^+ l^- / \chi\chi)$.

- *Drell-Yan*: a quark-antiquark pair annihilates into the dark photon, which then decays into a lepton pair (or hadrons): $q\bar{q} \rightarrow A'(\rightarrow l^+l^-, h^+h^-)$.

Detection of A' is usually through its decay products. Depending on whether they are visible or invisible, different searches are carried out as will be discussed in the next sections.

Constraints on decays to visible final states

There are two main types of experiments that have contributed to establishing the current limits on the visible massive dark photon in the region where its mass is greater than 1 MeV. These experiments are conducted at colliders and fixed-target or beam dump facilities. In both experiments, the idea is to look for resonances over a smooth background. In collider experiments, the decay vertex is prompt or slightly displaced from the beam interaction point. In contrast, beam dump experiments look for highly displaced vertices. Additionally, the former is most sensitive to region of the parameter space with higher masses and mixing ($\varepsilon > 10^{-3}$, $m_{A'} \sim O(10\text{ GeV})$), while the latter can probe regions with lower masses and mixing.

- **Experiments at colliders**. These look for resonances in the invariant mass distribution of e^+e^- and $\mu^+\mu^-$ pairs. The dark photon can be produced in different ways: meson decay (e.g. $\pi^0 \rightarrow \gamma A'$, NA48/2 [118]), *Bremsstrahlung* ($e^-Z \rightarrow e^-ZA'$, A1 [119]), annihilation ($e^+e^- \rightarrow \gamma A'$, BaBar [72]). In the case of a proton-proton (pp) collider, the dark photon can be produced via the γ - A' mixing in all the processes where an off-shell photon γ^* with mass $m(\gamma^*)$ is produced: meson decays (e.g. vector mesons), *Bremsstrahlung*, and Drell-Yan production [120].

- **Beam-dump experiments**. Electrons or proton beams are collided against a fixed target or dump in order to produce secondary particles. In this case, the dark photon can be produced by either *Bremsstrahlung*, mesons decay or QCD processes (the latter only in the case of proton beams). The products of the collisions are mostly absorbed in the dump and the dark photon is searched for as a displaced vertex with two opposite charged tracks in the decay volume of the experiment.

Searches for visible dark photons in collider/fixed target experiments are mainly carried out at BaBar [72], A1 [119], KLOE[121], CMS[122], NA48/2[118], while beam dump searches are done at ν-Cal[123] and CHARM[124]. Additional bounds can also come from supernovae[125]. Many additional experiments have been proposed to search for visibly decaying dark photons, as discussed in [117].

Constraints on decays to invisible final states

These dark photons are considered "invisible" as they do not leave a detectable signal in the particle detectors. In this context, experimental techniques such as measuring missing momentum,

missing energy, and missing mass are employed to look for potential massive dark photons. Experiments using the missing-mass method aim to detect and measure visible final-state particles, seeking events with energy and momentum imbalances. Avoiding backgrounds from processes generating neutrinos is crucial, as they can mimic signals. Precisely determining the initial state is essential, achieved using accelerator information or measuring the initial state's energy and momentum directly. To reduce backgrounds and enhance sensitivity, the detectors must be hermetic with extensive tracking and calorimetric systems to minimize losses. The main challenge is increasing luminosity while maintaining excellent background suppression, primarily arising from photo-nuclear effects in the calorimeters. The most stringent limits come from BaBar and NA64 experiments at CERN:

- **NA64** - this experiment looks for $A' \to$ *invisible states*. The dark photon is produced via *Bremsstrahlung* in the process $e^- Z \to e^- Z A'$, where the 100 GeV electron beam collides against an active ECAL target [126].
- **Belle II** - in this case the dark photon is produced via $e^+e^- \to A'$, and the A' subsequently decay into invisible states [127].
- **KLEVER** - this experiment could search for dark photons in invisible final states in the $K_L \to \pi^0 \nu\overline{\nu}$ rare decays [128].
- **PADME** - a 550 MeV positron beam collides on a diamond target. The search for invisible dark photon uses the missing momentum technique at the Beam Test Facility (BTF) at Laboratori Nazionali di Frascati (INFN) [129].

Model-independent limits

As anticipated before, the semi-visible dark photon model circumvents the visible and invisible limits we just discussed. The dominant branching ratio of the dark photon is into HNFs, which subsequently decay producing both visible and invisible final states. This implies that the branching ratio cannot be reconstructed as a visible resonance due to missing energy, and neither missing energy techniques can be applied due to the visible products. Thus, it becomes crucial to examine the present model-independent constraints on the masses and mixing of the dark photon. These constraints remain unaffected regardless of whether the dark photon's branching ratio results in visible or invisible phenomena.

Visible resonance searches. In the model discussed here, the dark photon can still decay into visible final states, such as $A' \to e^+e^-$. However, the branching ratios for visible states are smaller than those into dark sectors, being on the order of $\varepsilon^2\alpha/\alpha_D$.

For independent constraints on kinetic mixing, irrespective of the branching ratios of A', we can consider processes that are sensitive to the exchange of virtual dark photons. These

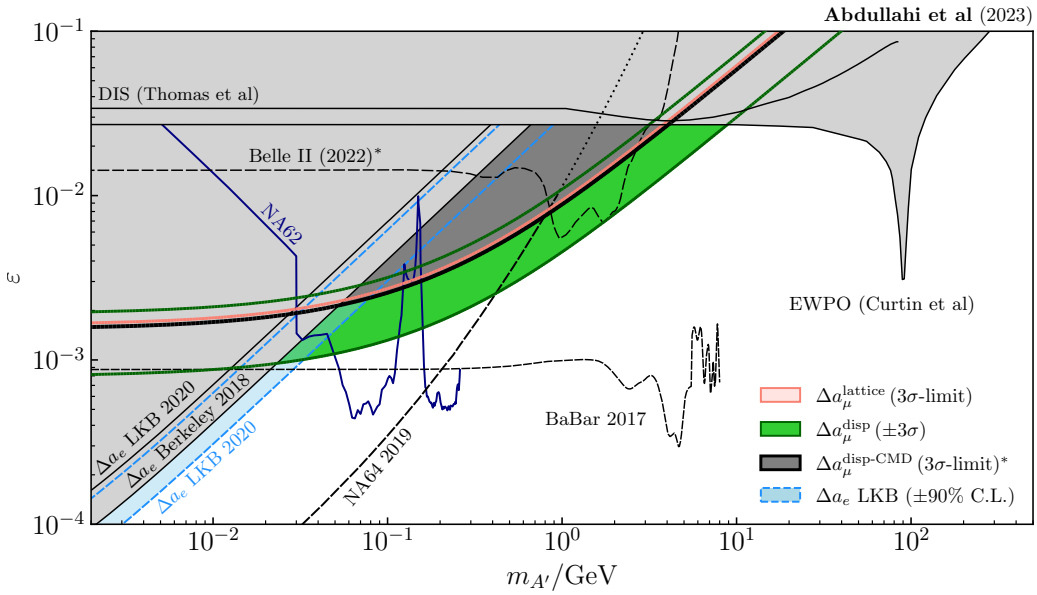

FIGURE 4.1: Model independent limits (grey colours) for the kinetic mixing ε of the dark photon alongside limits on the invisible dark photon (navy colours). Picture from [4].

constraints do not heavily rely on the specific branching ratios and can be considered model-independent, assuming no fine-tuning is present from other new-physics contributions to these observables.

Deep-inelastic scattering. The presence of a dark photon can influence the deep-inelastic scattering (DIS) involving charged leptons interacting with nuclei via t-channel exchange. As a result, the extracted values of Parton Distribution Functions (PDFs), which describe the momentum distributions of quarks and gluons within the nucleon, can be affected.

Electroweak precision observables. Among the EWPO modified by the kinetic mixing, the most important is $M_Z^2 \sim M_{Z^0}^2 - \varepsilon^2 M_{A'}$, and the corresponding shift in the mass of the W boson.

Electron $(g-2)$. Dirac's theory predicts that the magnetic moment of the electron should be exactly an integer value of two. However, experimental measurements [130] have revealed a departure from this prediction, which is referred to as the *electron anomalous magnetic moment*. Corrections at 1-loop using QED to the electron's magnetic dipole moment can make up for this deviation [131], giving the correct measured value.
Precision measurements of the electron's anomalous magnetic moment offer model-independent constraints on the parameter ε associated with the exchange of virtual dark photons. The dark photon's contribution introduces a negative sign and tends to reduce the magnetic moment's

value. By comparing these experimental results with high-precision Standard Model (SM) predictions, we can derive constraints on new physics. In general, these constraints exclude the Δa_μ explanation for dark photon masses below $m_{A'} \sim 30$ MeV.

Muon $(g-2)$. The muon magnetic moment can be calculated similarly to the electron magnetic moment. However, it has been found that experiments deviate from the Standard Model prediction [132] by 3.7σ[133], suggesting that new physics might be at play. Experiment E989 at FNAL [134] has reported $a_\mu^{FNAL} = 116\,592\,040\,(54) \times 10^{-11}$. Combining with results with Brookhaven National Laboratory (BNL) measurements $a_\mu^{BNL} = 116\,592\,920\,(63) \times 10^{-11}$, provides the experimental average: $a_\mu^{comb} = 116\ 592\ 061\ (41) \times 10^{-11}$. The Standard model prediction, obtained by combining QED, electroweak, and hadronic contributions, gives: a_μ^{disp}=116 591 810 (43) $\times 10^{-11}$ [132], leading to a tension between experiments and theory reaches 4.2σ. A strong ongoing effort is aiming at reducing uncertainties in the hadronic contributions, but there's no indication that these corrections alone can reconcile the discrepancy. The latest results published by Fermilab last August [135] bring the new world average for the measurement of $(g-2)_\mu$ to $a_\mu^{comb} = 116\ 592\ 059\ (22) \times 10^{-11}$, which deviates around 5.1σ compared to the SM prediction. This discrepancy is however expected to lower once the Muon $g-2$ Theory Initiative provides updated results.

A remark must be made about the anomalous muon magnetic moment. A lattice computation carried out by the BMW collaboration [136] has revealed a significant 2.1 σ deviation from the value reported in [132]. With the incorporation of the BMW findings, the disparity between theoretical predictions and experimental data diminishes to an average of 1.5 σ. The intricate nature of the muon magnetic moment continues to hold numerous unanswered questions, leaving its "anomalous" nature still uncertain. Despite this ambiguity, the focus of our study shifts towards investigating a Beyond the Standard Model explanation as a means to account for the observed discrepancy.

4.4 ProtoDUNE Searches for Dark Sectors particles

Constructed as part of the Deep Underground Neutrino Experiment (DUNE) project, ProtoDUNE consists of two prototype detectors designed to test and validate the technologies and design that will be applied to the construction of the DUNE Far Detector [137, 138].

ProtoDUNE is located at CERN Neutrino Platform. Secondary particles produced in the interaction between protons extracted from the CERN Super Proton Synchrotron (SPS) and targets in the CERN North Area targets, can reach the detectors. The proton collisions in the primary target may generate a flux of BSM particles that could leave a visible signal in the ProtoDUNE detectors, as suggested in [5]. The detectors are two kiloton-scale liquid Argon Time Projection Chambers (LArTPCs). The advantage of LArTPCs resides in their excellent imaging

capabilities: when a particle passes through the liquid argon, it ionizes the atoms, creating electron-ion pairs. An electric field then drifts the electrons towards a readout plane, where their positions are recorded in three dimensions. This allows to reconstruct the path and energy of the interacting particle. Additionally, the time synchronization with the beam can significantly reduce possible background sources, e.g. cosmic rays.

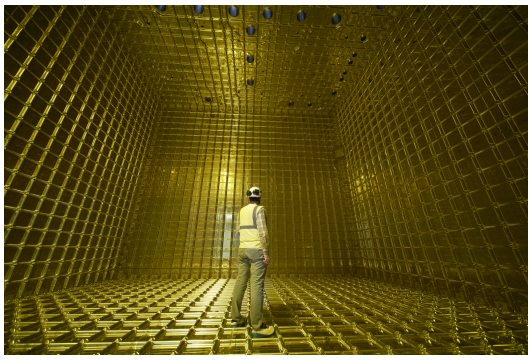

FIGURE 4.2: ProtoDUNE photo from [139]

A second advantage of this proposal is the possibility to explore wider regions of the phase space compared to other neutrino experiments, due to the highly energetic proton beam (∼400 GeV). This allows to abundantly produce light short-lived mesons (π_0, η, η', ..) and heavier short-lived mesons such as D, D_s, B, and Υ. This beam configuration does not allow to study longer lived mesons, such as charged kaons and pions, as they are deviated by a set of magnets located after the primary target. ProtoDUNE can be used to study both unstable and stable weakly interacting particles produced in this manner. In this work, we focus only on stable particles, which as we will see can be considered a dark matter candidate.

4.4.1 Experimental Setup

The two large DUNE Far Detector prototypes (NP02 and NP04) are located at the CERN Neutrino platform. The first ProtoDUNE detector, ProtoDUNE-SP (NP04), began taking data in 2018. With ∼750 tonnes of LAr, ProtoDUNE is the largest LArTPC ever operated. The second ProtoDUNE detector, ProtoDUNE-DP (NP02), started operations in 2019.
In order to generate the secondary beam within CERN's North Area, the high-energy proton beam, extracted from the SPS accelerator, is directed towards a thin (50cm) Beryllium target (T2). Secondary particles are then selected using magnetic spectrometers and transported to various experimental areas. The ProtoDUNE detectors are aligned with the secondary H2/H4 beamlines, and thus with the primary target T2.

Annually, approximately 3.5×10^{18} protons on target (PoT) are dumped against T2. The incoming angle of the proton beam is defined via a set of magnets, such that it can vary from 0 to 10 mrad. The remaining protons are redirected towards a 3.2-meter expanse of iron, which

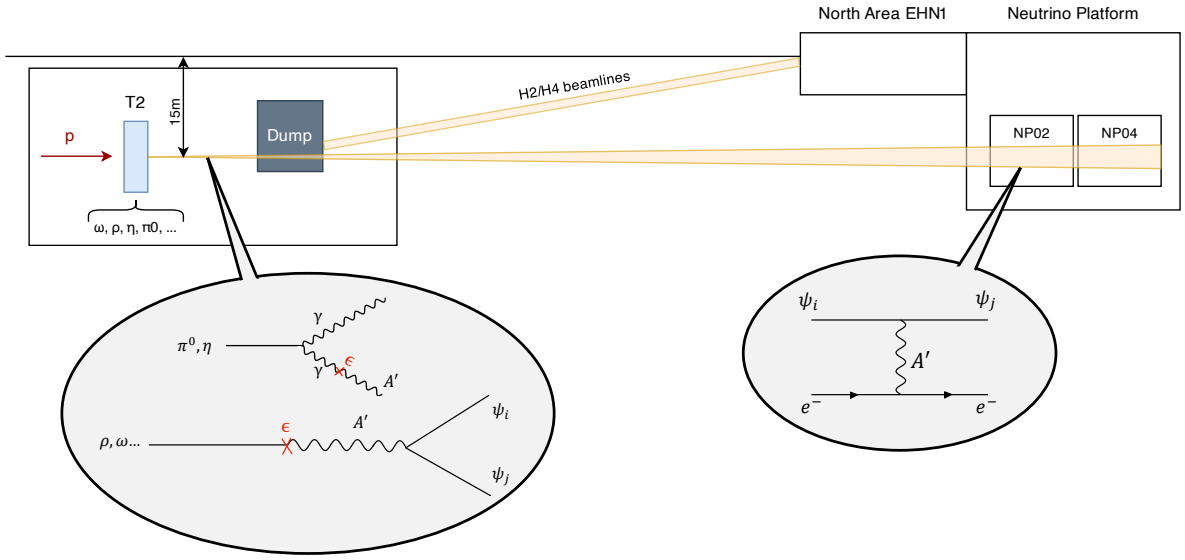

FIGURE 4.3: Sketch of ProtoDUNE experiment

acts as a dump (TAX). Positioned 15 meters below the surface for radiation containment, the T2 target is surrounded by an array of magnets, collimators, and additional beamline components.

This setup allows the production of a flux of BSM particles, capable of reaching the detectors. We only consider the first detector that they encounter, NP02, with fiducial volume V_{det}=6m $\times$ 7m $\times$ 6m, positioned at a distance of L =610 meters from T2. The background arising from standard model neutrinos is reduced by the presence of magnets, that redirect any residual protons and charged particles. Cosmic rays could still represent a potential source of interference, but the implementation of precise timing cuts has the potential to diminish this background noise as well.

4.4.2 ProtoDUNE dark photon searches

We will now delve into how the various models introduced in 4.2 can be investigated in ProtoDUNE. The goal is to study the sensitivity of ProtoDUNE to dark photon mixing ε and masses $m_{A'}$, complementing the work of [4]. We will first examine the different channels for dark photon production and its decay. The dark sectors HNFs originating from the dark photon decay will then reach the ProtoDUNE detectors, where they can interact with e.g. electrons.

The number of events in the detector can be written as [5]

$$N_{events} = \epsilon_{det} N_{PoT} N_{trg} \langle \sigma \rangle \Phi^{\chi}, \tag{4.25}$$

where N_{trg} is the number of targets in the fiducial volume of the detector. One can get the fluxes Φ^{χ} by integrating the values in the right panel of 4.4. We get:

$$N_{events} = \epsilon_{det} N_{PoT} N_{trg} \langle\sigma\rangle BR(M \to \psi_i \psi_j + ...) I \times \mathrm{PS}\left(\frac{m_\chi^2}{m_M^2}\right), \tag{4.26}$$

with

$$\langle\sigma\rangle = \frac{1}{\Phi}\int_0^\infty dE_{\psi_i} \int_{E_{e,min}}^{E_{e,max}} dE_e \frac{d\sigma}{dE_e}\left(E_{\psi_i}\right)\frac{d\Phi}{dE_{\psi_i}}. \tag{4.27}$$

I is simply the number obtained by integrating the plots in 4.4 and PS is the phase space suppression for massive final states, given by[140]

$$PS(x) = \frac{2}{3\pi}\int_{4x}^1 dz \sqrt{1-\frac{4x}{z}}\frac{1-z}{z^2}\left(12x^3 + 6x^2(3z-2) + x(5z-2)(z-1) + z(z-1)^2\right) \tag{4.28}$$

for the vector meson and by

$$PS(x,y) = \frac{(1+2x)\sqrt{1-4x}}{(1+2y)\sqrt{1-4y}} \tag{4.29}$$

for the pseudoscalar. In this case in 4.26 the phase space will be $PS\left(\frac{m_\chi^2}{m_M^2}, \frac{m_e^2}{m_M^2}\right)$, where m_e is the mass of the electron. From 4.26 it is possible to extrapolate ProtoDUNE sensitivities, as shown in the right panel in figure 4.4.

4.4.3 HNFs production

When the protons from SPS hit the T2 target, the proton collisions create unstable mesons that can produce dark photons as they decay.

π^0	η	ρ	ω	ϕ	J/ψ	Υ
4.03	0.46	0.54	0.53	0.019	$4.4 \cdot 10^{-5}$	$2.3 \cdot 10^{-8}$

TABLE 4.1: Production yield (normalized per PoT) for each of the parent particles considered in this work. [5]

We will focus on two classes of production processes: 1) secondary meson decay and 2) vector meson mixing. In proton fixed target experiments, it could also be produced in Drell-Yan processes [140–142], but we will not discuss this particular class of production mechanism. This leaves the ground for further analysis.

Pseudoscalar meson decay

For low mass vectors, the dominant production mode is via radiative decay of pseudoscalar mesons $\varphi = \pi^0, \eta$ [104]. For masses of the dark photon smaller than the mass of the parent

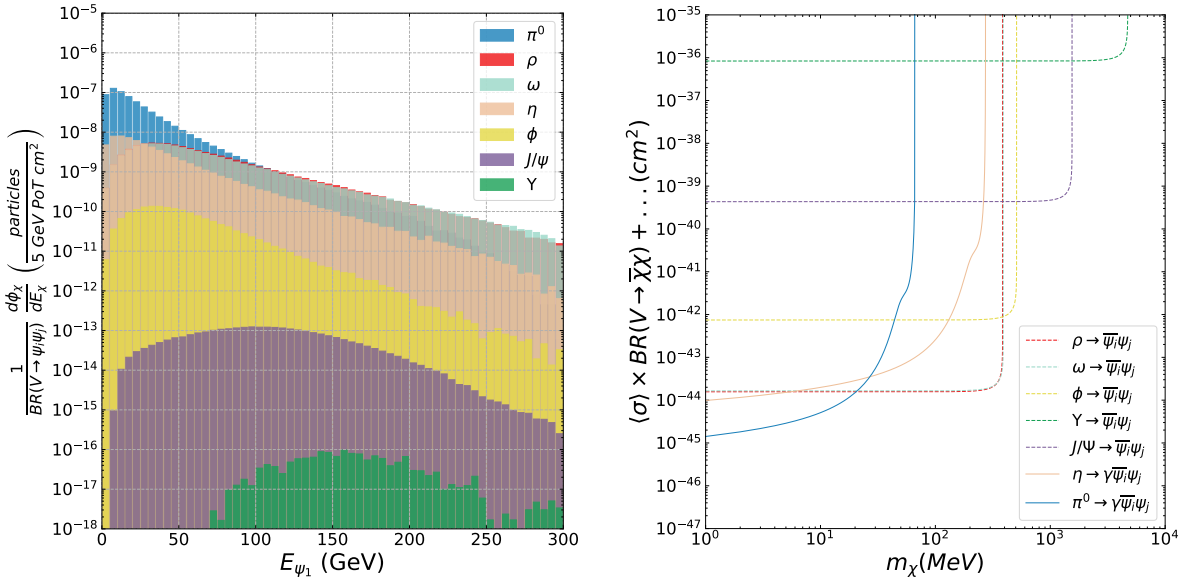

FIGURE 4.4: Expected fluxes and sensitivity to stable, weakly interacting particles in ProtoDUNE [5]. (Left) Flux of stable particles that would enter the fiducial volume of ProtoDUNE as a function of the energy of the stable particle. The fluxes have been computed for $m_\chi = 50$ GeV. (Right) Model-independent sensitivities, assuming no background and perfect detection efficiency, computed from eq. 4.26. The region above each line would lead to a number of events above 2.44 in 5 years of data taking.

meson, the DP is produced on-shell and subsequently decays into HNFs. This requires satisfying the condition $m_{A'} < m_{\pi^0,\eta}$. The branching ratio for this process is

$$BR(\varphi \to \gamma A' \to \gamma\overline{\psi_i}\psi_j) = BR(\varphi \to \gamma A') \times BR(A' \to \overline{\psi_i}\psi_j), \tag{4.30}$$

where

$$BR(\varphi \to \gamma A') = 2\varepsilon^2 \left(1 - \frac{m_{A'}^2}{m_\varphi^2}\right)^3. \tag{4.31}$$

In the limit $\alpha_D \ll \varepsilon^2\alpha_{QED}$, we can take $BR(A' \to \overline{\psi_i}\psi_j) \approx 1$.

When $m_{A'} \ll m_i + m_j$ or $m_{A'} \gtrsim m_\varphi$, the on-shell approximation is not applicable and the HNFs are produced through a tree-body decay [142]. In appendix D, we explore this point in more detail.

Vector meson mixing

For masses of the dark photon close to the mass of the vector meson, resonant production via mixing becomes relevant [143]. In this case, the dark photon is produced off-shell and subsequently decays into DS particles. The channel considered will be $V \to A'^* \to \overline{\psi_i}\psi_j$.

The branching ratio is

$$\frac{BR(V \to \overline{\psi}_i \psi_j)}{BR(V \to e^+e^-)} = \sum_{i,j} \left(\frac{V_{ij} g_D \varepsilon}{e}\right)^2 \frac{m_V^4}{(m_V^2 - m_{A'}^2)^2 + m_{A'}^2 \Gamma_{A'}^2} I_{ij}(m_i, m_j, m_V), \tag{4.32}$$

where I_{ij} is the phase-space suppression due to massive final states:

$$I_{ij}(m_i, m_j, m_V) = \left(1 - \frac{\delta_{ij}^2}{m_V^2}\right)\left(1 + \frac{m_{ij}^2}{2m_V^2}\right)\sqrt{\left(1 - \frac{\delta_{ij}^2}{m_V^2}\right)\left(1 - \frac{m_{ij}^2}{m_V^2}\right)}, \tag{4.33}$$

with $\delta_{ij} = m_i - m_j$ and $m_{ij} = m_i + m_j$. Details on the computation can be found in Appendix D

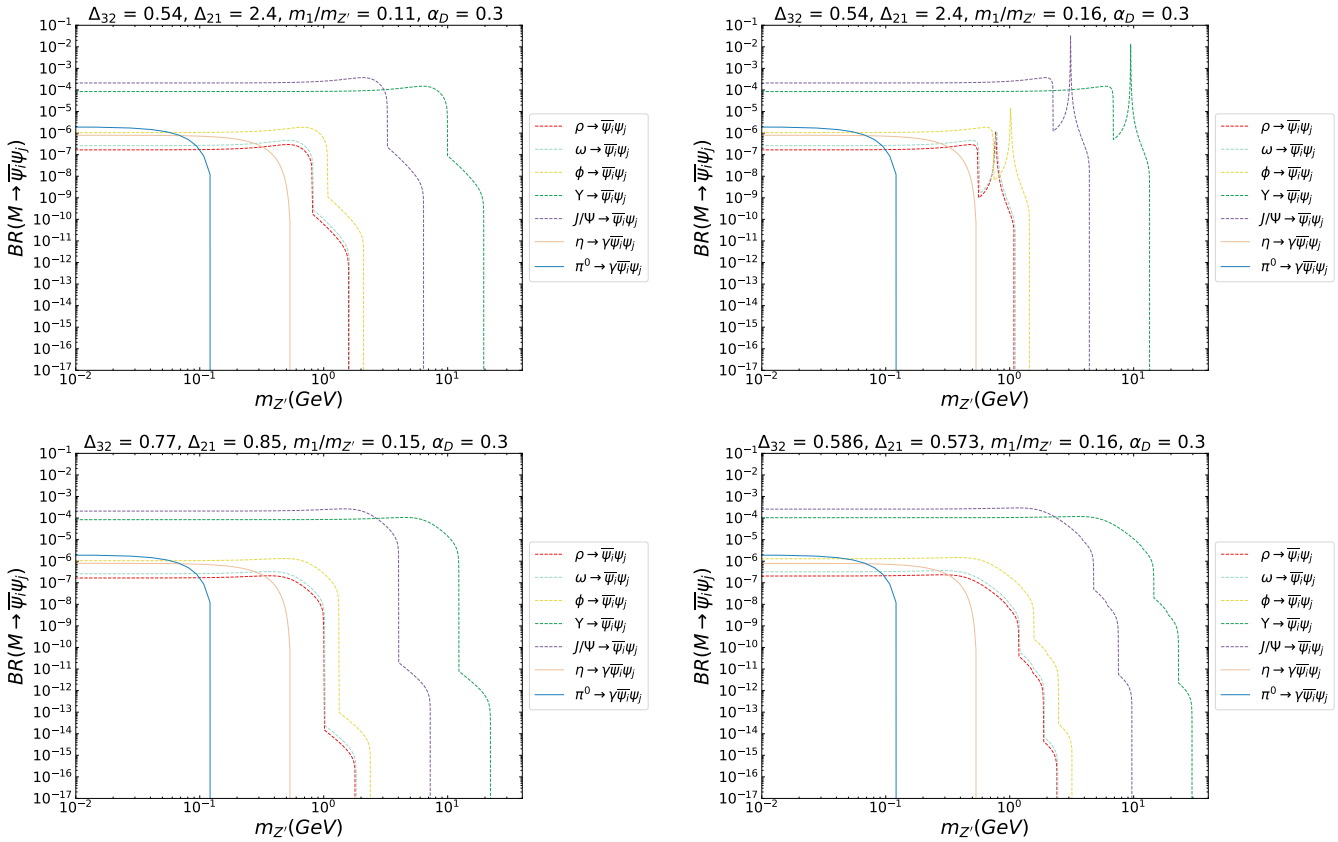

FIGURE 4.5: Branching ratio for the production of HNFs for different parent mesons for BP4a (top left), BP4b (top right), BP4c (bottom left) and BP5 (bottom right).

In 4.5 we plot the branching ratio for the different channels, taking the BP4a-c/5 in 4.2 and $\varepsilon \sim 10^{-3}$. As discussed above, the HNFs are produced through the decay of pseudoscalar or vector mesons. In the case of pseudoscalar decay, we consider on-shell production of the dark photon, which subsequently decays into dark currents. On the other hand, for vector meson decay, the dark photon is produced off-shell to ensure the mixing between the dark photon and the vector meson. This process is kinematically allowed for $m_i + m_j < m_V$.

We can make some comments on the shape of the curves in 4.5. In BP4b, the channel $A' \to \psi_2\psi_3$ is forbidden. In fact, in order to kinematically allow this channel, we must have:

$$m_{Z'} > m_2 + m_3 \implies r < \frac{1}{(\Delta_{21}+1)(\Delta_{32}+2)} \approx 0.116,$$

where $r = m_1/m_{A'}$ and $\Delta_{ij} = (m_i - m_j)/m_j$. We can observe that BP4a and BP4b are identical in the values of the different parameters, with the exception of the values of r. The above condition is indeed realized in BP4a, allowing an additional decay channel for the dark photon into dark current, leading to a longer lifetime for the dark photon $\Gamma_{A'}$. The change in the value of the decay width of the dark photon has an impact on the decay channel of the vector mesons. In equation 4.32, $\Gamma_{A'}$ appears in the denominator of the branching ratio. When the mass of the dark photon is comparable with the mass of the vector meson, $m_{A'} \sim m_V$, there will be a resonant production of the dark photon and the shape of this resonance will be dictated solely by the value of $\Gamma_{A'}$. Therefore, a higher value of the decay width will suppress the resonance, while a smaller value will result in a peak. For BP5, the resonance is particularly suppressed. This is reasonable in light of the fact that many more decay channels are allowed in the case of this benchmark, implying a larger dark photon width.

Instead, to explain the bumps that appear in the graphs, it is necessary to analyze which decay channels are allowed as the dark photon mass varies. Using $r = m_1/m_{A'}$, $\Delta_{21} = (m_2 - m_1)/m_1$ and $\Delta_{32} = (m_3 - m_2)/m_2$ is possible to find a relation between $m_{A'}$ and m_V starting from the condition $m_i + m_j \leq m_v$:

$$m_1 + m_2 < m_V \implies m_{A'} < \frac{m_V}{r(\Delta_{21}+2)},$$
$$m_2 + m_3 < m_V \implies m_{A'} < \frac{m_V}{r(\Delta_{21}+1)(\Delta_{32}+2)}.$$

For BP4a, this means that the second channel is forbidden for $m_{A'} \sim m_V$, while the first one is for $m_{A'} \sim 2m_V$.
For BP4b, this means that the second channel is forbidden for $m_{A'} \sim 0.7m_V$, while the first one is for $m_{A'} \sim 1.4m_V$.
For BP4c, this means that the second channel is forbidden for $m_{A'} \sim 1.3m_V$, while the first one is for $m_{A'} \sim 2.3m_V$.
In the case of BP5, since also the channels $\{\psi_1\psi_1,\ \psi_2\psi_2,\ \psi_3\psi_3,\ \psi_1\psi_3\}$ are allowed, more than two bumps appear. This is compatible with the results shown in Figure 4.5, explaining why the branching ratio for the vector mesons suddenly diminishes for specific values of $m_{Z'}$.

In the case of the pseudoscalar, the branching ratio does not depend on the BP considered. This is evident from eq. 4.31, where only the value of $m_{A'}$ enters. The total branching ratio of the pseudoscalar is $BR(\pi^0, \eta \to \gamma\psi_i\psi_j) = BR(\pi^0, \eta \to \gamma A') \times BR(A' \to \psi_i\psi_j)$, where $BR(A' \to \psi_i\psi_j)$ is approximately always 1.

4.4.4 HNFs detection

At this point we have a flux of dark sector particles produced by parent mesons that can reach the detector. In these computations, we have assumed that all HNFs decay promptly into the lightest, stable particle and that only the DM candidate reaches the detector. However, it's worth noticing that, depending on the specific BPs being considered, the lifetimes of the heaviest HNFs could be extended, potentially allowing them to reach the detector without decaying. To analyze more precisely this aspect, a more comprehensive Monte Carlo simulation could be conducted. Note that even if the heaviest HNFs were to reach the detector without decaying, they would still be capable of interacting and leaving a visible signature.
We will work under the assumption that only the ψ_1 particles arrive at the detector, interacting with the electrons through the exchange of a dark photon. The cross section for $\psi_i + e^+ \to \psi_j + e^-$ is [144]:

$$\frac{d\sigma}{dE_e} = 4\pi\varepsilon^2\alpha_{QED}\alpha_D V_{ij}^2 \frac{2E_{\psi_i}^2 m_e + g(E_e)/2}{(E_{\psi_i}^2 - m_i^2)(m_{A'}^2 + 2m_e E_e - 2m_e^2)^2}, \tag{4.34}$$

where

$$g(E_e) = 2E_{\psi_i}\big(m_i^2 - m_j^2 + 2m_e(m_e - E_e)\big) - m_i^2 E_e - (2m_e - E_e)\big(m_j^2 - 2m_e(m_e - E_e) - 2m_i m_j\big),$$

with V_{ij} the value of the dark photon coupling vertices to HNFs, m_i the mass of the i-th HNF, E_e the electron recoil energy and E_{ψ_i} the energy of the incoming HNF. The full computation can be found in Appendix E. Considering, in particular, the case of $E_{\psi_i} \gg m_j - m_i$, the cross section is given by:

$$\frac{d\sigma}{dE_e} = 4\pi\varepsilon^2\alpha_{QED}\alpha_D V_{ij}^2 \frac{2m_e E_{\psi_i}^2 - f(E_e)(E_e - m_e)}{(E_{\psi_i}^2 - m_i^2)(m_{A'}^2 + 2m_e E_e - 2m_e^2)^2} \tag{4.35}$$

with $f(E_e) = 2m_e E_{\psi_i} - m_e E_e + m_i^2 + 2m_e^2$. The differential cross section will be integrated between the minimal and maximal energy for electron recoils, where $E_{e,min}$ will be the detection threshold for electron recoils at ProtoDUNE, estimated to be (conservatively) 30 MeV. $E_{e,max}$ is the maximal achievable recoil, depending on the kinematic of the process.

Kinematic features. The maximum mass that the up-scattered particle ψ_j can have is $\sqrt{s} - m_e$, where $\sqrt{s}$ is the center-of-mass energy $s = m_e^2 + 2E_{\psi_i}m_e + m_{\psi_i}^2$. This means that:

$$m_{\psi_j} \leq \sqrt{m_e^2 + 2E_{\psi_i}m_e + m_{\psi_i}^2} - m_e. \tag{4.36}$$

This translates into a constraint on the minumum value that E_{ψ_i} can have to allow the process:

$$E_{\psi_i} \geq \frac{m_j^2 - m_i^2 + 2m_j m_e}{2m_e}. \tag{4.37}$$

The maximum achievable recoil energy is:

$$E_e^{max} = \frac{(s + m_e^2 - m_j^2)(E_{\psi_i} + m_e) + \lambda^{1/2}(s, m_e^2, m_j^2)p_i}{2s}, \tag{4.38}$$

with $p_i = \sqrt{E_{\psi_i}^2 - m_i^2}$ and $\lambda(x, y, z) = (x - y - z)^2 - 4yz$.

The relevant quantity in our computations is the average cross section $\langle\sigma\rangle$, expressed as:

$$\langle\sigma\rangle = \frac{1}{\Phi}\int_0^\infty dE_{\psi_i} \int_{E_{e,min}}^{E_{e,max}} dE_e \frac{d\sigma}{dE_e}(E_{\psi_i}) \frac{d\Phi}{dE_{\psi_i}}, \tag{4.39}$$

where $E_{e,min}$ is the minimum observable recoil energy (taken to be 30 MeV), and $E_{e,max}$ depends on the kinematics. The value Φ is the flux of incoming particles whose trajectories intersect the detector, as displayed in 4.4. The result obtained for the average cross section for BP4a and a mass of the dark photon of 100 MeV is shown in 4.6.

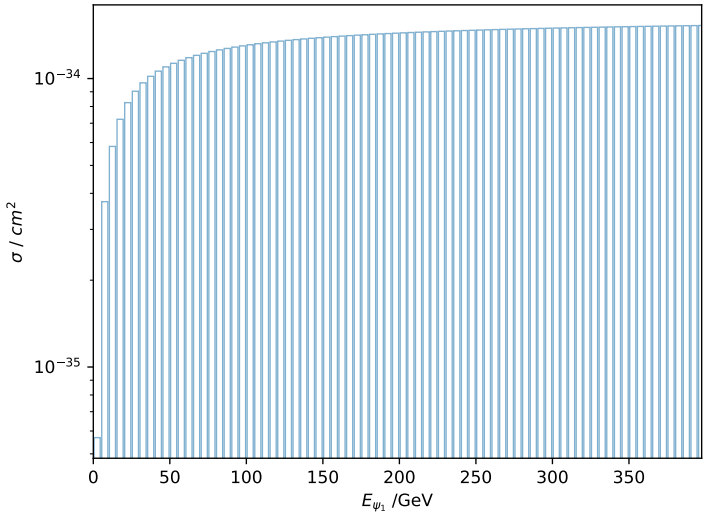

FIGURE 4.6: Inelastic electron scattering cross section for different values of the energy of the incoming stable particle.

We are then left to compute:

$$\langle\sigma\rangle = \frac{1}{\Phi}\int_0^\infty dE_{\psi_1}\sigma(E_{\psi_1})\frac{d\Phi}{dE_{\psi_1}}. \tag{4.40}$$

To compute the total flux, we need to consider the information provided in Figure 4.4. The flux can be approximated by discretizing the integral.

$$\Phi = \sum_i \left(\frac{d\Phi}{dE_{\psi_1}}\right)_i \Delta E_{\psi_1} BR(V \to \psi_i\psi_j).$$

In a similar fashion, we also discretize the integral in 4.40:

$$\langle\sigma\rangle = \frac{\sum_i \sigma_i \left(\frac{d\Phi}{dE_{\psi_1}}\right)_i \Delta E_{\psi_1} BR(V \to \psi_i\psi_j)}{\sum_i \left(\frac{d\Phi}{dE_{\psi_1}}\right)_i \Delta E_{\psi_1} BR(V \to \psi_i\psi_j)}.$$

Since both the integral and the branching ratios are constants, they can be factored out of the summation. Thus, the final expression can be simplified as follows:

$$\langle\sigma\rangle = \frac{\sum_i \sigma_i \left(\frac{d\Phi}{dE_{\psi_1}}\right)_i}{\sum_i \left(\frac{d\Phi}{dE_{\psi_1}}\right)_i}. \tag{4.41}$$

4.5 Results

In this section, we show the results from the recasting of ProtoDUNE sensitivities in [5] to the semi-visible dark photon model presented in this thesis. A rough estimate of the kinetic mixing can be done considering the cross section in E. We have:

$$\sigma \sim \varepsilon^2 10^{-38} cm^2 \tag{4.42}$$

$$\begin{aligned} \frac{\sigma \times BR(\pi^0 \to \gamma\psi_i\psi_j)}{10^{-38}cm^2} &\sim \varepsilon^2 BR(\pi^0 \to \gamma A') \times BR(A' \to \overline{\psi_i}\psi_j) \\ &\sim 2\varepsilon^4 \left(1 - \frac{m_{A'}^2}{m_\pi^{02}}\right)^3 BR(\pi^0 \to \gamma\gamma). \end{aligned} \tag{4.43}$$

If we take the sensitivities in Figure4.4 and the $BR(\pi^0 \to \gamma\gamma) = 99\%$, we can be sensitive to values of $\varepsilon \sim 10^{-2}$, in the absence of background.

A summary of the values considered for this BP is given here:

BP	model	r	Δ_{21}	Δ_{32}	α_D	V_{11}	V_{21}	V_{22} /10^{-2}	V_{31}	V_{32}	V_{33}	Comments
1a	iDM	1/3	0.5	-	0.5	0	1	0	-	-	-	-
1b	iDM	1/3	0.4	-	0.1	0	1	0	-	-	-	-
2a	mixed-iDM	1/3	0.3	-	0.5	0	$s_\alpha c_\alpha$	c_α^2	-	-	-	$\alpha = 8°$
2b	mixed-iDM	1/3	0.3	-	0.5	0	$s_\alpha c_\alpha$	c_α^2	-	-	-	$\alpha = 4°$
3a	i2DM	1/3	0.4	-	0.5	s_β^2	$s_\beta c_\beta$	c_β^2	-	-	-	$\beta = 8.6°$
3b	i2DM	1/3	0.4	-	0.5	s_β^2	$s_\beta c_\beta$	c_β^2	-	-	-	$\beta = 4.6°$
3c	i2DM	1/3	0.4	-	0.5	s_β^2	$s_\beta c_\beta$	c_β^2	-	-	-	$\beta = 2.3°$
3d	i2DM	1/3	0.4	-	0.5	s_β^2	$s_\beta c_\beta$	c_β^2	-	-	-	$\beta = 1.1°$
4a	3HNFs	0.11	2.44	0.54	0.3	0	3.9	0	0	99	0	-
4b	3HNFs	0.16	2.44	0.54	0.3	0	3.9	0	0	99	0	-
4c	3HNFs	0.15	0.85	0.77	0.3	0	0.10	0	0	99	0	-
5	3HNFs	0.16	0.573	0.586	0.3	0.40	7.8	8.3	2.8	98	69	-

TABLE 4.2: Summary of the benchmark points considered in [4]. In particular, $r = m_1/m_{A'}$ and $\Delta_{ij} = (m_i - m_j)/m_j$. V_{ij} are the dark photon coupling vertices.

4.5.1 Inelastic Dark Matter

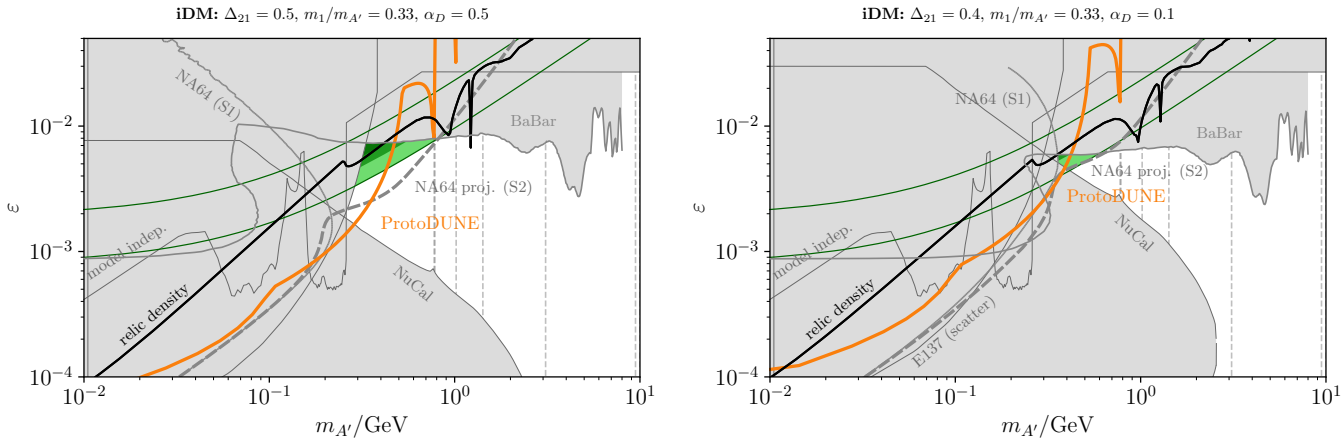

FIGURE 4.7: The kinetic mixing ε as a function of the mass $m_{A'}$ for BP1a (left), BP1b (right), corresponding to the inelastic Dark Matter model. Assuming the lightest HNF to be a dark matter candidate, the relic density is displayed in black. Sensitivities from ProtoDUNE are shown in orange. The grey areas are constraints on the semi-visible dark photon model from [4].

BP1a/b - The results of the iDM benchmark are depicted in Figure 4.7. The preferred region for the explanation of the Δa_μ is already covered by searches at NA64 with signatures of the type S2, as discussed in [4]. Searches at ProtoDUNE are able to cover only a small part of the parameter space that has not already been excluded by other searches.

BP1a and BP1b differs only for the values of $\Delta_{21} = (m_2 - m_1)/m_1$ and α_D. Varying Δ_{21} has an impact on the lifetime of ψ_2, but this is beyond the reach of our computations. However, also the branching ratio of the mesons in HNFs and the scattering cross sections depend on these

two parameters. An increase in the value of α_D translates into a bigger branching ratio and cross sections since both are $\propto \alpha_D$. This implies an enhanced sensitivity to the kinetic mixing ε, which is indeed what we observe in 4.7. In particular, both in the case of iDM and 3HNFs, we have Majorana fermions, with the implications that this has on the Feynman rules as discussed in Appendix C. As anticipated, the semi-visible dark photon model relaxes constraints coming from BaBar and NA64, opening up the part of the parameter space that could account for the anomalous muon magnetic moment. In particular, in BP1a, this region would also be able to account for the DM relic density. In figures 8 and 9 in [4] it has additionally been explored the parameter space of $\alpha_D/m_{A'}$ and $\Delta_{21}/m_{A'}$ to check whether it was possible to accommodate the constraints coming from experiments and the relic density, fixing the value of ε to that necessary to explain Δa_μ. CMB limits, in this case, are not applicable since DM self-annihilation is forbidden by the C-symmetry.

4.5.2 Mixed iDM

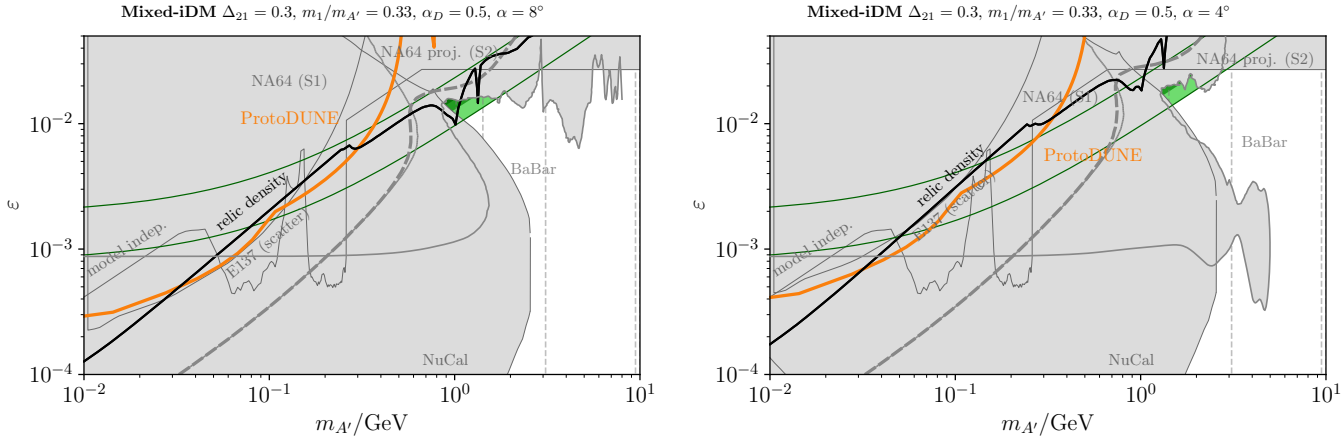

FIGURE 4.8: Same as 4.7 but for BP2a (left), BP2b (right), corresponding to the mixed-iDM model. The two BP differs only for the value of the angle α.

BP2a/b - The mixed-iDM benchmark results are illustrated in Figure 4.8. In this scenario, there is only a small window open for the explanation of the anomalous muon magnetic moment. In contrast to the case of inelastic dark matter, one of the two hidden neutral fermions (HNFs) in this scenario is a Dirac fermion, while the other is a Majorana fermion. Additionally, the channel $A' \to \psi_2\psi_2$ becomes accessible with a mixing of $V_{22} \sim 10^{-2}$ for small values of the angle, while the channel $A' \to \psi_1\psi_2$ is subdominant. The difference between BP2a and BP2b resides solely in the value of α, that enters in our computations only through V_{12} ($V_{22} \sim 10^{-2}$ for $\alpha = 4°, 8°$). For those values of the angle, $V_{12} \propto \alpha$. In BP2b we therefore expect a reduced sensitivity in the value of ε, as observed in 4.8. No new region of the parameter space is covered by searches for this model at ProtoDUNE as the sensitivities found are already excluded by other dark photon searches.

For this specific model, DM relic density and the explanation of Δa_μ can be simultaneously achieved for masses $m_{A'} \sim 0.9 - 1.2$ GeV in BP2a, while in BP2b ψ_1 would be overabundant in the region of parameter space that explain Δa_μ.

4.5.3 Inelastic Dirac Dark Matter

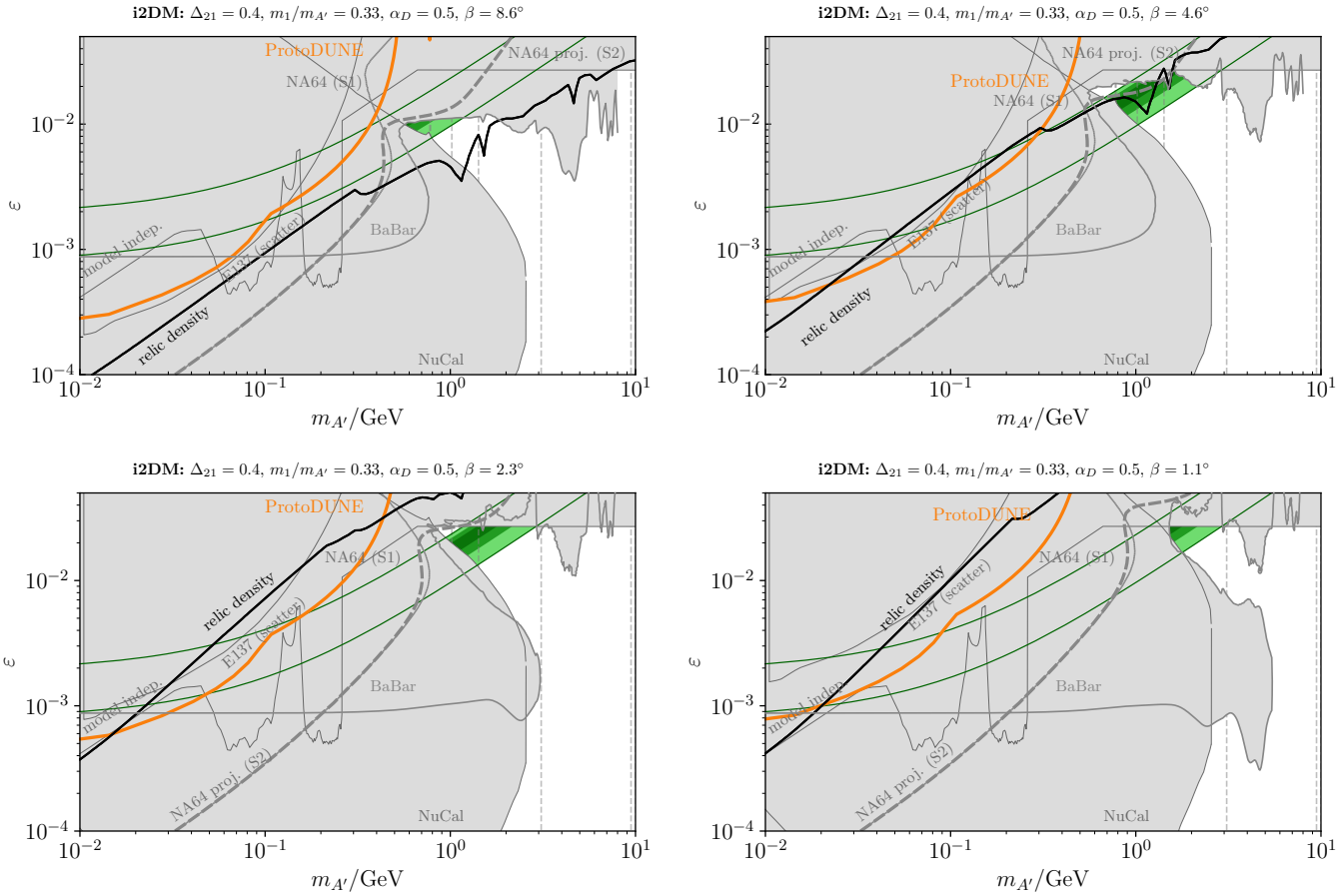

FIGURE 4.9: Same as 4.7 but for BP3a (top left), BP3b (top right), BP3c (bottom left) and BP3d (bottom right), corresponding to the inelastic Dirac dark matter model. The three plots differ only for the value of β.

BP3a-d - The results of i2DM are shown in figure 4.9. This BP is similar to the case of mixed-iDM, with the exception that now both HNFs are Dirac and that the dark photon can also decay in $\psi_1\psi_1$. This channel is however very suppressed as $V_{11} = s_\beta^2$, where β takes very small values, meaning $s_\beta^2 \to 0$. As in the previous case, we expect the sensitivity to diminish as the angle β gets smaller. For this model, searches at ProtoDUNE do not seem to yield any positive results, as the sensitivities found here are already excluded by other dark photon searches.

For what concerns a DM explanation in the inelastic Dirac dark matter scenario, we see that in BP3a the whole region for the explanation of Δa_μ can give the correct DM relic density. In BP3c and BP3d, ψ_1 would be overabundant in the entire region of parameter space that explain

Δa_μ. In figure 13 of [4], also bounds from CMB are shown as in this benchmark self-annihilation of ψ_1 are allowed, even if suppressed. What is observed is that the regions of parameter space where ψ_1 is underabundant and compatible with other constraints are excluded by CMB bounds.

4.5.4 Three Majorana HNFs

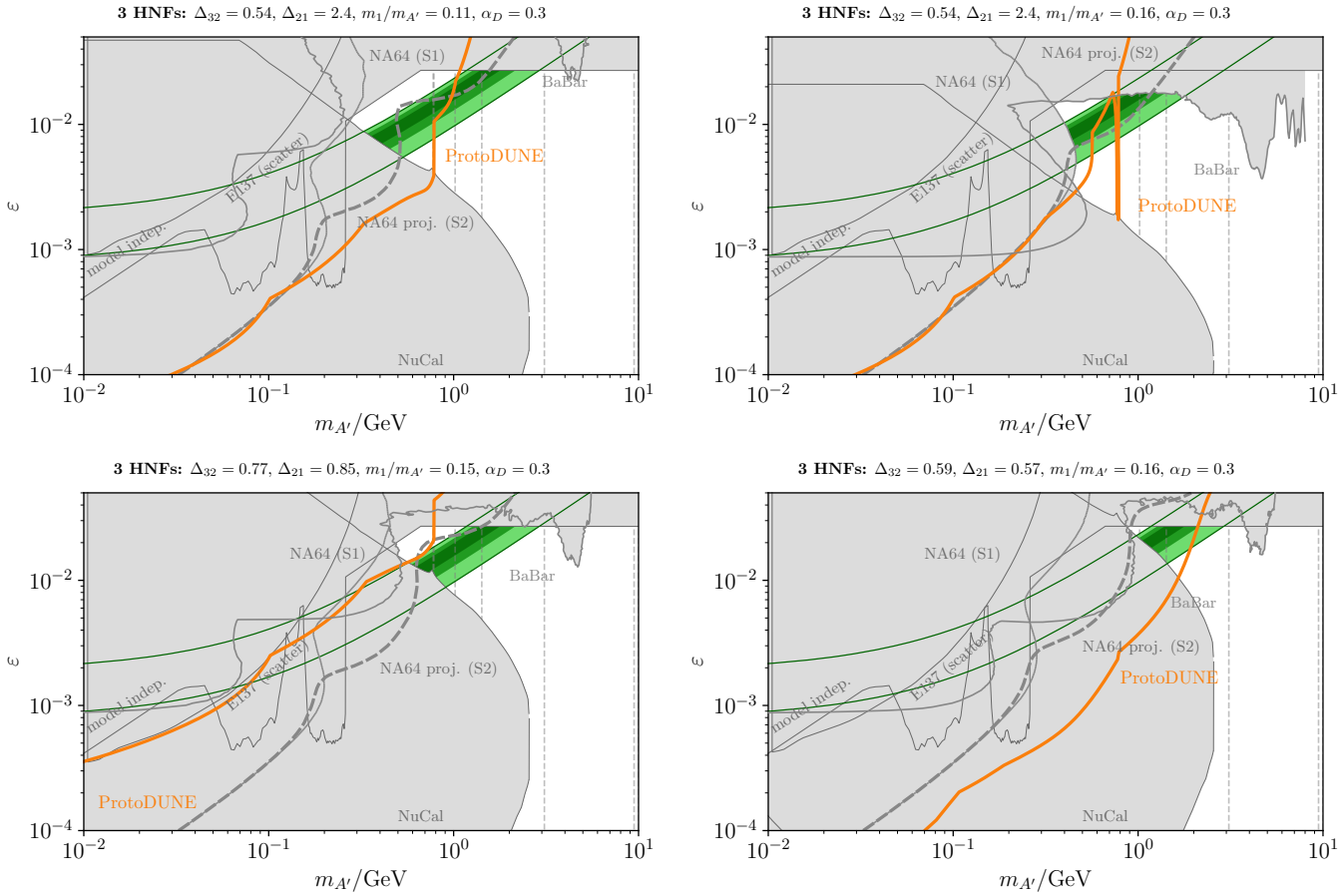

FIGURE 4.10: Same as 4.7 but for BP4a (top left), BP4b (top right), BP4c (bottom left) and BP5 (bottom right), corresponding to the 3 Majorana HNFs model.

BP4a-c - In figure 4.10 we show the expected sensitivity of ProtoDUNE compared to previous limits in the literature for the semi-visible dark photon as a function of the kinetic mixing ε with respect to the mass of the dark photon $m_{A'}$. In both BP4a and BP4b, the expected sensitivity would allow us to test part of the parameter space for the explanation of Δa_μ. The best result would be obtained for BP4a, where it expands the sensitivity reached by NA64-proj., covering masses for the dark photon between 5×10^{-1} - 1 GeV. In BP4b only a very small part of the parameter space is opened by searches at ProtoDUNE. For BP4c the analysis doesn't reveal any new sector of the parameter space. The drop in sensitivity stems from a diminished value of $|V_{21}|^2$. In BP4a, this value stands at 3.9×10^{-2}, whereas in BP4c, it's reduced further to 0.10×10^{-2}. This leads to a substantial ratio of 4×10^{-1} between ε_a and ε_c, as can be observed

in the plot. In BP4b the spike corresponds to the resonance in the vector meson decay that we discussed before. Due to the peculiar model considered, we expect that most ψ_2 produced in the up-scattering will promptly decay, leaving a unique signature in the detector with an excess of electron recoil.

BP5 - This benchmark differs from the previous one for a stronger hierarchy between the HNFs masses. In this case, all possible decay channels are available. While in BP4 only off-diagonal couplings were allowed, namely:

$$\begin{aligned} &A' \to (N_2 \to N_1 e^+ e^-)(N_3 \to ((N_2 \to N_1 e^+ e^-)e^+ e^-) \\ &A' \to (N_2 \to N_1 e^+ e^-)N_1, \end{aligned} \tag{4.44}$$

in this benchmark all couplings are possible. This results in an enhancement of both the branching ratio and the cross-section, leading to improved sensitivities in the parameter space and covering almost the entire region for the Δa_μ explanation up to $m_{A'} \sim 2$ GeV.

This model is usually more studied in the context of neutrino mass generation, for example in [103], since coannihilations are strongly suppressed.

4.6 Outlook

In the preceding section, we presented the outcomes of our analysis concerning the semi-visible dark photon model at ProtoDUNE. As elucidated in [4], this model extends the parameter space available for explaining the $(g-2)_\mu$ anomaly through the existence of a dark photon. Our findings corroborate that ProtoDUNE searches can effectively probe previously unexplored regions within the dark photon's mass $m_{A'}$ and mixing parameter space ε. This is especially pertinent when considering scenarios involving three distinct Majorana HNFs, characterized by hierarchical masses, in contrast to pseudo-Dirac pairs with negligible mass differences, as observed in the mixed-iDM scenario.

In BP1, the simplest case of Inelastic Dark Matter, we observed that ProtoDUNE can complement the projected investigations by NA64 for the semi-visible dark photon, as discussed in [4], represented by the dotted line labelled N2 in 4.7. The presence of two distinct Majorana states significantly enhances both the cross section and branching ratio, resulting in heightened sensitivities at ProtoDUNE. In the cases of BP2 and BP3, corresponding to mixed-iDM and Inelastic Dirac dark matter, respectively, ProtoDUNE's sensitivity is markedly lower. In these instances, ProtoDUNE does not yield additional positive results, as the parameter space covered by these searches has already been excluded by other experiments.

Notably, in BP4/5, involving the presence of three Majorana fermions, ProtoDUNE demonstrates the capability to extend the parameter space further, encompassing regions previously unexplored by any other experiment. Particularly promising results are obtained for BP4a and

BP5. The distinction between BP4a and BP4b lies primarily in the value of the parameter $r = m_1/m_{A'}$, with a value of 0.11 in BP4a and 0.16 in BP4b. This has implications for the possible decay channels of the dark photon; in BP4b, the decay into $A' \to \psi_2\psi_3$ is kinematically prohibited, leading to a reduction in the branching ratio of parent mesons and the decay width of the dark photon. Moreover, this has a specific impact on the resonance's shape, as discussed in 4.4.3, resulting in a prominent spike in the curve.

In BP4c, the coupling constant V_{21} is ten times smaller, resulting in reduced sensitivity. Finally, in BP5, all possible couplings between the HNFs are permitted, leading to an increased cross section and branching ratio, thereby offering the opportunity to explore previously uncharted portions of the parameter space.

ProtoDUNE serves as an ideal experimental platform for investigating the semi-visible dark photon model, effectively extending the parameter space $\varepsilon/m_{A'}$ in certain scenarios while complementing other searches for this model. This makes it an intriguing venue for the exploration of new theoretical models. Furthermore, ProtoDUNE's operational status at CERN, without interference with other ongoing experiments in the North Area, underscores its potential as an important resource for future searches.

Conclusions

Dark sector dark matter is particularly interesting as it constitutes a different paradigm to the most common searches and studies of WIMP dark matter. The presence of light dark matter in the MeV range necessitates the existence of a new mediator that interacts both with ordinary matter and dark matter. This mediator can be a new fermion (neutrino portal), a new scalar (Higgs portal), or a new gauge boson (vector portal). In this thesis we have studied the case of a dark photon that decays semi-visibly, as presented in [4] and derived the sensitivity of ProtoDUNE to this model. Thanks to a symmetry that distinguishes DS fields from SM fields, the lightest dark sector particle appearing in the model considered here can be made stable, constituting a reasonable DM candidate. In the absence of this symmetry, the HNFs can mix with SM neutrinos and are identified as HNLs. Although ProtoDUNE is in principle capable of conducting searches for both HNFs and stable particles, our focus in this thesis has been directed solely towards the latter. Long-lived particles can be produced by SM neutrinos and decay in the detector volume, leaving visible signatures. Stable particles, on the other hand, reach the detector without decaying, interacting with the liquid Argon inside ProtoDUNE and leading to excess electron recoil. Although long-lived particles can also be searched for in this manner, we simplified our discussion to the case where only stable particles reach the detectors. It is worth noting that in our model, the stable particle can up-scatter to a heavier dark sector particle, which can subsequently decay within the detector volume. While this aspect wasn't thoroughly investigated in this particular study, it could prove useful when considering background analyses.

We have considered different models where the fermionic content in the dark sector was systematically increased, from two to four HNFs, always reducing the phenomenological model to, at most, three distinguishable states. In particular, we were interested in checking whether ProtoDUNE could cover the newly-open parameter space in the case of a semi-visible dark photon, in the region $\varepsilon \sim 10^{-3}$ - $10^{-}2$ and $m_{A'} \sim 0.3$ - 1.3 GeV. Dark photons in this mass range and with this kinetic mixing could in principle be able to explain the discrepancy between the measured anomalous magnetic moment of the muon and the SM predictions, Δa_μ. In the case of iDM and mixed-iDM, the lightest particle could also constitute a DM candidate. In the case of the i2DM, however, CMB constraints exclude the Δa_μ region. ProtoDUNE could be able to improve significantly current sensitivities in the case of the 3HNFs, in particular for BP4a and BP5, as can be seen in Fig. 4.10. In the case of BP4a, ProtoDUNE's investigations encompass a noteworthy portion of the parameter space, ranging from $\varepsilon \sim 5 \times 10^{-3}$ for $m_{A'} \sim 500$ MeV, extending up to $\varepsilon \sim 2 \times 10^{-2}$ for $m_{A'} \sim 1$ GeV, which holds significance for explaining the Δa_μ

anomaly through the dark photon 1-loop correction. For BP5, ProtoDUNE's sensitivities span from $\varepsilon \sim 10^{-2}$ for $m_{A'} \sim 1.5$ GeV to $\varepsilon \sim 2 \times 10^{-2}$ for $m_{A'} \sim 2$ GeV, effectively encompassing nearly the entire parameter region that could provide a dark photon-based explanation for the Δa_μ discrepancy.

This study exclusively relies on analytical computations to assess ProtoDUNE's sensitivities. However, it might be of interest to delve into a more comprehensive investigation of shower development using a dedicated Monte Carlo (MC) simulator tailored to this setup. Additionally, a background analysis could shed light on whether the model's sensitivities remain robust or are influenced under more realistic conditions.

This simplified study, nonetheless, offers additional proof that the semi-visible dark photon model is indeed within the scope of current experimental capabilities. In a relatively short span of time, it could be possible to understand whether an explanation for the anomalous muon magnetic moment through a dark photon is possible, showing that richer dark sectors are preferred by nature.

Appendix A

Self-energy computations for neutrino masses

A.1 Loop corrections to neutrino masses

In this section, we compute the correction at one-loop to neutrino masses.
We work with the on-shell renormalization scheme. This is ensured by requiring that the off-diagonal elements in the self-energy be diagonal when the external particles are on their mass shell, and that the residue of the renormalized propagator are equal to one.

Assuming Majorana neutrino fields, we can write the self-energy tensor in the most general form:

$$\Sigma_{ij}(\not{q}) = \not{q} P_L \Sigma^L_{ij}(q^2) + \not{q} P_R \Sigma^R_{ij}(q^2) + P_L \Sigma^M_{ij}(q^2) + P_R \Sigma^{M*}_{ij}(q^2), \tag{A.1}$$

and due to the Majorana nature:

$$\Sigma^L_{ij}(q^2) = \Sigma^{R*}_{ij}(q^2), \quad \Sigma^M_{ij}(q^2) = \Sigma^M_{ji}(q^2)$$

The neutrino mass at one-loop is then given by:

$$m^{one-loop}_{ij} = Re\left[\Sigma^M_{ij}(0)\right], \quad i,j < 4 \tag{A.2}$$

A.1.1 Self-energy

We compute explicitly the self-energy corrections. We ignore the kinetic and scalar mixing effects, as these can be shown to only give small corrections given the current experimental bounds. The contributions from the scalar fields $s = h, \varphi$, the Goldstones $G = G_h, G_\varphi$ and the vector fields

$V = Z, A'$ are:

$$\begin{aligned}
-i\Sigma^s_{ij}(p^2) &= (-i)^2 \left(\Delta_s P_R + \Delta_s^* P_L\right)_{ik} \times \\
&\qquad \int \frac{d^d k}{(2\pi)^d} \frac{i\left(\not{p} + \not{k} + m_k\right)}{(p+k)^2 - m_k^2} \frac{i}{k^2 - m_s^2} \left(\Delta_s P_R + \Delta_s^* P_L\right)_{kj} \\
-i\Sigma^G_{ij}(p^2) &= (-i)^2 \left(\Delta_G P_R + \Delta_G^* P_L\right)_{ik} \times \\
&\qquad \int \frac{d^d k}{(2\pi)^d} \frac{i\left(\not{p} + \not{k} + m_k\right)}{(p+k)^2 - m_k^2} \frac{i}{k^2 - \xi_V m_V^2} \left(\Delta_G P_R + \Delta_G^* P_L\right)_{kj} \\
-i\Sigma^V_{ij}(p^2) &= -(-i)^2 \gamma^\mu \left(C_V P_R - C_V^T P_L\right)_{ik} \times \\
&\qquad \int \frac{d^d k}{(2\pi)^d} \frac{i\left(\not{p} + \not{k} + m_k\right)}{(p+k)^2 - m_k^2} \frac{i P_{\mu\nu}}{k^2 - m_V^2} \gamma^\nu \left(C_V P_R - C_V^T P_L\right)_{kj}
\end{aligned} \tag{A.3}$$

[feynman]
In the latter self-energy, we have defined the vector boson propagator numerator, that can be rewritten as:

$$\begin{aligned}
\gamma^\mu P_{\mu\nu} \gamma^\nu =& \gamma^\mu \left[g_{\mu\nu} - (1-\xi_V)\frac{k_\mu k_\nu}{k^2 - \xi_V m_V^2}\right] \gamma^\nu \\
=& d - (1-\xi_V)\frac{k^2 - m_k^2}{k^2 - \xi_V m_V^2} - \frac{m_k^2}{m_V^2}\frac{(k^2 - \xi_V m_V^2) - (k^2 - m_k^2)}{(k^2 - \xi_V m_V^2)}
\end{aligned}$$

This allows us to write the relevant part of the self-energy as functions of the scalar two-point loop function:

$$B_0(l, m_a^2, m_c^2) = \mu^{2\epsilon} \int \frac{d^d k}{(2\pi)^k} \frac{1}{(k^2 - m_a^2)((l+k)^2 - m_c^2)} \tag{A.4}$$

Using this, we can rewrite:

$$\begin{aligned}
\Sigma^s_{ij}(0) P_R &= -\frac{\pi^2}{(2\pi)^4} \mu^{d-4} \left[(\Delta_s)_{ik} m_k B_0(0, m_k^2, m_s^2)(\Delta_s)_{kj}\right] P_R \\
\Sigma^G_{ij}(0) P_R &= -\frac{\pi^2}{(2\pi)^4} \mu^{d-4} \left[(\Delta_G)_{ik} m_k B_0(0, m_k^2, \xi_V m_V^2)(\Delta_G)_{kj}\right] P_R \\
\Sigma^s_{ij}(0) P_R &= -\frac{\pi^2}{(2\pi)^4} \mu^{d-4} \left[(C_V)_{ik} m_k B_0(m_k^2, m_V^2, \xi_V m_V^2)(C_V^*)_{kj}\right] P_R
\end{aligned} \tag{A.5}$$

where the rearrangement of the boson propagator allowed us to write $f(m_k^2, m_V^2, \xi_V m_V^2)$ as:

$$\begin{aligned}
f(m_k^2, m_V^2, \xi_V m_V^2) =& d B_0(0, m_k^2, m_s^2) - (1-\xi_V) B_0(0, m_k^2, \xi_V m_V^2) + \\
& \frac{m_k^2}{m_V^2} B_0(0, m_k^2, \xi_V m_V^2) - \frac{m_k^2}{m_V^2} B_0(0, m_k^2, m_s^2)
\end{aligned}$$

Finally, the scalar loop function can be computed giving:

$$\begin{aligned} B_0(0, m_a^2, m_c^2) &= \frac{1}{\epsilon} - \gamma_E + ln4\pi - \int_0^1 dx ln \frac{m_a^2 - x(m_a^2 - m_b^2)}{\mu^2} \\ &= \frac{1}{\epsilon} - \gamma_E + ln4\pi - \frac{m_a^2}{m_a^2 - m_b^2}\left[ln\frac{m_a^2}{\mu^2} - 1\right] + \frac{m_a^2}{m_a^2 - m_b^2}\left[ln\frac{m_b^2}{\mu^2} - 1\right] \end{aligned} \tag{A.6}$$

For light neutrinos $i, j = 1, 2, 3$ the final result is:

$$\Sigma_{ij} P_R = \frac{\pi^2}{(2\pi)^4} C\hat{m}\left[dB_0(0, \hat{m}^2, m_V^2) + \frac{\hat{m}^2}{m_V^2}\left(B_0(0, \hat{m}^2, m_s^2) - B_0(0, \hat{m}^2, m_V^2)\right)\right] C^T P_R \tag{A.7}$$

After some algebra, we get:

$$m_{ij} = \frac{1}{4\pi^2}\sum_{k=4}^{5}\left[C_{ik}C_{jk}\frac{m_k^3}{m_Z^2}F(m_k^2, m_Z^2, m_h^2) + D_{ik}D_{jk}\frac{m_k^3}{m_Z^2}F(m_k^2, m_Z^2, m_\varphi^2)\right] \tag{A.8}$$

where

$$F(a, b, c) \equiv \frac{3ln(a/b)}{a/b - 1} + \frac{ln(a/c)}{a/c - 1}$$

Appendix B

HNFs three-body decay

If the mass of the dark photon is bigger than the mass of any of the HNFs, only three-body decays are allowed.

We consider the following process:

$$\psi_j(p) \to \psi_i(k1) + l^+(k2) + l^-(k3)$$

Where ψ_j and ψ_i are the HNFs in the theory under consideration, and l^+ and l^- are the Standard Model leptons. We want to compute the total width for this decay. All particles in the final state are massive. For this process to be kinematically allowed, we must have that $m_j > m_i + 2m_l$.

We only consider processes mediated by the dark photon A'. The coupling of the dark photon with the dark sector current is given by $g_D V_{ij}\gamma^\mu$. For Dirac HNFs, the full amplitude reads:

$$i\mathcal{M} = \overline{u}(k_1)V_{ij}g_D\gamma^\mu u(p)\frac{\overline{u}(k_3)e\varepsilon\gamma_\mu v(k_2)}{(p-k_1)^2 - m_{A'}^2} \tag{B.1}$$

Squaring the amplitude gives the following expression:

$$\begin{aligned}|\mathcal{M}|^2 =& \frac{(g_D e\varepsilon)^2}{m_{A'}^4}|V_{ij}|^2 \left[\overline{u}(k_1)\gamma^\mu u(p)\right]\left[\overline{u}(k_3)\gamma_\mu v(k_2)\right] \\ & \left[\overline{u}(p)\gamma^\nu u(k_1)\right]\left[\overline{v}(k_2)\gamma_\nu u(k_3)\right]\end{aligned} \tag{B.2}$$

Performing the sum over spin, averaging over initial states and using the identities for the traces of gamma matrices we find:

$$\begin{aligned}\frac{1}{2}\sum|\mathcal{M}|^2 =& \frac{1}{2}\frac{(g_D e\varepsilon)^2}{m_{A'}^4}|V_{ij}|^2 Tr\left[(\not{k}_1 + m_i)\gamma^\mu(\not{p} + m_j)\gamma^\nu\right] Tr\left[(\not{k}_3 + m_l)\gamma_\mu(\not{k}_2 - m_l)\gamma_\nu\right] \\ =& \frac{1}{2}\frac{(g_D e\varepsilon)^2}{m_{A'}^4}|V_{ij}|^2\left[(\not{k}_1 + m_i)\gamma^\mu(\not{p} + m_j)\gamma^\nu\right]\left(Tr\left[\not{k}_3\gamma_\mu\not{k}_2\gamma_\nu\right] - m_l^2 Tr\left[\gamma_\mu\gamma_\nu\right]\right) \\ =& \frac{1}{2}\frac{(g_D e\varepsilon)^2}{m_{A'}^4}|V_{ij}|^2 16(p^\mu k_1^\nu - p.k_1 g^{\mu\nu} + p^\nu k_1^\mu + m_i m_j g^{\mu\nu})(k_{2\mu}k_{3\nu} - k_2.k_3 g_{\mu\nu} + k_{2\nu}k_{3\mu} - m_l^2 g_{\mu\nu}) \\ =& 16\frac{(g_D e\varepsilon)^2}{m_{A'}^4}|V_{ij}|^2(p.k_2 k_1.k_3 + p.k_3 k_1.k_2 + p.k_1 m_l^2 - m_i m_j k_2.k_3 - 2m_i m_j m_l^2)\end{aligned} \tag{B.3}$$

For parametrizing the phase space, we use the Dalitz variables defined as $m_{ij}^2 = k_{ij}^2$ where $k_{ij} = k_i + k_j$. We find:

$$\begin{aligned} m_{12}^2 &= (k1 + k2)^2 = (p - k3)^2 \\ m_{23}^2 &= (k2 + k3)^2 = (p - k1)^2 \\ m_{13}^2 &= (k1 + k3)^2 = (p - k2)^2 \end{aligned} \tag{B.4}$$

We can also notice that $m_{12}^2 + m_{23}^2 + m_{13}^2 = m_i^2 + 2m_l^2$. Using these identities, we can rewrite the scalar products appearing in the squared amplitude as:

$$\begin{aligned} p.k_2 &= \frac{1}{2}(m_{12}^2 + m_{23}^2 - m_i^2 - m_l^2) \\ k_1.k_3 &= \frac{1}{2}(m_5^2 + m_l^2 - m_{12}^2 - m_{23}^2) \\ p.k_3 &= \frac{1}{2}(m_j^2 + m_l^2 - m_{12}^2) \\ k_1.k_2 &= \frac{1}{2}(m_{12}^2 - m_i^2 - m_l^2) \\ p.k_1 &= \frac{1}{2}(m_j^2 + m_i^2 - m_{23}^2) \\ k_2.k_3 &= \frac{1}{2}(m_{23}^2 - 2m_l^2) \end{aligned} \tag{B.5}$$

The phase space can be parameterized using the Dalitz variables (ref. PDG kinematics):

$$d\Gamma = \frac{1}{(2\pi)^3}\frac{1}{32m_i^3}\left(\frac{1}{2}\sum|\mathcal{M}|^2\right)dm_{12}^2 dm_{23}^2 \tag{B.6}$$

For a given value of m_{12}, the range of m_{23} is determined by its values when k_2 is parallel or anti-parallel to k_3:

$$\begin{aligned} (m_{23}^2)_{max} &= (E_2^* + E_3^*)^2 - \left(\sqrt{E_2^{*2} - m_l^2} - \sqrt{E_3^{*2} - m_l^2}\right)^2 \\ (m_{23}^2)_{min} &= (E_2^* + E_3^*)^2 - \left(\sqrt{E_2^{*2} - m_l^2} + \sqrt{E_3^{*2} - m_l^2}\right)^2 \end{aligned} \tag{B.7}$$

where now $E_2^* = (m_{12}^2 - m_i^2 + m_l^2)/2m_{12}$ and $E_3^* = (m_j^2 - m_{12}^2 - m_\mu^2)/2m_{12}$. Doing some algebra and defining the values as did for the ν_4 decay, we get:

$$\Gamma = \frac{1}{768\pi^3}\frac{(g_D e\varepsilon)^2}{m_{A'}^4}|V_{ij}|^2 m_j^5 I\left(x_i, x_l\right) \tag{B.8}$$

with:

$$I\big(x_i, x_l\big) = 6 \int_{(x_i+x_l)^2}^{(1-x_l)^2} ds_{12} \int_{(s_{23})_{min}}^{(s_{23})_{max}} ds_{23} \Big[s_{23}(1-x_i^2)^2 - 2(x_i + x_l^2)^2 \\ - (s_{12}+s_{23})^2 + s_{12}(2x_{tot}^2 - s_{12}) \Big] \tag{B.9}$$

where $x_{tot}^2 = 1 + x_i^2 + 2x_l^2$, $s_{12} = x_{12}^2$, $s_{23} = x_{23}^2$ and $x_i = m_i/m_j$.

Appendix C

Majorana Feynman rules

Constructing Feynman rules for Majorana fermions necessitates additional considerations due to the inherent self-conjugacy of these particles. Ambiguities can arise in the directions of momentum flows and the relative signs of various graphs contributing to a given amplitude. Therefore, careful attention is essential to accurately account for these unique features in the rule construction process. In this Appendix we briefly review how to do that, following references [145] [146].

Let's first introduce the charge conjugation matrix, satisfying the following properties:

$$\begin{aligned} &(i)\ C^\dagger = C^{-1} \\ &(ii)\ C^T = -C \\ &(iii)\ C^{-1}\Gamma_i C = \eta_i \Gamma_i^T \end{aligned} \tag{C.1}$$

where $\Gamma_i = 1,\ i\gamma_5,\ \gamma_\mu\gamma_5,\ \gamma_\mu,\ \sigma_{\mu\nu} = \frac{1}{2}i[\gamma_\mu, \gamma_\nu]$ and $\eta_i = +1$ for $\Gamma_i = 1,\ i\gamma_5,\ \gamma_\mu\gamma_5$, while $\eta_i = -1$ for $\Gamma_i = \gamma_\mu,\ \sigma_{\mu\nu}$.

A Majorana field satisfy the following condition:

$$\psi_M = \psi_M^c \equiv C\overline{\psi}_M^T, \tag{C.2}$$

where $\overline{\psi} \equiv \psi^\dagger\gamma^0$. In general, the u and v spinors for either Dirac or Majorana fermions are related via:

$$u(k,s) = C\overline{v}^T(k,s) \qquad v(k,s) = C\overline{u}^T(k,s), \tag{C.3}$$

where $s = \pm 1/2$ labels spin.

Following the convention used in [145][146], we define λ, ψ, and ϕ to be respectively a Majorana fermion, a Dirac fermion and a vector boson (either spin 0 or 1) fields. The interaction Lagrangian will be of the form:

$$\begin{aligned} \mathcal{L}_{int} =& \frac{1}{2}\overline{\lambda}_a\left(i\partial\!\!\!/ - M_a\right)\lambda_a + \overline{\psi}_a\left(i\partial\!\!\!/ - m_a\right)\psi_a \\ &+ \frac{1}{2}g^i_{abc}\overline{\lambda}_a\Gamma_i\lambda_b\phi_c + \frac{1}{2}g^{i*}_{abc}\overline{\lambda}_b\Gamma_i\lambda_a\phi^*_c + k^i_{abc}\overline{\lambda}_a\Gamma_i\psi_b\phi^*_c + k^{i*}_{abc}\overline{\psi}_b\Gamma_i\lambda_a\phi_c \end{aligned} \tag{C.4}$$

Using C.1 and the definition of a Majorana field, we find that $g^i_{abc} = \eta_i g^i_{bac}$. We want to find the Feynman diagrams for the Lagrangian given above. All external fermions are denoted by a straight solid line and an arrow. While for Dirac fermions the direction of the arrow indicates the flow of the lepton number, for Majorana fermion we will have to choose a convention for the direction.

Each external fermion line is associated with a u or v spinor. For Dirac fermions, the notation $u(p)[\overline{u}(p)]$ is used for an incoming [outgoing] particle state, while $\overline{v}(p)[v(p)]$ is used for an incoming [outgoing] antiparticle state. For Majorana fermions, being particle and antiparticle indistinguishable, this rule appear ambiguous. The correct procedure involves first choosing a direction for the arrow on a given Majorana fermion line, although this choice is arbitrary. Subsequently, an *incoming* Majorana fermion line is termed a particle line when the arrow points in an incoming direction (i.e., into the Feynman diagram). Conversely, if the arrow points in an outgoing direction, the line is referred to as an antiparticle line. Similarly, an *outgoing* Majorana fermion line is considered a particle line when the arrow points in an outgoing direction, and it is regarded as an antiparticle line when the arrow points in an incoming direction.

For Dirac fields, the sum over spins gives:

$$\begin{aligned} \sum_s u^s(p)\overline{u}^s(p) &= \not{p} + M \\ \sum_s v^s(p)\overline{v}^s(p) &= \not{p} - M \end{aligned} \tag{C.5}$$

For Majorana fermios, other combinations of the u and v spinors arise.

$$\begin{aligned} \sum_s u^s(p)v^{sT}(p) &= \left(\not{p} + M\right) C^T \\ \sum_s \overline{u}^{sT}(p)\overline{v}^s(p) &= C^{-1}\left(\not{p} - M\right) \\ \sum_s \overline{v}^{sT}(p)\overline{u}^s(p) &= C^{-1}\left(\not{p} + M\right) \\ \sum_s v^s(p)u^{sT}(p) &= \left(\not{p} - M\right) C^T \end{aligned} \tag{C.6}$$

The Feynman rules can be read off the Lagrangian, following what is done in [146], obtaining the rules in C.1.

Note that the factor $1/2$ appearing in the Lagrangian, is not present in the Feynman rules. Let's delve into this point further to understand the reason behind this. A Majorana fermion field can be expanded as:

$$\lambda_i \sim \sum_{s_i} b_i^{s_i} u_i^{s_i} + \left(b_i^{s_i}\right)^\dagger v_i^{s_i}, \quad \overline{\lambda_j} \sim \sum_{s_j} \overline{u_j^{s_j}} \left(b_j^{s_j}\right)^\dagger + \overline{v_j^{s_j}} b_j^{s_j} \tag{C.7}$$

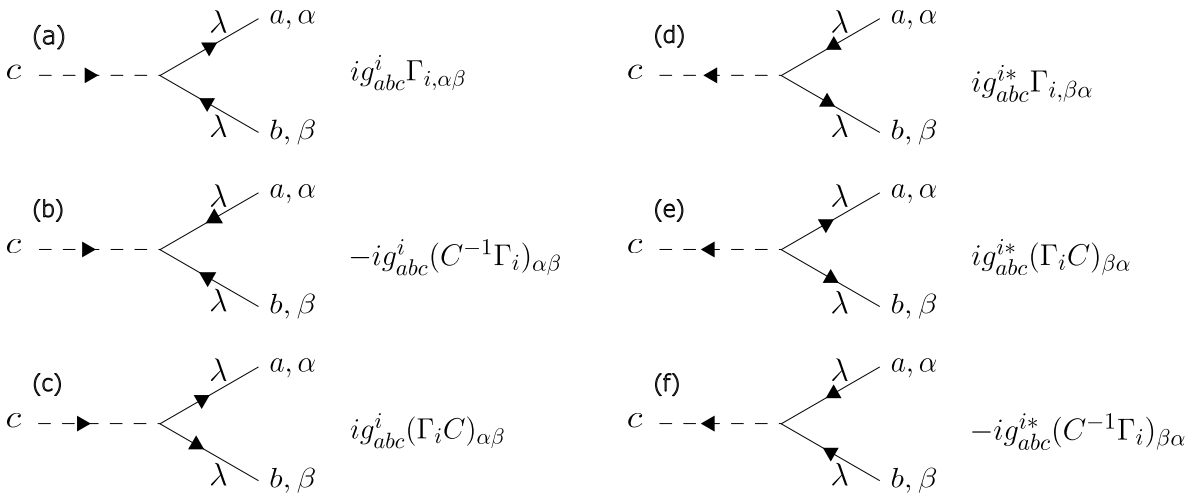

FIGURE C.1: Majorana feynman rules for the scalar (vector) field with a pair of Majorana fermions as computed in [146]

where we have omitted integrals, momenta, and factor of π. The s_i are the spin of the particles. In order to compute the transition $\phi + \lambda_b \to \lambda_a$, we have to evaluate the matrix element:

$$\langle 0 \mid b_{a,s_2}\overline{\lambda_a}\frac{1}{2}g^i_{abc}\Gamma_j\lambda_b b^\dagger_{b,s_1} \mid 0\rangle. \tag{C.8}$$

Inserting C.7, we obtain:

$$\frac{1}{2}[g^i_{abc}\overline{u}_a\Gamma_j u_b - g^j_{bac}\overline{v}_b\Gamma_j v_a]. \tag{C.9}$$

where the minus sign comes from the fact that $\{b_i, b_j\} = 0$. Using the relations defined previously, we find that the two terms in C.9 are equal and therefore:

$$g^j_{abc}u_a\Gamma_j u_b. \tag{C.10}$$

In [147], they were able to simplify the rules for the two-Majorana-boson vertices, reducing the number of diagrams from six to two and avoiding using the charge-conjugation matrix. In [145] a similar but more general algorithmic approach for constructing the Feynman rules is presented, applicable to any fermion-number-violating interactions. [here you should insert some images for both references]

Let's consider the model of the semi-visible dark photon analyzed in this thesis. We consider the simplest example of inelastic Dark Matter presented in 4.5.1. The interaction Lagrangian for that model is:

$$\mathcal{L}_{int-iDM} \supset g_D A'_\mu(V_{12}\overline{\psi_1}\psi_2 + V_{21}\overline{\psi_2}\psi_1). \tag{C.11}$$

Using the general Feynman rules depicted in [147] in the appendix, this should simply result in the diagram:

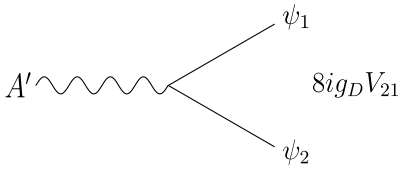

FIGURE C.2: Majorana Feynman rule for the $A' \to \psi_1\psi_2$ vertex in the inelastic Dark Matter model

Appendix D

Dark Matter production at ProtoDUNE

Production from pseudoscalars mesons decay

The HNFs in our model can be produced from the dark photon through the process:

$$\pi^0, \eta \to \gamma A'^{(*)} \to \gamma \overline{\psi_i} \psi_j$$

where the A' can either be on-shell or off-shell, depending on its mass. If $m_{A'} < m_{\pi_0,\eta}$, A' can be produced on-shell and then decay to dark matter. The branching ratio for this process will then simply be:

$$BR(\pi^0, \eta \to \gamma \overline{\psi_i} \psi_j) = BR(\pi^0, \eta \to \gamma\gamma) \times 2\varepsilon^2 \left(1 - \frac{m_{A'}^2}{m_{\pi^0\eta}^2}\right)^3 \times BR(A' \to \overline{\psi_i}\psi_j). \tag{D.1}$$

For $\alpha_D \gg \varepsilon^2 \alpha_{QED}$, the branching ratio of the dark photon $BR(A' \to \overline{\psi_i}\psi_j) \approx 1$.

If $m_{A'} > m_{\pi_0,\eta}$, the dark photon cannot be produced on-shell and the HNFs are produced through a three-body decay. In this case this expression for the branching ratio is more complicated and is given by [142]:

$$BR(\pi^0, \eta \to \gamma \overline{\psi_i} \psi_j) = \frac{1}{\Gamma_{\pi^0,\eta}} \frac{\varepsilon^2 \alpha_D}{2 m_{\pi^0,\eta}} \int d\Phi_{\pi^0,\eta \to \gamma A'} d\Phi_{A' \to \overline{\psi_i}\psi_j} \frac{ds}{2\pi} \langle \mid \mathcal{M}_{\pi^0,\eta \to \gamma \overline{\psi_i}\psi_j} \mid^2 \rangle \tag{D.2}$$

where s is the centre-of-mass energy, $\Gamma_{\pi^0,\eta}$ is the total π^0, η decay width and $\langle \mid \mathcal{M}_{\pi^0,\eta \to \gamma \overline{\psi_i}\psi_j} \mid^2 \rangle$ is the three-body decay amplitude. Following Appendix A.3-4 in [142], we have that the matrix element for this process is:

$$\mathcal{M}_{\pi^0,\eta \to \gamma \overline{\psi_i}\psi_j} = \varepsilon g_D \frac{e^2}{4\pi^2} \frac{1}{f_{\pi^0,\eta}} \epsilon_\lambda^{(\gamma)} \epsilon^{\lambda\mu\alpha\beta} p_\alpha q_\beta \frac{-i(g_{\mu\nu} - q_\mu q_\nu / m_{A'}^2)}{s - m_{A'}^2 + i m_{A'} \Gamma_{A'}} (\overline{v}(k2) \gamma^\mu u(k1)), \tag{D.3}$$

where $f_{\pi^0,\eta}$ is the pion decay constant, namely the coefficient in front of the kinetic term for the pseudoscalar in the low-energy effective action. The momentum of the photon is p, while the momenta of the HNFs are k_1 and k_2 and $q = k_1 + k_2$. Squaring the amplitude and summing over

spin, we get:

$$\langle \mid \mathcal{M}_{\pi^0,\eta\to\gamma\overline{\psi_i}\psi_j} \mid^2 \rangle = \frac{4\varepsilon^2\alpha_{QED}^2\alpha_D}{\pi f_{\pi^0,\eta}^2[(s-m_{A'}^2)^2+m_{A'}^2\Gamma_{A'}^2]}\left[\left(s+m_i^2+m_j^2\right)\left(m_{\pi^0,eta}^2-s\right)^2-8s(p\cdot k_1)(p\cdot k2)\right] \tag{D.4}$$

In the on-shell limit, we can use the narrow with approximation:

$$\frac{1}{(s-m_{A'}^2)^2+m_{A'}^2\Gamma_{A'}^2}\to\frac{\pi}{m_{A'}\Gamma_{A'}}\delta(s-m_{A'}^2). \tag{D.5}$$

By integrating over the phase space and making the above substitution in the matrix element, we recover the expression in 4.31:

$$\Gamma_{\pi^0,\eta\to\gamma\psi_i\overline{\psi_j}} = \Gamma_{\pi^0,\eta\to\gamma A'}\times BR(A'\to\psi_i\overline{\psi_j}). \tag{D.6}$$

In this work for the pseudoscalar meson decay, we only consider the on-shell regime. Indeed, for higher masses of the dark photon, production through vector meson mixing dominates.

Production from vector meson mixing

According to the vector meson dominance model (VMD)[148], the photon couples to hadronic states through mixing with intermediate QCD vector mesons. Following the convention in which the SM photon (A^μ) and vector mesons (V^μ) mass-mix, the corresponding effective Lagrangian is given by [149]:

$$-\mathcal{L}\subset(em_V^2/g_V)A^\mu V_\mu \tag{D.7}$$

where g_V is the vector meson-pion interaction strength. When a dark photon mixes with the standard model photon, we obtain an effective mass-mixing between the dark photon and the vector meson:

$$-\mathcal{L}\subset(\varepsilon em_V^2/g_V)A'^\mu V_\mu \tag{D.8}$$

In order to compute the decay width of the vector mesons into HNFs, we consider the Proca propagator for a massive vector field, which subsequently decays into $\overline{\psi_i}\psi_j$. The final result yields:

$$\Gamma(V\to\overline{\psi_i}\psi_j) = \frac{1}{4\pi}\sum_{i,j}\left(\frac{V_{ij}g_De\varepsilon m_V^2}{g_V}\right)^2\frac{m_V^5}{(m_V^2-m_{A'}^2)^2+m_{A'}^2\Gamma_{A'}^2}I_{ij}(m_i,m_j,m_V), \tag{D.9}$$

where $I_{ij}(m_i,m_j,m_V)$ is the phase space suppression term, given by:

$$I_{ij}(m_i,m_j,m_V) = \left(1-\frac{\Delta_{ij}^2}{m_V^2}\right)\left(1+\frac{m_{ij}^2}{2m_V^2}\right)\sqrt{\left(1-\frac{\Delta_{ij}^2}{m_V^2}\right)\left(1-\frac{m_{ij}^2}{m_V^2}\right)}, \tag{D.10}$$

The branching ratio for the process $V \to A'^{*} \to \overline{\psi_i}\psi_j$, will then be:

$$\frac{BR(V \to \overline{\psi_i}\psi_j)}{BR(V \to e^+e^-)} = \sum_{i,j} \left(\frac{V_{ij} g_D \varepsilon}{e}\right)^2 \frac{m_V^4}{(m_V^2 - m_{A'}^2)^2 + m_{A'}^2 \Gamma_{A'}^2} I_{ij}(m_i, m_j, m_V). \tag{D.11}$$

Appendix E

Inelastic DM scattering cross section

The lightest HNFs produced from the dark photon decay as discussed in the previous section, enter the detector and scatter off of target particles in the detector. The scattering process is $\psi_i T \to \psi_j T$, where $i, j = 1, 2(3)$ depends on the couplings allowed in the model under consideration. In this work, we assumed that only ψ_1 reaches the detector. However, here we maintain a more general discussion considering the most general scattering written before.

The matrix element for the process $\psi_i(p_1)T(p_2) \to \psi_j(k_1)T(k_2)$ is:

$$\mathcal{M} = \frac{\varepsilon e g_D V_{ij}}{(t - m_{A'}^2)}[\overline{u}(k_2)\gamma_\mu u(p_2)][\overline{u}(k_1)\gamma^\mu u(p_1)]. \tag{E.1}$$

The squared, spin-average matrix will then be:

$$\begin{aligned}\langle \mid \mathcal{M} \mid^2 \rangle = \frac{128\pi^2 V_{ij}^2 \varepsilon^2 \alpha_{QED}\alpha_D}{(t - m_{A'}^2)^2}\Big[&(k_1 \cdot k_2)(p_1 \cdot p_2) + (k_2 \cdot p_1)(p_2 \cdot k_1) \\ &- m_i m_j (k_2 \cdot p_2) - m_T^2 (p_1 \cdot k_1) + 2 m_i m_j m_T^2\Big]\end{aligned} \tag{E.2}$$

The differential scattering cross section in the centre-of-mass frame is:

$$\frac{d\sigma}{d_\Omega} = \frac{1}{2\pi}\frac{d\sigma}{dcos\theta} = \frac{\langle \mid \mathcal{M} \mid^2 \rangle}{64\pi^2 s}\frac{\mid \vec{k} \mid}{\mid \vec{p} \mid} \tag{E.3}$$

where $\vec{p}$ and $\vec{k}$ are the initial/final state momenta, given by[150]:

$$\mid \vec{p} \mid^2 = \frac{(s - m_T^2 - m_i^2)^2 - 4m_T^2 m_i^2}{4s}, \tag{E.4}$$

$$\mid \vec{p} \mid^2 = \frac{(s - m_T^2 - m_j^2)^2 - 4m_T^2 m_j^2}{4s}, \tag{E.5}$$

. In the laboratory frame, with a stationary target T, we have:

$$\begin{aligned} p_1 &= (E_{\psi_i}, \vec{p_1}) \\ p_2 &= (m_T, 0) \\ k_1 &= (E_{\psi_j}, \vec{k_1}) \\ k_2 &= (E_T, \vec{k_2}) \end{aligned} \tag{E.6}$$

From these values of the momenta:

$$s = (p_1 + p_2)^2 = m_i^2 + m_T^2 + 2m_T E_{\chi_i}, \tag{E.7}$$

$$(k_1 \cdot p_1) = -\frac{1}{2}(2m_T^2 - m_i^2 - m_j^2 - 2m_T E_T), \tag{E.8}$$

To obtain the differential recoil distribution:

$$dcos\theta = \frac{m_T}{\mid \vec{p} \mid\mid \vec{k} \mid} dE_T \tag{E.9}$$

Substituting in E.3,

$$\frac{d\sigma}{dE_T} = \frac{m_T \langle \mid \mathcal{M} \mid^2 \rangle}{32\pi s \mid \vec{p} \mid^2} \tag{E.10}$$

For the scattering against electrons considered here, it sufficed to substitute the value of the mass of the electrons m_e in m_T.

Bibliography

[1] F. Zwicky. In: *Helvetica Physica Acta* 6 (1933). ISSN: 0018-0238.

[2] V. C. Rubin and Jr Ford. In: *Astrophys. J. 159: 379-403(Feb 1970).* (1970). DOI: 10.1086/150317.

[3] D. Clowe, A. Gonzalez, and M. Markevitch. In: *The Astrophys. J.* 604.2 (2004), pp. 596–603. DOI: 10.1086/381970.

[4] A. M. Abdullahi et al. "Semivisible dark photon phenomenology at the GeV scale". In: *Phys. Rev. D* 108.1 (2023), p. 015032. DOI: 10.1103/PhysRevD.108.015032. arXiv: 2302.05410 [hep-ph].

[5] P. Coloma et al. 2023. arXiv: 2201.08409 [hep-ph].

[6] S. Weinberg. In: *Phys. Rev. Lett.* 19.21 (1967), pp. 1264–1266. DOI: 10.1103/PhysRevLett.19.1264.

[7] A. Salam. In: *Conf.Proc.C* 680519 (1968). DOI: 10.1142/9789812795915_0034.

[8] S. L. Glashow. In: *Nuclear Physics* 22 (1961), pp. 579–588. ISSN: 0029-5582. DOI: 10.1016/0029-5582(61)90469-2.

[9] David J. Gross and Frank Wilczek. In: *Phys. Rev. Lett.* 30.26 (1973). DOI: 10.1103/PhysRevLett.30.1343.

[10] S. Weinberg. In: *Phys. Rev. Lett.* 31.7 (1973). DOI: 10.1103/PhysRevLett.31.494.

[11] H. Fritzsch, M. Gell-Mann, and H. Leutwyler. In: *Physics Letters B* 47.4 (1973). ISSN: 0370-2693. DOI: 10.1016/0370-2693(73)90625-4.

[12] P. W. Higgs. In: *Phys. Rev. Lett.* 13.16 (1964). DOI: 10.1103/PhysRevLett.13.508.

[13] F. Englert and R. Brout. In: *Phys. Rev. Lett.* 13.9 (1964). DOI: 10.1103/PhysRevLett.13.321.

[14] CMS Collaboration. In: *Physics Letters B* 716.1 (2012). DOI: 10.1016/j.physletb.2012.08.021. arXiv: 1207.7235 [hep-ex].

[15] ATLAS Collaboration. In: *Phys. Lett. B* 716 (2012). DOI: 10.1016/j.physletb.2012.08.020. arXiv: 1207.7214 [hep-ex].

[16] CMS Collaboration. In: *Nature* 607.7917 (2022). DOI: 10.1038/s41586-022-04892-x. arXiv: 2207.00043 [hep-ex].

[17] ATLAS Collaboration. Tech. rep. Geneva: CERN, 2021. URL: http://cds.cern.ch/record/2789544.

[18] G. 't Hooft and M. Veltman. en. In: *Nuclear Physics B* 44.1 (1972). ISSN: 0550-3213. DOI: 10.1016/0550-3213(72)90279-9.

[19] J. Goldstone. In: *Nuovo Cim* 19.1 (1961). ISSN: 1827-6121. DOI: 10.1007/BF02812722.

[20] Jeffrey Goldstone, Abdus Salam, and Steven Weinberg. In: *Phys. Rev.* 127.3 (1962). DOI: 10.1103/PhysRev.127.965.

[21] N. Cabibbo. In: *Phys. Rev. Lett.* 10.12 (1963). DOI: 10.1103/PhysRevLett.10.531.

[22] M. Kobayashi and T. Maskawa. In: *Progress of Theoretical Physics* 49.2 (1973). ISSN: 0033-068X. DOI: 10.1143/PTP.49.652.

[23] C. Csáki, S. Lombardo, and O. Telem. 2018. arXiv: 1811.04279 [hep-ph].

[24] The Super-Kamiokande Collaboration and Y. Fukuda et al. In: *Phys. Rev. Lett.* 81.8 (1998). ISSN: 0031-9007, 1079-7114. DOI: 10.1103/PhysRevLett.81.1562. arXiv: 9807003 [hep-ex].

[25] W. H. Furry. In: *Phys. Rev.* 56.12 (1939). Publisher: American Physical Society. DOI: 10.1103/PhysRev.56.1184.

[26] K.-H. Ackermann et al. In: *Eur. Phys. J. C* 73.3 (2013). ISSN: 1434-6052. DOI: 10.1140/epjc/s10052-013-2330-0.

[27] CUORE Collaboration. In: *Astroparticle Physics* 20.2 (2003). ISSN: 09276505. DOI: 10.1016/S0927-6505(03)00180-4. arXiv: 0302021 [hep-ex].

[28] D. G. Phillips II et al. In: *J. Phys.: Conf. Ser.* 381 (2012). ISSN: 1742-6588, 1742-6596. DOI: 10.1088/1742-6596/381/1/012044. arXiv: 1111.5578 [nucl-ex].

[29] KamLAND-Zen Collaboration. In: *Phys. Rev. C* 85.4 (2012). ISSN: 0556-2813, 1089-490X. DOI: 10.1103/PhysRevC.85.045504. arXiv: 1201.4664 [hep-ex].

[30] C. L. Bennett et al. In: *The Astrophysical Journal Supplement Series* 148.1 (2003), pp. 1–27. DOI: 10.1086/377253.

[31] A. D. Sakharov. In: *Pisma Zh.Eksp.Teor.Fiz.* 5 (1967). DOI: 10.1070/PU1991v034n05ABEH002497.

[32] M. Fukugita and T. Yanagida. In: *Physics Letters B* 174.1 (1986). ISSN: 0370-2693. DOI: 10.1016/0370-2693(86)91126-3.

[33] V. A. Kuzmin, V. A. Rubakov, and M. E. Shaposhnikov. In: *Physics Letters B* 155.1 (1985). ISSN: 0370-2693. DOI: 10.1016/0370-2693(85)91028-7.

[34] B. Famaey and S. McGaugh. In: *Living Rev. Relativ.* 15.1 (2012). ISSN: 2367-3613, 1433-8351. DOI: 10.12942/lrr-2012-10. arXiv: 1112.3960 [astro-ph.CO].

[35] Kühnel Carr B., F., and M. Sandstad. In: *Phys. Rev. D* 94.8 (2016). DOI: 10.1103/PhysRevD.94.083504.

[36] G. Bertone, D. Hooper, and J. Silk. In: *Physics Reports* 405.5-6 (2005), pp. 279–390. DOI: 10.1016/j.physrep.2004.08.031. arXiv: hep-ph/0404175.

[37] M. Lisanti. 2017. DOI: 10.1142/9789813149441_0007. arXiv: 1603.03797 [hep-ph].

[38] T. Lin. 2019. DOI: 10.48550/arXiv.1904.07915. arXiv: 1904.07915 [hep-ph].

[39] V. C. Rubin et al. In: *The Astrophysical Journal* 238 (1980). ISSN: 0004-637X. DOI: 10.1086/158003.

[40] Planck Collaboration, N. Aghanim, and et al. "Planck 2018 results. VI. Cosmological parameters". In: *A&A* 641 (2020). ISSN: 0004-6361, 1432-0746. DOI: 10.1051/0004-6361/201833910. arXiv: 1807.06209 [astro-ph].

[41] R. J. Cooke and et al. In: *ApJ* 781.1 (2014). ISSN: 0004-637X. DOI: 10.1088/0004-637X/781/1/31.

[42] V. Springel et al. In: *Mon. Not. Roy. Astron. Soc.* 391.4 (2008), pp. 1685–1711. DOI: 10.1111/j.1365-2966.2008.14066.x. arXiv: 0809.0898 [astro-ph].

[43] J. Diemand et al. In: *Nature* 454.7205 (2008), pp. 735–738. DOI: 10.1038/nature07153. arXiv: 0805.1244 [astro-ph].

[44] D. Bhattacharjee et al. 2022. DOI: 10.36227/techrxiv.20590452.

[45] A. De Rújula, S. L. Glashow, and U. Sarid. In: *Nuclear Physics B* 333.1 (1990), pp. 173–194. ISSN: 0550-3213. DOI: 10.1016/0550-3213(90)90227-5.

[46] S. D. McDermott, H. Yu, and K. M. Zurek. In: *Physical Review D* 83.6 (2011). DOI: 10.1103/physrevd.83.063509. arXiv: 1011.2907 [hep-ph].

[47] B. Audren et al. In: *Journal of Cosmology and Astroparticle Physics* 2014.12 (2014), pp. 028–028. DOI: 10.1088/1475-7516/2014/12/028. arXiv: 1407.2418 [hep-ph].

[48] P. F. Depta et al. In: *Journal of Cosmology and Astroparticle Physics* 2019.04 (2019), pp. 029–029. DOI: 10.1088/1475-7516/2019/04/029. arXiv: 1901.06944 [hep-ph].

[49] S. W. Randall et al. In: *The Astrophysical Journal* 679.2 (2008), pp. 1173–1180. DOI: 10.1086/587859. arXiv: 0704.0261 [astro-ph].

[50] D. Harvey et al. In: *Science* 347.6229 (2015), pp. 1462–1465. DOI: 10.1126/science.1261381. arXiv: 1503.07675 [astro-ph].

[51] S. Tulin and H. Yu. In: *Physics Reports* 730 (2018), pp. 1–57. DOI: 10.1016/j.physrep.2017.11.004. arXiv: 1705.02358 [hep-ph].

[52] S. Kazama. "Physics in LHC and Beyond". 2022. URL: https://indico.cern.ch/event/1102363/contributions/4820766/.

[53] W. Hu, R. Barkana, and A. Gruzinov. In: *Phys.Rev.Lett.* 85.6 (2000), pp. 1158–1161. DOI: 10.1103/physrevlett.85.1158.

[54] S. Tremaine and J. E. Gunn. In: *Phys. Rev. Lett.* 42 (6 1979), pp. 407–410. DOI: 10.1103/PhysRevLett.42.407.

[55] P. Villanueva-Domingo, O. Mena, and S. Palomares-Ruiz. In: *Front. Astron. Space Sci.* 8 (2021). DOI: 10.3389/fspas.2021.681084. arXiv: 2103.12087 [astro-ph].

[56] M. Oncins. 2022. arXiv: 2205.14722 [astro-ph].

[57] Y. Bai, A. J. Long, and S. Lu. In: *Phys. Rev. D* 99.5 (2019). DOI: 10.1103/physrevd.99.055047. arXiv: 1810.04360 [hep-ph].

[58] J. Lee and I. Koh. In: *Phys. Rev. D Part. Fields* 53.4 (1996), pp. 2236–2239. ISSN: 0556-2821. DOI: 10.1103/physrevd.53.2236.

[59] A. Kusenko and M. Shaposhnikov. In: *Phys.Lett.B* 418.1-2 (1998), pp. 46–54. DOI: 10.1016/s0370-2693(97)01375-0.

[60] K. Griest and M. Kamionkowski. In: *Phys. Rev. Lett.* 64 (6 1990), pp. 615–618. DOI: 10.1103/PhysRevLett.64.615.

[61] E. W. Kolb and M. S. Turner. *The early universe*. Westview Press, 1990. DOI: 10.1201/9780429492860.

[62] M. L. Graesser, I. M. Shoemaker, and L. Vecchi. In: *JHEP* 2011.10 (2011). DOI: 10.1007/jhep10(2011)110. arXiv: 1103.2771 [hep-ph].

[63] T. Lin, H. Yu, and K. M. Zurek. In: *Phys. Rev. D* 85.6 (2012). DOI: 10.1103/physrevd.85.063503. arXiv: 1111.0293 [hep-ph].

[64] R. T. D'Agnolo, D. Pappadopulo, and J. T. Ruderman. In: *Phys. Rev. Lett.* 119.6 (2017). DOI: 10.1103/physrevlett.119.061102. arXiv: 1705.08450 [hep-ph].

[65] Gordon L. Kane et al. In: *Phys. Rev. D* 93.6 (2016). DOI: 10.1103/physrevd.93.063527. arXiv: 1502.05406 [hep-ph].

[66] L. J. Hall et al. In: *JHEP* 2010.3 (2010). DOI: 10.1007/jhep03(2010)080. arXiv: 0911.1120 [hep-ph].

[67] S. Giagu. In: *Front. in Phys.* 7 (2019), p. 75. DOI: 10.3389/fphy.2019.00075.

[68] M. W. Goodman and E. Witten. In: *Phys. Rev. D* 31 (12 1985), pp. 3059–3063. DOI: 10.1103/PhysRevD.31.3059.

[69] LUX Collaboration and D.S. Akerib et al. In: *Phys. Rev. Lett.* 112.9 (2014). DOI: 10.1103/physrevlett.112.091303. arXiv: 1310.8214 [hep-ph].

[70] XENON100 Collaboration et al. In: *Astropart. Phys.* 35.9 (2012), pp. 573–590. DOI: 10.1016/j.astropartphys.2012.01.003. arXiv: 1107.2155 [hep-ph].

[71] L. Baudis. "26th International Conference on Supersymmetry and Unification of Fundamental Interactions". SUSY 2018. 2018. URL: https://indico.cern.ch/event/689399/contributions/2953589/.

[72] J.P. Lees et al. (BaBar). In: *Phys. Rev. Lett.* 113.20 (2014). DOI: 10.1103/physrevlett.113.201801. arXiv: 1406.2980 [hep-ex].

[73] L. Hsu. "40th International Conference on High-Energy Physics". ICHEP 2020. 2020. URL: https://indico.cern.ch/event/868940/contributions/3905692/.

[74] D. Hooper. 2018. arXiv: 1812.02029 [hep-ph].

[75] E. A. Baltz et al. In: *JCAP* 2008.07 (2008), p. 013. DOI: 10.1088/1475-7516/2008/07/013. arXiv: 0806.2911 [astro-ph].

[76] T. Bringmann and C. Weniger. In: *Physics of the Dark Universe* 1.1-2 (2012), pp. 194–217. DOI: 10.1016/j.dark.2012.10.005. arXiv: 1208.5481 [hep-ph].

[77] M. Lisanti et al. In: *Phys. Rev. Lett.* 120.10 (2018). DOI: 10.1103/physrevlett.120.101101. arXiv: 1708.09385 [astro-ph].

[78] S. Ando and K. Ishiwata. In: *JCAP* 2015.05 (2015), pp. 024–024. DOI: 10.1088/1475-7516/2015/05/024. arXiv: 1502.02007 [astro-ph].

[79] The Fermi LAT collaboration. In: *JCAP* 2015.09 (2015). DOI: 10.1088/1475-7516/2015/09/008. arXiv: 1501.05464 [astro-ph].

[80] Fermi/LAT Collaboration et al. In: *Astrophys.J.* 697.2 (2009), pp. 1071–1102. DOI: 10.1088/0004-637x/697/2/1071. arXiv: 0902.1089 [hep-ph].

[81] HESS Collaboration et al. In: *Phys. Rev. D* 75.4 (2007). DOI: 10.1103/physrevd.75.042004.

[82] MAGIC Collaboration: M.L. Ahnen et al. In: *JCAP* 2018.03 (2018), pp. 009–009. DOI: 10.1088/1475-7516/2018/03/009. arXiv: 1712.03095 [astro-ph].

[83] M. Actis et al. (CTA). In: *Experimental Astronomy* 32.3 (2011), pp. 193–316. DOI: 10.1007/s10686-011-9247-0. arXiv: 1008.3703 [astro-ph].

[84] i. Cholis et al. In: *JCAP* 2009.12 (2009). DOI: 10.1088/1475-7516/2009/12/007. arXiv: 0810.5344 [astro-ph].

[85] L. Feng et al. In: *Phys. Lett. B* 728 (2014). DOI: 10.1016/j.physletb.2013.12.012. arXiv: 1303.0530 [astro-ph].

[86] A. Cuoco, M. Krämer, and M. Korsmeier. In: *Phys. Rev. Lett.* 118 (19 2017). DOI: 10.1103/PhysRevLett.118.191102. arXiv: 1610.03071 [astro-ph].

[87] M. G. Aartsen et al. (IceCube). In: *Eur. Phys. J.* 77.3 (2017). DOI: 10.1140/epjc/s10052-017-4689-9. arXiv: 1612.05949 [astro-ph].

[88] S. Desai et al. (SuperKamiokande). In: *Phys. Rev. D* 70.10 (2004). DOI: 10.1103/PhysRevD.70.109901.

[89] J. Silk, K. Olive, and M. Srednicki. In: *Phys. Rev. Lett.* 55 (2 1985). DOI: 10.1103/PhysRevLett.55.257.

[90] G. P. Salam. *Theory Vision talk at LHCP2018*. 2018. arXiv: 1811.11282 [hep-ph].

[91] A. Boveia and C. Doglioni. In: *Annual Review of Nuclear and Particle Science* 68.1 (2018). DOI: 10.1146/annurev-nucl-101917-021008. arXiv: 1810.12238 [hep-ex].

[92] O. Buchmueller, C. Doglioni, and L. Wang. In: *Nature Phys.* 13.3 (2017). DOI: 10.1038/nphys4054. arXiv: 1912.12739 [hep-ex].

[93] P. Agrawal and et al. In: *Eur. Phys. J. C* 81.11 (2021). DOI: 10.1140/epjc/s10052-021-09703-7. arXiv: 2102.12143 [hep-ph].

[94] J. Alexander and et al. In: (2016). arXiv: 1608.08632 [hep-ph].

[95] M. Battaglieri and et al. In: (2017). arXiv: 1707.04591 [hep-ph].

[96] C. et al. Argüelles. In: *Rep. Prog. Phys.* 83.12 (2020). ISSN: 0034-4885, 1361-6633. DOI: 10.1088/1361-6633/ab9d12. arXiv: 1907.08311 [hep-ph].

[97] J. L. Feng, H. Tu, and H. Yu. In: *J. Cosmol. Astropart. Phys.* 2008.10 (2008). ISSN: 1475-7516. DOI: 10.1088/1475-7516/2008/10/043. arXiv: 0808.2318 [hep-ph].

[98] J. L. Feng et al. In: *J. Cosmol. Astropart. Phys.* 2009.07 (2009). ISSN: 1475-7516. DOI: 10.1088/1475-7516/2009/07/004. arXiv: 0905.3039 [hep-ph].

[99] Peter Ballett, Matheus Hostert, and Silvia Pascoli. In: *Phys. Rev. D* 99.9 (2019). ISSN: 2470-0010, 2470-0029. DOI: 10.1103/PhysRevD.99.091701. arXiv: 1903.07590 [hep-ph]. URL: http://arxiv.org/abs/1903.07590.

[100] P. Ballett, M. Hostert, and S. Pascoli. In: *Phys. Rev. D* 101.11 (2020). ISSN: 2470-0010, 2470-0029. DOI: 10.1103/PhysRevD.101.115025. arXiv: 1903.07589 [hep-ph].

[101] N. Haba and S. Matsumoto. In: *Progress of Theoretical Physics* 125.6 (2011). ISSN: 0033-068X, 1347-4081. DOI: 10.1143/PTP.125.1311. arXiv: 1008.2487 [hep-ph].

[102] T. Bringmann et al. In: (2023). arXiv: 2306.09411 [hep-ph]. URL: http://arxiv.org/abs/2306.09411.

[103] A. Abdullahi, M. Hostert, and S. Pascoli. In: *Physics Letters B* 820 (2021). ISSN: 03702693. DOI: 10.1016/j.physletb.2021.136531. arXiv: 2007.11813 [hep-ph].

[104] B. Batell, M. Pospelov, and Adam Ritz. In: *Phys. Rev. D* 80.9 (2009). ISSN: 1550-7998, 1550-2368. DOI: 10.1103/PhysRevD.80.095024. arXiv: 0906.5614 [hep-ph]. URL: http://arxiv.org/abs/0906.5614.

[105] H. Zhang. In: *Physics Letters B* 714.2-5 (2012). DOI: 10.1016/j.physletb.2012.06.074. arXiv: 1110.6838 [hep-ph].

[106] B. Holdom. In: *Phys. Lett. B* 166.2 (1986). DOI: 10.1016/0370-2693(86)91377-8.

[107] C. Cheung et al. In: *Phys. Rev. D* 80.3 (2009). DOI: 10.1103/physrevd.80.035008. arXiv: 0902.3246 [hep-ph].

[108] B. Abi et al. In: *Phys. Rev. Lett.* 126.14 (2021). DOI: 10.1103/physrevlett.126.141801. arXiv: 2104.03281 [hep-ex].

[109] T. Albahri et al. In: *Phys. Rev. D* 103.7 (2021). DOI: 10.1103/physrevd.103.072002. arXiv: 2104.03247 [hep-ex].

[110] KamLAND-Zen Collaboration and S. et al. Abe. In: *Phys. Rev. Lett.* 130.5 (2023). ISSN: 0031-9007, 1079-7114. DOI: 10.1103/PhysRevLett.130.051801. arXiv: 2203.02139 [hep-ex].

[111] M. Pospelov. In: *Phys. Rev. D* 80.9 (2009). DOI: 10.1103/physrevd.80.095002. arXiv: 0811.1030 [hep-ph].

[112] G. Mohlabeng. In: *Phys. Rev. D* 99.11 (2019). DOI: 10.1103/physrevd.99.115001. arXiv: 1902.05075 [hep-ph].

[113] A. M. Abdullahi and et al. In: *J. Phys. G: Nucl. Part. Phys.* 50.2 (2023). ISSN: 0954-3899, 1361-6471. DOI: 10.1088/1361-6471/ac98f9. arXiv: 2203.08039 [hep-ph].

[114] D. Smith and N. Weiner. In: *Phys. Rev. D* 64.4 (2001). DOI: 10.1103/physrevd.64.043502.

[115] A. Filimonova et al. In: *J. High Energ. Phys.* 2022.6 (2022). ISSN: 1029-8479. DOI: 10.1007/JHEP06(2022)048. arXiv: 2201.08409 [hep-ph].

[116] A. et al. Abada. *Snowmass Letter of Interest: Testable neutrino mass models.*

[117] M. Fabbrichesi, E. Gabrielli, and G. Lanfranchi. *The Physics of the Dark Photon.* Springer International Publishing, 2021. DOI: 10.1007/978-3-030-62519-1. arXiv: 2005.01515 [hep-ph].

[118] NA48/2 collaboration. *Search for the dark photon in π^0 decays.* 2015. arXiv: 1504.00607 [hep-ex].

[119] H. Merkel et al. (A1). In: *Phys. Rev. Lett.* 112.22 (2014). DOI: 10.1103/physrevlett.112.221802. arXiv: 1404.5502 [hep-ex].

[120] D. Curtin et al. In: *JHEP* 2015.2 (2015). DOI: 10.1007/jhep02(2015)157. arXiv: 1412.0018 [hep-ph].

[121] (KLOE) F. Archilli et al. In: *Phys. Lett. B* 706.4-5 (2012). DOI: 10.1016/j.physletb.2011.11.033.

[122] Tech. rep. CERN, 2019. URL: https://cds.cern.ch/record/2684861.

[123] J. Blümlein and J. Brunner. In: *Physics Letters B* 701.2 (2011). DOI: 10.1016/j.physletb.2011.05.046.

[124] S.N. Gninenko. In: *Phys. Lett. B* 713.3 (2012). DOI: 10.1016/j.physletb.2012.06.002.

[125] Jae Hyeok Chang, Rouven Essig, and Samuel D. McDermott. In: *JHEP* 2017 (2017). DOI: 10.1007/jhep01(2017)107.

[126] E. Cortina Gil et al. (NA64). In: *JHEP* 2019.5 (2019). DOI: 10.1007/jhep05(2019)182. arXiv: 1903.08767 [hep-ex].

[127] E Kou et al. (Belle II). In: *Prog. Theor. Exp. Phys.* 2019.12 (2019). DOI: 10.1093/ptep/ptz106. arXiv: 1808.10567 [hep-ex].

[128] F. Ambrosino et al. (KLEVER). 2019. arXiv: 1901.03099 [hep-ex].

[129] M. Raggi, V. Kozhuharov, and P. Valente (PADME). 2015. arXiv: 1501.01867 [hep-ex].

[130] X. Fan et al. In: *Phys. Rev. Lett.* 130 (7 2023). DOI: 10.1103/PhysRevLett.130.071801.

[131] J. Schwinger. In: *Phys. Rev.* 73 (4 1948). DOI: 10.1103/PhysRev.73.416.

[132] T. Aoyama et al. In: *Phys. Rept.* 887 (2020), pp. 1–166. DOI: 10.1016/j.physrep.2020.07.006. arXiv: 2006.04822 [hep-ex].

[133] G. W. Bennett et al. In: *Phys. Rev. Lett.* 92.16 (2004). DOI: 10.1103/physrevlett.92.161802. arXiv: hep-ex/0401008.

[134] J. Grange et al. 2018. arXiv: 1501.06858 [physics.ins-det].

[135] D. P. Aguillard et al. 2023. arXiv: 2308.06230 [hep-ex].

[136] Sz. Borsanyi et al. In: *Nature* 593.7857 (2021). DOI: 10.1038/s41586-021-03418-1. arXiv: 2002.12347 [hep-lat].

[137] B. Abi et al. 2017. arXiv: 1706.07081 [physics.ins-det].

[138] B. Abi et al. 2020. arXiv: 2002.02967 [physics.ins-det].

[139] M. Brice. "Inside ProtoDune". In: (2017). URL: https://cds.cern.ch/record/2288139.

[140] K. J. Kelly and Y. Tsai. In: *Phys. Rev. D* 100.1 (2019). DOI: 10.1103/physrevd.100.015043. arXiv: 1812.03998 [hep-ph].

[141] B. Batell et al. In: *Phys. Rev. D* 90.11 (2014). DOI: 10.1103/physrevd.90.115014. arXiv: 1405.7049 [hep-ph].

[142] Y. Kahn et al. In: *Phys. Rev. D* 91.5 (2015). DOI: 10.1103/physrevd.91.055006. arXiv: 1411.1055 [hep-ph].

[143] D. E. Morrissey and A. P. Spray. In: *JHEP* 2014.6 (2014). DOI: 10.1007/jhep06(2014)083. arXiv: 1402.4817 [hep-ph].

[144] D. Kim, J. Park, and S. Shin. In: *Phys. Rev. Lett.* 119.16 (2017). DOI: 10.1103/physrevlett.119.161801.

[145] A. Denner et al. In: *Nuclear Physics B* 387.2 (1992), pp. 467–481. ISSN: 05503213. DOI: 10.1016/0550-3213(92)90169-C.

[146] H Haber. In: *Physics Reports* 117.2-4 (1985), pp. 75–263. ISSN: 03701573. DOI: 10.1016/0370-1573(85)90051-1.

[147] Evalyn I. Gates and Kenneth L. Kowalski. In: *Phys. Rev. D* 37.4 (1988). DOI: 10.1103/PhysRevD.37.938.

[148] H.B. O'Connell et al. In: *Prog.Part.Nucl.Phys* 39 (1997). DOI: 10.1016/s0146-6410(97)00044-6. arXiv: hep-ph/9501251.

[149] A. Berlin and F. Kling. In: *Phys. Rev. D* 99.1 (2019). DOI: 10.1103/physrevd.99.015021. arXiv: 1810.01879 [hep-ph].

[150] R. L. Workman et al. "Review of Particle Physics". In: *PTEP* 2022 (2022), pp. 743–747. DOI: 10.1093/ptep/ptac097.